The role of $Ca_v3.2$ Ca^{2+} channels in influencing the activity of the layer II stellate cells of the Medial Entorhinal Cortex

Aleksandra Paulina Topczewska

UCL School of Pharmacy

Department of Pharmacology

University College London

29-39 Brunswick Square, London WC1N 1AX

A thesis submitted for the degree of Doctor of Philosophy for the UCL School of Pharmacy 2017

I, Aleksandra Paulina Topczewska, confirm that the work presented in this thesis is my own. Where information has been derived from other sources, I confirm that this has been indicated in the thesis.

Signature: Date: 04/08/2017

Acknowledgements

Firstly, I would like to thank my husband, Elia, for his continuous support and endless patience. Thank you for encouraging me with a smile to carry on during all difficult moments and believing in me. It would not be possible for me to accomplish this without you. I would also like to thank my Mother, Father and Sister who were always there for me, ready to listen and help whenever needed. It was their phone calls and skype conversations which always made me feel better. Thank you for your continuous trust in my choices and support during this past four years.

Furthermore, I wish to thank my friends, in particular Archie Khan and Jody Phelan, for their support and help. Thank you for helping me to overcome so many difficulties and sharing all the ups and downs with me. I would like to thank my colleagues from School of Pharmacy, all of the people from the 6th floor, in particular Joana Manuel, Kimberley Reid and Laura Pellegrini, who made this experience so much more enjoyable. Special thanks to two amazing post-docs, Dr Edward Maguire and Dr Katiuscia Martinello, that helped me overcome numerous problems both in the laboratory and outside of it. Electrophysiology would be impossible without you two. Thank you for your never--ending patience and support.

Finally, I would like to thank my two supervisors, Professor Mala Shah and Professor Annette Dolphin for giving me the opportunity to do this PhD. Thank you for sharing your expertise with me as well as for your valuable feedback and the training I was given during the course of my PhD.

Lastly, I would like to acknowledge Talfan Evans for his collaboration and help on data analysis, Dr David Gathercole for his advices on confocal microscopy, Martin Stuart for all the brilliant genotyping work and Mr Victor Diran for his help and support.

Abstract

Layer II (L II) Medial Entorhinal Cortex (MEC) stellate cell (SC) intrinsic membrane properties vary along the MEC dorsal-ventral axis. This has been attributed partly to altered HCN and K^+ conductances (Garden et al. 2008; Giocomo and Hasselmo 2008). The subthreshold active T-type $Ca_V3.2$ Ca^{2+} channels, though, are also expressed in the MEC (Huang et al. 2011). $Ca_V3.2$ channels are known to influence neuronal excitability but their effects on dorsal and ventral LII MEC SC properties remain unknown. To investigate this, I obtained acute brain slices from $Ca_V3.2$ wild type ($Ca_V3.2^{+/+}$) and null ($Ca_V3.2^{-/-}$) 5-8 week old mice and made electrophysiological recordings from dorsal and ventral L II MEC SC. $Ca_V3.2^{-/-}$ ventral neurons displayed significantly reduced input resistance but little difference in resting membrane potential (RMP) compared with $Ca_V3.2^{+/+}$ ventral neurons. Consequently, depolarizing steps resulted in fewer action potentials in $Ca_V3.2^{-/-}$ ventral SC than in wild type neurons. In contrast, dorsal $Ca_V3.2^{-/-}$ and $Ca_V3.2^{+/+}$ SC properties were similar. Furthermore, $Ca_V3.2^{+/+}$ ventral cells had a significantly higher α excitatory post synaptic potentials (αEPSP) summation ratio (at 50 Hz) in comparison to $Ca_V3.2^{-/-}$ ventral neurons. The Ca_V3 inhibitors, $NiCl_2$ and TTA-P2, also significantly reduced input resistance and action potential firing in $Ca_V3.2^{+/+}$ ventral neurons, whilst having little effect on $Ca_V3.2^{+/+}$ dorsal or $Ca_V3.2^{-/-}$ neurons. Furthermore, voltage-clamp experiments revealed a significantly greater T-type $Ca_V3.2$ Ca^{2+} current in ventral than dorsal neurons. Our results suggest that $Ca_V3.2$ channels selectively affect L II MEC ventral SC properties, thereby contributing to the intrinsic membrane gradient across the MEC dorsal-ventral axis.

Impact statement

In my work, I investigated the role of specific type of ion channels, T-type $Ca_v3.2$ Ca^{2+} channels, and their contribution towards the so-called dorsal-ventral gradient in the MEC SC L II.

The dorsal-ventral gradient in the intrinsic properties of SC is believed to make an important contribution towards grid cell firing patterns. Grid cells encode for an animal's position in the environment and thus, these neurons play a significant role in spatial navigation (Fyhn et al. 2004). Therefore, it is vital to understand the cellular processes regulating MEC SC excitability.

Multiple ion channels have been shown to control the activity of the L II SC. However, the role of T-type $Ca_v3.2$ Ca^{2+} channels has not been investigated so far. The work presented here positively answers the basic research question of whether these channels are present in MEC SC, and therefore opens up new doors for further research. One possibility is to see how the data presented hereby fits into a computational model of grid cells (Hasselmo et al. 2007; McNaughton et al. 2006). Moreover, *in vivo* experiments could be conducted to understand the role of T-type Ca^{2+} currents in modulating grid cell activity and spatial navigation. Additionally, understanding cellular processes setting up the dorsal-ventral gradient of L II SC could help us to define whether these two subregions of MEC have different mechanisms for synaptic integration and therefore information processing.

Further, dysfunction of the MEC has been associated with multiple diseases including schizophrenia, temporal lobe epilepsy and mild cognitive impairment (Arnold et al. 1991; deToledo-Morrell et al. 2004). For example, MEC is the first brain structure to be affected in the Alzheimer's Disease (Braak and Braak 1985). Therefore, understanding the cellular mechanisms controlling the activity of this brain region are crucial in order to answer questions on how the brain processes information under healthy and

pathological conditions. In summary, through answering the question regarding the presence and the role of T-type Ca^{2+} channels in MEC L II SC, this research has a great potential to contribute towards the neuroscience field through increasing the understanding of basic cellular mechanisms controlling the brain.

Table of contents

List of figures

List of tables

Abbreviations

ACSF - artificial cerebral spinal fluid

ADP – afterdepolarisation

AHP – afterhyperpolarisation

AIS – axon initial segment

Ca_{HVA} - high voltage activated calcium channels

Ca_{LVA} - low voltage activated calcium channels

CamKII - calmodulin-dependent protein kinase II

cAMP – cyclic adenosine monophosphate

DAP - depolarising after potential

DG – dentate gyrus

EC – entorhinal cortex

EPSP - excitatory post synaptic potential

fAHP – fast afterhyprepolarisation

HCN – hyperpolarisation activated cyclic nucleotide gated channels

I_h – hyperpolarisation activated cyclic nucleotide gated current

$I_{Twindow}$ - non-inactivating inward calcium current

K_A – A-type potassium current

K_{Ca} - Calcium-activated potassium channel

K_{DR} - delayed rectifier potassium

K_{leak} - potassium leak current

L II – layer II

LEC- lateral entorhinal cortex

LTP - long term potentiation

LTS – low threshold spike

mAHP – medium afterhyperpolarisation

MCI – Mild Cognitive Impairment

MEC - medial entorhinal cortex

MEC L II – layer II of the MEC

min – minutes

NA$_P$ – persistent sodium current

NA$_T$ – transient sodium current

NMDA - N-methyl-D-aspartate

NRT – thalamic reticular neurons

OI- Oscillatory interference (model)

PCR- polymerase chain reaction

PKA – protein kinase A

PKC – protein kinase C

RMP – resting membrane potential

s – seconds

SC – stellate cells

sMPOs - subthreshold membrane potential oscillations

TC – thalamocortical relay neurons

TTA-P2 - 3,5-dichloro-N-[1-(2,2-dimethyl-tetrahydro-pyran-4-ylmethyl)-4-fluoro-piperidin-4-ylmethyl]-benzamide

1. Introduction

In this thesis, I will asses the influence of T-type $Ca_v3.2$ Ca^{2+} channels on the dorsal-ventral gradient of medial entorhinal cortex (MEC) layer II (L II) stellate cells (SC). In this introduction, I will first outline the general position of the entorhinal cortex (EC) in the brain and highlight its physiological significance. Next, I will introduce the EC subdivision into lateral entorhinal cortex (LEC) and MEC outlining the differences in their connectivity with dentate gyrus (DG) and hippocampal formation. I will then explain what cell types can be found within the six layers of EC (both MEC and LEC) and outline the connections between, and within, these layers. This will lead to the main topic of this research, which is MEC L II and its primary excitatory neurons, SC. Finally, this chapter will summarize the different ion channels found in SC, with a particular focus on the T-type Ca^{2+} channels. Lastly, I will explain the different properties of SC in the context of the dorsal-ventral gradient.

1.1 Entorhinal cortex

The EC owes its name to the fact it is surrounded by the rhinal sulcus (Canto et al. 2008). The significance of the EC was first appreciated in the 20th century, when Ramon y Cajal characterised it as a part of the posterior temporal cortex associated with the hippocampus (y Cajal 1902). Today, the localisation of the EC is known in more detail (Figure 1.1). Anteriorly, the EC adheres to the amygdaloid and olfactory cortices (piriform and periamygdaloid cortices and the posterior cortical nucleus of the amygdala). Medially, the EC meets hippocampal and parahippocampal regions e.g. parasubiculum. The lateral part of the EC merges with the perirhinal cortex, whereas the posterior part lies next to the parahippocampal cortex (Canto et al. 2008)

Figure 1.1. Graphical representation of the position of the medial entorhinal cortex in the rat brain (left) and the surrounding structures (right). This picture was adapted from Canto et al. (2008).

1.1.1 Physiological significance of the EC and its pathologies

The EC is linked to numerous important functions of the brain. Multiple rat studies involving damage to the EC and associated areas, including subiculum, perirhinal cortex or entire retrohippocampal region, highlighted its importance in spatial navigation. More specifically, lesions to these brain regions caused impairments in spatial alternation (Ramirez and Stein 1984), place learning (Nagahara et al. 1995), integration of geometric information during spatial exploration (Oswald and Good 2000) and spatial memory (Schenk and Morris 1985). These impairments were tested during various behavioural tasks, mainly the variations of the water maze test. More recently, neurons within the MEC were shown to fire in a 'grid-like' pattern to encode for an animal's position within the environment, providing significant evidence that this region of the brain has a substantial role in spatial navigation (Fyhn et al. 2004; Hafting et al. 2005).

The role of EC is not limited to computing the spatial information. EC has also been associated with different forms of learning and memory processes. For example, animal studies involving lesions of EC (and perirhinal cortex) showed severe visual recognition decline in monkeys (Meunier et al. 1993) and rats (Otto and Eichenbaum

1992). Furthermore, behavioural studies on rats showed that spatial representations of EC can contribute towards the formation of episodic memories (Lipton and Eichenbaum 2008) by supplementing the activity of the hippocampus. Authors of this study suggested that hippocampus encodes sequences of events contributing towards spatial and temporal episodes, while the EC in some way connects sequential episodes to form a concrete memory. Furthermore, neurotoxic inactivation of EC (using *N*-methyl-D-aspratate (NMDA)) showed a significant decrease in the rats' performance during behavioural memory tasks, highlighting the importance of EC in memory retention (Levisohn and Isacson 1991). Additionally, pharmacological experiments on rats illustrated that changes to the cholinergic inputs to the EC can interfere with memory processes. Particularly, the infusion of a cholinergic antagonist, scopolamine, was shown to disrupt spatial encoding and learning, whereas application of carbachol (a cholinergic agonist) enhanced these processes (Hasselmo 2006; Elvander et al. 2004; Blokland et al. 1992). The EC has also been proposed to play an important role in the recollection-associated processes (summarised in: Eichenbaum et al. 2007).

These and multiple other animal studies have highlighted the significance of EC in cognitive functions. In order to investigate whether the EC is as equally important in the human brain, experiments involving human participants were performed. MRI studies on healthy participants showed that the EC volume is correlated with the performance during memory-related tasks (Goto et al. 2011). Multiple fMRI studies also illustrated that the EC is highly engaged while performing memory-associated tasks, including face recognition (Kirwan and Stark 2004), object and spatial recognition memory (Bellgowan et al. 2009), and novel object representations tests (Stern et al. 2001). Another fMRI study showed that EC is responsible for working memory processes (Newmark et al. 2013). In addition, a fMRI study on human participants exploring virtual reality environment confirmed the involvement of EC in navigation processes (Doeller et al. 2010). Finally, deep-brain stimulation of EC helped to improve memory during

spatial learning tasks in humans (Suthana et al. 2012). Altogether, these studies greatly illustrate the importance of EC in cognitive functions in both animals and humans.

Consistent with the significant role of the EC in cognition, L II of the EC appears to be the first region of the brain in which the pathological changes associated with Alzheimer's disease (AD) are observed (Braak and Braak 1985). Studies showed that patients with Mild Cognitive Impairment (MCI) are characterised by progressively decreasing EC volume, which in turn leads to the development of AD (deToledo-Morrell et al. 2004). Dysfunction in the EC has also been associated with diseases other than AD. A study based on the cases of four patients with temporal lobe epilepsy found pronounced neurodegeneration in layer III of the EC (Du et al. 1993). Similar neurodegeneration in this region was also observed in animal models of epilepsy (Du et al. 1995). A more recent study in humans, however, showed (using Nissl staining) that there was no obvious cell loss in EC layer III in tissue from temporal lobe epilepsy patients (Dawodu and Thom 2005). Furthermore, disruption of EC layers and neuronal displacement was observed in schizophrenic patients. This suggests that EC neuropathologies contribute to some neuropsychiatric diseases (Arnold et al. 1991). Due to the obvious significance of the EC in numerous physiological processes and its role in the pathologies of various diseases, it is important to understand the cellular properties and functional connections within the EC.

1.1.2 Extrinsic connectivity

The EC has a very diverse connectivity. Studies showed that EC is interconnected with both cortical and subcortical structures. In primates, the rostral EC receives an input from perirhinal cortex, whereas parahippocampal cortex sends projections to caudal EC (Insausti et al. 1987a). Other EC cortical inputs arise from medial orbital prefrontal area, insular regions (Insausti 1987a; Van Hoesen et al. 1975; van Hoesen and

Pandya 1975), and retrosplenial cortex (Morris et al. 1999). Additionally, the EC receives inputs from claustral regions (Witter et al. 1988), the basal forebrain (Insausti et al. 1987a), the temporal piriform cortex, the inferior and anterior area TE, as well as the superior temporal gyrus (Suzuki and Amaral 1994; Saleem and Tanaka, 1996). Studies on monkey also showed that EC is connected with amygdala (Aggleton et al. 1980; Amaral and Insausti 1992), thalamus (Aggleton et al. 1986) as well as midbrain structures (Insausti et al. 1987b).

In rodents, the EC cortical afferents arise from the perirhinal (sends projections to LEC and caudal EC) and postrhinal cortex (projects to MEC; Burwell and Amaral 1998). Further afferents in the EC come from the piriform: frontal, cingular, retrosplenial, insular, visual and parietal regions (Amaral and Witter 1995; Figure 1.1). Furthermore, the EC processes information from the medial septum nucleus and the nucleus basalis of Meynart. The EC also receives inputs from the band of Broca (Beckstead 1978). Studies on rats also showed that the inputs to the EC come from the striatum (Krayniak et al. 1981), ventral tegmental area (Beckstead et al. 1979), amygdala (Krettek and Price 1974), thalamic and hypothalamic structures (Beckstead 1978; van Groen et al. 1999; Canteras et al. 1994) as well as the dorsal raphe nucleus, median raphe, locus coeruleus and ventral tegmental area (Beckstead 1978).

There are also multiple reciprocal connections coming from diverse structures to the EC. In primates, EC have reciprocal connections with substantia innominate (Mesulam and Mufson 1984), insular regions (Carmichael and Price 1995), parahippocampal and perirhinal regions (Suzuki and Amaral 1994) as well as claustrum (Insausti 1987a). In rodents, inputs from perirhinal and postrhinal regions and pre- and para-subiculum are also reciprocal as well as the inputs coming from claustrum (Witter et al. 1988). Furthermore, the EC projects back to medial septum and Broca area (Alonso and Kohler 1984). CA1 and subiculum also project reciprocally to deep layers of the EC.

The detailed functional significance of these connections remains to be established (Kloosterman et al. 2003).

1.1.3 EC subdivisions

Over the years, the EC was defined based on multiple factors, including its cytoarchitecture, location and connectivity (Canto et al. 2008). The most common and efficient description of the EC is based on its connections with the DG. This approach allows the EC of rodents to be subdivided into two major subgroups: LEC and MEC, based on the termination of their projections. MEC was shown to send projections to middle thirds of the DG molecular layer, whereas LEC outputs in the DG terminate in the outer third of the molecular layer (Steward 1976, van Groen et al. 2003). This description corresponds to Brodmann's classification (cytoarchitectonic) and his subdivision of the EC into areas 28 a and b (Brodmann 1909). Although the work presented in this thesis will focus on the findings from mice, it is important to note that studies on macaque monkey showed that EC projections in primates terminate diffusely across the outer two-thirds of DG molecular layer rather than being bilaminal as in rodents (Witter et al. 1989). The MEC and LEC in primates can however be distinguished based on the fact that their inputs terminate in the caudal and rostral DG, respectively (Witter et al. 1989).

Whereas the description of the outputs termination differs between rodents and primates, the inputs from the presubiculum can be used to define the MEC in all species, including rodents (Alonso and Kohler et al. 1984) and primates (Amaral et al. 1984). Using this method of classification, the MEC was defined to be the area where the presubicular innervation is confined to its caudal and dorsal parts (Caballero-Bleda and Witter 1993). Both MEC and LEC can also be distinguished by their connections with hippocampal regions, particularly CA1. LEC primarily sends information to the parts of CA1 near the subiculum, whereas MEC excites CA1 pyramidal neurons closer to the CA2 region (Steward 1976; Witter 1993).

20

Since this project is focused on MEC, I will discuss the connection of this brain region to the hippocampal formation in more detail. The major outputs of the MEC neuronal projections to the hippocampus are via perforant path. Here, L II of the MEC projects to the middle one-third of the molecular layer of the DG (Figure 1.2). Furthermore, neurons of L II project to hippocampal regions CA2 and CA3 (Steward and Scovile 1976). Some studies also suggest that MEC L II additionally projects to subiculum (Tamamaki and Nojyo 1993). In contrast, neurons of layer III of the MEC terminate their projections in the CA1 and subiculum, via temporoammonic branch of the perforant path (Amaral 1993). Finally, some studies showed that also MEC layers IV to VI sends their projections to DG, though these are sparse compared with the dense projections of layers II/III (Kohler 1985; Witter and Amaral 1991; van Groen et al. 2003).
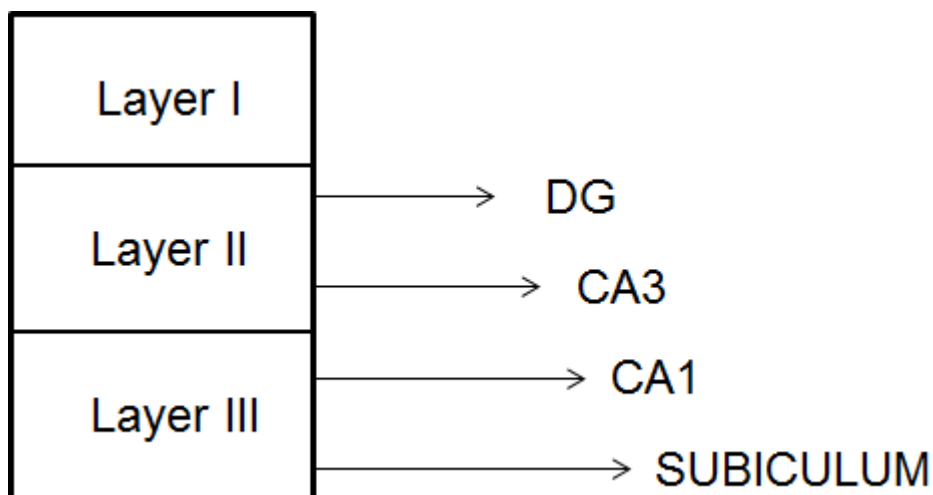
Figure 1.2. The schematic diagram showing the extrinsic connections of the MEC. The major output of L II and III go to DG, hippocampal regions CA1 and CA3 and subiculum.

Having different connections, it is not surprising that MEC and LEC display functional differences. LEC neurons are involved in odour discrimination (Young et al. 1997; Leitner et al. 2016; Chapuis et al. 2013). In addition to processing olfactory information, LEC is also responsible for object recognition (Tsao et al. 2013; Hargreaves et al. 2005; Deshmukh and Knierim 2011). Furthermore, LEC receives inputs from insular

cortex which could potentially lead to the processing of contextual information and their emotional significance (Kerr et al. 2007). LEC cells, however, in contrast with MEC neurons, are not spatially modulated (Deshmukh and Knierim 2011; Hargreaves et al. 2005; Fyhn et al. 2004). Based on these differences, for many years MEC and LEC were subdivided into spatial (Zhang, Ye, et al. 2013) and non-spatial (Hargreaves et al. 2005) neural structures, respectively. Although it has been recently discovered that the involvement of MEC and LEC in processing these two types of information can be modulated by the environment and depends on the complexity of the surroundings (Keene et al. 2016; Rodo et al. 2017), the major functions of MEC and LEC in the context of information processing are described as 'where' and 'what', respectively (Figure 1.3). LEC is a structure that is responsible for passing content related information to hippocampus (i.e. about the object itself), whereas MEC processes direct contextual information (i.e. about the object location, Figure 1.3).
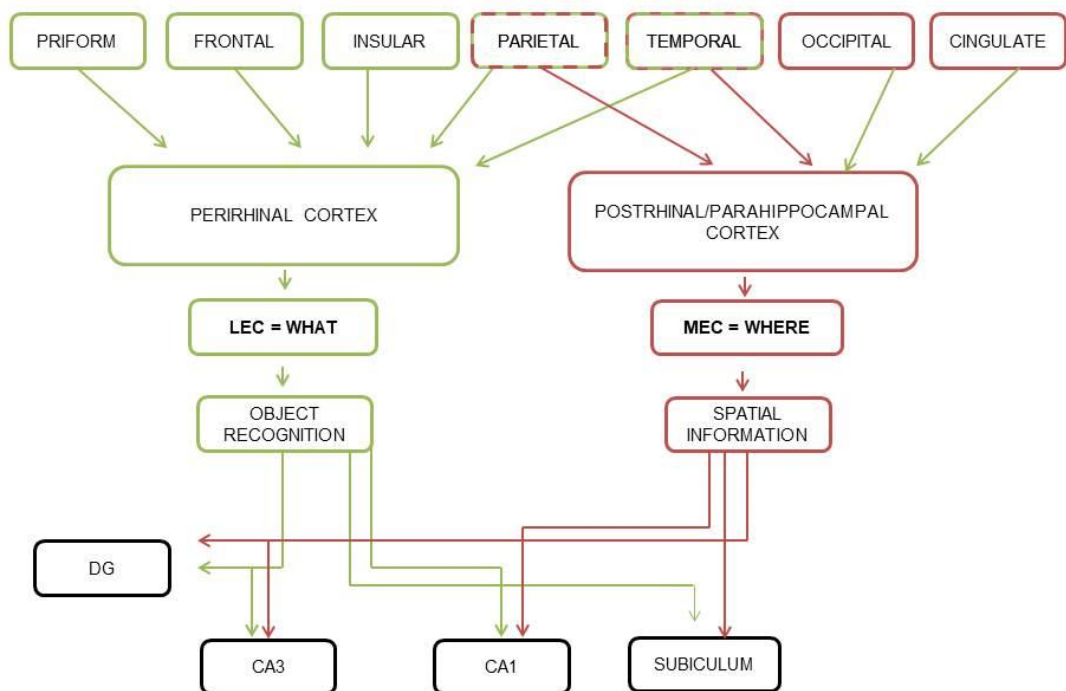
Figure 1.3. The representative diagram explaining 'what' and 'where' concept. The diagram was simplified and shows only the most important cortical afferents reaching perirhinal and postrhinal/parahippocampal regions. It was based on the information obtained from Burwell and Amaral 1998.

1.1.4 Cell types within the EC

The EC consists of six layers. The layer I, which is the most superficial, is composed of transversely orientated fibres and is typically devoid of neurons. Layer III consists primarily of medium pyramidal cells, which in contrast to L II, are arranged more randomly. Layer IV, also known as lamina dissecans, is composed of the cell-sparse fibres. Layer V can be subdivided into layers Va and Vb (sometimes called Vb/c). Large and medium pyramidal cells are typically found within layer Va and small and fairly dense pyramidal neurons are commonly present in layer Vb. The last and deepest layer of the EC outlined by the white matter is layer VI. Notably, the lamination of the EC differs between species (Canto et al. 2008). Furthermore, each of the molecular layers is composed of an even bigger variety of cells including excitatory neurons and

interneurons (summarised in Table 1.1). In contrast to the other layers, the L II is different in MEC and LEC (Canto et al. 2008). The most abundant MEC cell type is the stellate neuron, which is substituted by the fan cell in LEC (Lingenhohl and Finch 1991; Tahvildari and Alonso 2005). Fan cells, in contrast to MEC stellate neurons, are characterised by the presence of small descending dendrites and harbour different electrophysiological properties (Tahvildari and Alonso 2005).

Layer	Cell type	Short characteristic
I	Horizontal cells	On transition between layer I & II, soma 13-15 µm, GABAergic, positive for vasoactive intestinal polypeptide (VIP) and cholecystokinin (CKK).
I	Short axis cylinder cells/multipolar neurons (MPNs)	Calretinin (CR) positive, GABAergic, dendritic tree 100-150 µm long. Some also glutamatergic and calbindin (CB) or neuropeptide Y (NPY) positive
II	Stellate cells	Glutamatergic, CB positive, more abundant in MEC than LEC, superficial and medium layer II.
II	Pyramidal cells	Deep layer II, prominent apical dendrite and smaller dendritic tree in comparision to stellates
II	Fan cells	Found within LEC, probably a equivalent of stellate cells in the MEC
II	Interneurons	MPNs, bipolar, basket and chandelier.
III	Pyramidal cells	Devided into spiny (LEC & MEC) and non spiny (MEC only) subgroup.
III	Stellate cells	Upper part of Layer III
III	Interneurons	MPNs, pyramidal looking interneurons (PLIs), bipolar cells
IV	Pyramidal-shaped	Have transitional properties between the neurons of layers III and V
IV	Bipolar cells	Horizontally orientated dendrites, VIP, CCK and corticotrophin releasing factor (CRF) positive
V	Pyramidal cells	Axons extending to the more superficial layers of the EC
V	Horizontal cells	Polygonal somata
V	Polymorphic MPNs	Spherical or pyramidal soma, PV, SOM, NPY and substance P positive
V	Fusiform cells	Project to hippocampus, CR positive
V	Bipolar cells	Somatostatin (SOM), substance P, NPY and GABA positive
VI	MPNs	Spherical soma of 14 µm
VI	Pyramidal cells	Dominant dendrites are not only vertically but also horizontally orientated to the pial surface

Table 1.1. The variety of the cells found in layers I-VI of the EC (Wouterlood and Pothuizen 2000; Wouterlood et al. 1985; Wouterlood et al. 2000; Schwerdtfeger et al. 1990; Klink and Alonso 1997a; Yoshida et al. 1987; Tahvildari and Alonso 2005; Germroth et al. 1989; Gloveli et al. 1997; Kohler et al. 1986; Hamam et al. 2002; Lorente de Nó 1933; Kohler and Chan-Palay 1983; Lingenhohl and Finch1991).

1.1.5 Intrinsic organisation

The EC also possesses a high level of intrinsic connections. A study using paired whole-cell *in-vitro* recordings in rats' entorhinal neurons showed that inhibitory cells within the MEC are primarily connected to L II SC. This study therefore suggests the existence of local (inter-hemispheric) connections between these neurons (Couey et al. 2013). A different study, using immunohistochemistry tracing on rat brain slices showed that some inhibitory neurons project to the contralateral EC. This illustrates the existence of inter-hemispheric connections between neurons in the EC (Varga et al. 2010). Additionally, the EC also possesses inter-laminar connections. Anatomical tracing experiments made it possible for the connections between intra-entorhinal, transversely orientated fibres to be explained in detail. Generally, the projections of layers II and III terminate in the superficial layers of the EC; however, projections arising in deeper EC layers tend to terminate not only in the superficial but also in the deep layers of the EC. More recent experiments using electrophysiology and immunohistochemistry techniques showed however that L II SC can also excite cells found in EC layer Vb (Surmeli et al. 2015).

In more detail, the axons of the EC layer I interneurons can be found in layers II and III. Here they are believed to be responsible for feedforward inhibition of the principal neurons (Finch et al. 1988). L II pyramidal neurons were shown to have axons spanning across layers I-III (Klink and Alonso 1997b). The collaterals of layer III spiny pyramidal cells were shown to extend through layers II, III, and V and the axons of multipolar interneurons found within this layer span through layers I-III (Gloveli et al. 1997). The apical dendrites of layer V pyramidal neurons can be found within the superficial layers I and II, whereas the basal dendrites extend all the way to layer VI (Gloveli et al. 2001). The collaterals of these cells span in multiple directions, including the superficial parts of EC. Also layer V horizontal cells have dendritic processes that

reach layer I and axons that span through EC layers V and VI (Hamam et al. 2000). Finally, layer VI interneurons possess dendritic processes that reach layer III (Lingenhohl and Finch 1991) and axons that extend to more superficial parts of EC (Canto et al. 2008). As for the extrinsic connectivity, also the intrinsic connections differ between MEC and LEC. For example, the axons of L II MEC SC extend their collaterals to layers III-VI (Tamamaki and Nojyo 1993) and LEC fan cells to L II-III (Tahvildari and Alonso 2005).

The complexity of the EC also extends to intra-laminar connectivity. For example, pyramidal neurons within layer III have recurrent collateral innervation between them (Dhillon and Jones 2000). Some studies previously suggested that there are L II intralaminar excitatory and inhibitory connectivity within the EC (Kumar and Buckmaster 2006). Multiple studies attempted to identify the excitatory connections between the principal neurons found in this layer. These include an *in vitro* experiments, where none of 135 paired recordings revealed excitatory connections (Dhillon and Jones 2000), as well as an *in vivo* study where only 12 principal neurons showed some degree of paired connectivity (Quilichini et al. 2010). Noteworthy, studies using caged glutamate photostimulation suggesting the existence of excitatory connectivity within L II (Kumar et al. 2007; Beed et al. 2010), were criticised for their non-specificity due the extrinsic inputs potentially affecting the data (Couey et al. 2013). These findings forced researchers to investigate the possibility that MEC L II SC are interconnected through inhibitory, rather than excitatory, neural networks. Indeed, a study in which recordings from over 600 pairs of SC were performed, and confirmed that fast-spiking interneuron networks are a major way of connecting SC (Couey et al. 2013). The detailed intra-entorhinal connections remain to be fully established at present.

1.2 MEC L II

Due to the presence of so-called grid cells, L II of the MEC has drawn particular attention over the past decades. Neurons found within MEC L II are present in densely packed groups. This layer is composed of two types of excitatory neurons: stellate and pyramidal (Table 1.1), with the former ones being the most abundant (Klink and Alonso 1997). Pyramidal cells of the MEC L II are present mainly in deep parts of L II. These types of neurons can be distinguished from other cells by the presence of a single, thick, apical dendrite running all the way up to the most superficial regions of MEC layer I. They also have a distinctive triangular cell body (Figure 1.4 A). The shape of the soma of SC is diverse, but they can be clearly distinguished from other cell types by their spiny dendritic tree projecting in all directions away from the cell body. The widely branched (497±154 µm) dendritic tree of L II SC is composed of multiple dendrites of approximately equal size, which after reaching the pial surface align parallel to it. The basal dendritic tree, in contrast, is only 231±69 µm wide. The axon of SC runs from the base of the soma towards the angular bundle, where it branches into multiple thin collaterals that run through the subiculum into the CA3 region of the hippocampus and the DG (Klink and Alonso 1997a). Additionally, the collaterals of L II SC axons sometimes reach layers III-VI (Tamamaki and Nojyo 1993). Whereas the majority of the L II SC are reelin-positive (Varga et al. 2010), some are also positive for calbindin (Wouterlood 2002). The majority of the L II SC synapses are glutamatergic (Yoshida et al. 1987).

Figure 1.4. The morphology of the L II MEC excitatory neurons. A) An example of a typical pyramidal neuron B) The reconstruction of a typical SC found within MEC L II. Scale bars represent the distance of 40 μm. The picture was adapted from Klink and Alonso (1997a).

1.2.1 Properties of SC at RMP

In addition to the morphological characteristics, the electrophysiological properties of the SC can be used to distinguish them from other cell types in the MEC L II. The typical RMP of a SC during *in vitro* recordings varies from -60 mV to -70 mV. The input resistance is usually in the range of 20 to 80 MΩ with a membrane time constant value of around 5 -15 ms (Alonso and Klink 1993).

1.2.2 Membrane sag potential

A typical feature of electrophysiological recordings obtained from SC is the presence of a so-called membrane potential sag (Figure 1.5). This is due to the hyperpolarisation-activated cyclic nucleotide-gated (I_h) current, which is activated during a hyperpolarizing potential, resulting in a depolarizing current. The antagonistic effect of I_h arises after a brief delay, giving rise to a characteristic "sag" response (Alonso and Llinás 1989)

Figure 1.5. An example of a patch clamp recording obtained from a L II SC. The recordings were made from $HCN^{+/+}$ and $HCN1^{-/-}$ neurons at the membrane potential of approximately – 70 mV. The $HCN^{+/+}$ trace displays a clear membrane potential sag. The figure was adapted from Nolan et al. (2007).

1.2.3 The action potential properties

When the membrane potential of the SC depolarizes to -50 mV, it can generate an action potential. The spike threshold for this type of neuron is -50.9±2.4 mV (Alonso and Klink 1993). Typically, SC are characterised by relatively short first spike generation latency (from 23.85±0.7 ms (Fuchs et al. 2016) to 42±17 ms (Alonso and Klink 1993)). After the initiation of the action potential there is a brief fast afterhyperpolarisation (fAHP), followed by a short after-depolarisation (ADP) (Figure 1.6 A). A medium afterhyperpolarisation (mAHP) then takes place. The slow mAHP sustains the membrane potential at the levels below the action potential threshold (Alonso and Klink 1993). It was shown that mAHP in SC is likely to be mediated by a mixture of Ca^{2+}-dependent potassium (Khawaja et al. 2007) and HCN channels (Nolan et al.2007). However, further experiments are needed to establish which particular potassium channels are responsible for it since the small conductance (such as the ampimin-sensitive) Ca^{2+}-dependent potassium channels, which usually mediate this type of AHP in neurons, were shown to not be responsible for mAHP in L II SC (Khawaja et al. 2007).

The membrane potential recovery from the AHP is tightly regulated by I_h currents (Nolan et al. 2007). The action potential of the SC is dependent upon the transient sodium current (Na_T) but not the persistent sodium current (Na_P) (Alonso and Llinas 1989; Dorval and White 2005). When firing, the action potentials of SC form a clustered

pattern (Figure 1.6 B) which appears to be most apparent at a spiking frequency less than 5 Hz (Nolan et al. 2007). Although the details of the cluster pattern generation remain unclear, the basic mechanisms responsible for it seem to be different from those underlying sub-threshold theta-frequency resonance (described below in the section 1.2.4 (Dudman and Nolan 2009)). This idea was supported by the experiment where the potassium leak currents (K_{leak}) were introduced into a computational model. This affected the clustering by changing the spike frequency, however both the resonance and the membrane oscillations remained unchanged (Fernandez and White 2008). One conductance proposed to regulate spike clustering is I_h. Alterations in I_h leads to the changes in AHP amplitude and duration which in turn has a diminishing effect on spike clustering pattern (Nolan et al. 2007). This, however, has to be investigated further.

Figure 1.6. L II SC action potential properties. A) Representative current-clamp traces of five subsequent L II SC action potentials. Typical components are indicated by arrows: fAHP, mAHP, ADP. B) A trace showing the typical clustering pattern of the action potentials of L II SC. Both traces show features typical of the dorsal cells of the MEC. These figures were adapted from Pastol, Ramsden, et al. (2012).

1.2.4 Resonant properties of SC

When the sinusoidal inputs at theta frequency (4-12 Hz) are applied, SC resonate making them very distinctive amongst other neighbouring neurons (Haas and White

2002). The frequency of the resonance peak is usually between 4 to 6 Hz and its amplitude varies between 1.6 to 2 mV (Pastoll, Ramsden, et al. 2012). Interestingly both values differ depending on the membrane potential at which they are measured. This could suggest that different mechanisms are involved in the resonance modulation depending on the membrane voltages (Pastoll, Ramsden, et al. 2012). The resonance probably arises from the slow changes in membrane potentials being opposed by the I_h current (Nolan et al. 2007). Other ion channels, such as Na_p and potassium M-current can affect resonance in different cells (Hu et al. 2007). Furthermore, blocking of M-current in SC reduces both the amplitude and the frequency of the resonance. Additionally, the resonance of the membrane potential is also susceptible to cholinergic modulation (Heys et al. 2010). The role of different ionic currents affecting the SC membrane potential resonance has to be investigated in the future.

Furthermore, the importance of the link between SC resonance and physiological synaptic inputs is yet to be fully determined (Pastoll, Ramsden, et al. 2012). It is thought that the intrinsic theta resonance may play an important role in filtering of inputs and their transformation (Haas and White 2002).

1.2.5 Oscillatory activity of SC

In contrast to theta frequency resonance, which arises in response to sinusoidal current inputs at a particular frequency, MEC L II SC also show intrinsic membrane potential oscillations. They were first described by Alonso and Llinas (1989). Using rat brain slices, they observed membrane fluctuations between 5.1 and 11.7 Hz (theta range). Interestingly, the amplitude of oscillations was shown to be dependent on the membrane voltage, with the maximal amplitude occurring between -59 and -54 mV. Furthermore, Alonso and Llinas showed that the oscillations were highly dependent on the activity of Na_p channels. These findings were later confirmed by multiple groups (Alonso and Klink 1993; Erchova et al. 2004; Nolan et al. 2007; Dodson et al. 2011; Yoshida et al. 2011).

The mechanisms explaining the existence of the peri-threshold membrane potential oscillations were proposed to be different to the ones underlying resonant properties described above (paragraph 1.2.4). To date, two different theories describing the generation of peri-threshold membrane oscillations were proposed. The first one suggests that the ion channels found in L II SC tune their activity to control subthreshold oscillations period, i.e. allow them to repeat at a regular cycle (Fransen et al. 2004; Hutcheon and Yarom 2000). This model was supported by biophysical stimulations, where different ion channels (primarly I_h and Na_p) were modelled in a way that indeed allowed SC to show the peri-threshold oscillations (Fransen et al. 2004) The problem with this model is that it requires theta-activity in SC to be periodic. This was shown not to be the case (Nolan et al. 2007; Dodson et al. 2011) and thus, an alternative model was proposed. In this model, it was suggested that the ion channels involved in the generation of membrane potential oscillations, e.g. Na_p, open and close in a stochastic (random) manner. It was indeed possible to reproduce the peri-threshold membrane potential oscillations using this model (Dorval and White 2005; Dodson et al. 2011). Nevertheless, the more specific mechanisms of the oscillations occurring in the L II SC remain unclear and has to be further investigated. The physiological importance of the MEC L II SC membrane oscillations is also not yet fully understood. However, it was suggested that they may be a cellular counterpart of the theta rhythms observed during MEC (and hippocampus) *in vivo* recordings (Stewart et al. 1992; Mizuseki et al. 2009). As observed in other cell types, such as hippocampal neurons, the rhythmic oscillatory activity can potentially promote synchronic activity of different brain structures, e.g. when the animal explores the environment. More importantly, the oscillations can contribute towards synaptic input filtering or modulate temporal information (Haas and White 2002).

1.3 Ion channels of the L II SC

1.3.1 Sodium channels

To improve our understanding of the properties of the L II SC, the cellular and molecular details of these neurons have to be thoroughly explained. SC have a very rich and diversified repertoire of ion channels that regulate the intrinsic excitability of these neurons. Although my project does not directly focus on all of them, it is important to explain the basic properties of the SC channels as this is essential for a proper assessment of the field and thus the interpretation of the results. Two sodium conductances are present in the L II SC. The first kind of conductance is mediated by Na_T channels, which activate at membrane potentials around – 50 mV (White et al. 1993). Na_T–mediated current has two components: larger TTX-sensitive and smaller TTX-insensitive (White et al. 1993). The second component can be blocked by Cd^{2+}, La^{3+} and Zn^{2+} ions (White et al. 1993). The second kind of sodium conductance found in L II SC is mediated by the voltage gated Na_p channels that open at around – 60 mV and can be blocked by 1 µM TTX (Magistretti and Alonso 1999; Alonso and Llinas 1989). Na_p channels were shown to have complex kinetic properties. For example, it has been suggested that Na_p can be found in six sub-states between open and closed modes (Magistretti and Alonso 2006). Additionally, two different gating models (called intraburst mode 1 and 2, differing in their opening and closing time) have been proposed for Na_p. Furthermore, individual channels can alternate between these gating modalities (Magistretti et al. 2003). The complex kinetics of Na_p channel can play an important role in the L II SC computation mechanisms as its different gating mechanisms can tightly regulate the amount of intracellular Na^+. This can in turn influence all the processes taking place in the cell, for example membrane potential oscillations of L II SC (Dorval and White 2005).

1.3.2 Potassium channels

Several types of potassium channels are present in the L II SC. One of the most common currents is the K_{leak}. This current is membrane potential independent and mediated by the two pore domain potassium channels (Deng et al. 2009). The delayed rectifier potassium (K_{DR}) and the A-type (K_A) currents, which activate at - 45 mV and - 50 mV respectively, are also present (Eder et al. 1991). Calcium-activated potassium channels (K_{Ca}), which are activated by the depolarisation induced calcium influx through the voltage-gated calcium channels, are also expressed in the L II SC (Khawaja et al. 2007). Also the K_v7 channel-mediated M-currents can be found in the SC of the MEC L II where they were shown to reduce the SC excitability, particularly at the membrane potentials near and higher than spike threshold (Nigro et al. 2014). Recently, the presence of K_v2 channels in the MEC L II SC was also confirmed experimentally. The application of Guangxitoxin-1E, a K_v2 antagonist, resulted in excitability increase, enhanced ADP, decreased fAHP and mAHP as well as action potential broadening and decreased spike clustering (Honigsperger et al. 2017). Together, the data show the importance of K_v2 channels in influencing the physiology of L II SC.

1.3.3 HCN channels

The hyperpolarisation-activated cyclic nucleotide-gated channels (HCN), conducting I_h current, do not have typical voltage-gated properties. They become active when the membrane is hyperpolarised below -50 mV and de-activate during depolarisation (Nolan et al. 2007). I_h has half-maximal activation at around – 80 mV (Dickson et al. 2000; Nolan et al. 2007; Figure 1.7). This HCN mediated current is carried by a mixture of sodium and potassium ions (with 1:3-1:5 $P_{Na}:P_K$ permeability ratio) and is inwardly directed at rest. I_h therefore contributes to the RMP by depolarising it (Biel et al. 2009). I_h has slow kinetics, in comparison to sodium and potassium currents (Day et al. 2005). Furthermore, I_h has a fast and slow component, with a time constant of approximately

80 ms and 400 ms, respectively (Dickson et al. 2000; Nolan et al. 2007; Figure 1.7). I_h is encoded by four genes HCN1-4 (Robinson and Siegelbaum 2003). Deletion of the HCN1 causes a prominent I_h amplitude reduction in L II SC and removes fast I_h current activation (Nolan et al. 2007). In agreement with electrophysiological experiments, there is a high mRNA expression level of HCN1 and HCN2 in L II of the MEC (Lein et al. 2007).

Figure 1.7. An example of I_h half-activation curve determined using tail currents obtained from L II SC (middle). The left panel shows an example trace of SC responses to hyperpolarizing voltage steps (starting from -50 mV). Additionally, the right panel shows an average I_h activation curve obtained from tail currents recorded in $HCN^{+/+}$ and $HCN^{-/-}$ L II SC (closed and open circles, respectively). The maximal average amplitude was shown to be 410 pA and an average half-maximal activation was achieved at -83.1 mV. The figures were adapted from Nolan et al. (2007).

1.3.4. Voltage gated calcium channels

L II SC of the MEC possess two types of calcium currents mediated by high voltage activated (Ca_{HVA}) and low-voltage activated (Ca_{LVA}) channels. The first type is activated at potentials more positive than -50 mV. In contrast, Ca_{LVA} open at –60 mV (from studies on acutely isolated neurons (Bruehl and Wadman 1999)). Ca_{HVA}–mediated currents come from L-type, N-type and P/Q-type Ca^{2+} channels which contribute to approximately 50 %, 23-30 % and 22-24 % of the Ca_{HVA}–mediated current, respectively. The remaining current is yet to be identified (Castelli and Magistretti 2006). In contrast, Ca_{LVA} have properties corresponding to the T-type Ca^{2+} channels, which are the focus of my research and I will, therefore, discuss the properties and function of these in detail below.

1.3.5. T-type Ca^{2+} channels

1.3.5.1 Molecular structure of T-type Ca^{2+} channels

T-type Ca^{2+} channels are formed by a Ca$_v$α1 subunit monomer (Figure 1.8 A) This is composed of four transmembrane domains (I-IV), each comprised of six helices that span the membrane (S1-S6) and a re-entrant poor loop used as a permeation pathway (Figure 1.8 B). The loop contains key negatively charged amino acid residues which make it selective for particular ions, in this case Ca^{2+} (Ellinor et al. 1995). Cytoplasmic linkers hold the domains together, regulate the channel modulation coming from second messengers and are also crucial for protein-protein interactions, including G proteins (Zamponi et al. 1997). One of the most important parts of the structure is the transmembrane segment IV that can be found in each domain, which acts as a voltage sensor using positively charged amino acids (for review see Simms and Zamponi 2014).

Figure 1.8. Diagram of a T-type Ca^{2+} channel. A) A drawing representing the Ca$_v$α1 subunit spanning through the cell membrane. The picture was adapted from Simms and Zamponi (2014). B) A schematic drawing showing the four domains of Ca$_v$α1 subunit, each composed of six helices and cytoplasmic linkers.

1.3.5.2 Biophysical properties of T-type Ca^{2+} channels

Multiple studies on primary sensory neurons made it possible to establish the biophysical properties of T-type Ca^{2+}channels (Bossu and Feltz 1986; Carbone and Lux 1984). At physiological Ca^{2+} concentrations, they are activated from approximately – 60 mV and have reversal potentials of +40 mV. T-type Ca^{2+}channels, like any other

voltage-gated channels, can be found in three main states: open (activated), closed (resting) and inactivated (refractory), due to the activity of voltage-sensitive gates. T-type Ca^{2+} channels are unique because their activation occurs at much lower voltages than HVA channels. At hyperpolarised membrane potentials, usually 10-15 mV less than a standard RMP of neurons (-60 mV), they start to shift from a closed state to an active state (for review see Senatore et al. 2014). The gating of the channels as this stage is controlled by the S4 voltage sensor movements induced by the membrane potential alterations. The movements of voltage sensor causes rearrangements in the structure of the channels, which subsequently shifts it from a closed to an active state (Frazier et al. 2001). T-type Ca^{2+} channels generate transient inward currents which reach peak in few milliseconds. This is followed by a rapid decay (time constant of approximately 10 milliseconds) due to open-state inactivation. Detailed kinetic activation and inactivation time constants of these processes are highly variable and depend on the Ca_v3 subtype and will be described below. During membrane repolarization, a unique slow deactivation of the channels occurs, resulting in a tail current, due to increased driving force for the current after repolarization, which ensures prolonged current flow (for review see Senatore et al. 2014).

T-type Ca^{2+} channels are well known to be responsible for production of the so-called window current ($I_{Twindow}$). This can be visualised as the overlap between activation and steady-state inactivation curves. $I_{Twindow}$ can be recorded at membrane potentials when a fraction of T-type Ca^{2+} channels have not reached full inactivation and are available to open at the membrane potentials close to rest (Figure 1.9; Crunelli et al. 2005).

Figure 1.9. T-type window current. Window current arises as a result of fraction of the channels remaining open at the RMP. The figure shows current mediated by $Ca_v3.1$, $Ca_v3.2$ and $Ca_v3.3$ channels recorded from HEK293 cells. The figure was copied from Chemin et al. (2002).

Although window currents are relatively small in comparison to the peak amplitude of T-type Ca^{2+} current, they produce a continuous, slow influx of calcium ions (Cain and Snutch 2010) which can have important physiological consequences. For example, the window current participates in the process of slowing sleep oscillations in thalamic neurons (Blethyn et al. 2006).

1.3.5.3 T-type channel subtypes and their kinetic properties

T-type Ca^{2+} channel $Ca_v\alpha1$ subunit can be further subdivided into three types: $Ca_v3.1$, $Ca_v3.2$ and $Ca_v3.3$. All three subtypes can be found not only in neurons within the brain, but also across the entire human body where they play multiple important functions. They share low-threshold and transient activation but can be easily distinguished by other kinetic properties (Table 1.2; Figure 1.9; Chemin et al. 2007). In brief, $Ca_v3.1$ and $Ca_v3.2$, when expressed in heterologous cells, both open and inactivate at membrane potentials of -48 mV to -49 mV and -74 mV to -75 mV, respectively. In contrast, $Ca_v3.3$ open and inactivate at potentials approximately 10 mV and 5 mV more depolarised, respectively to those of $Ca_v3.1$ and $Ca_v3.2$ (Chemin,

Monteil, et al. 2002). Additionally, both $Ca_v3.1$ and $Ca_v3.2$ have similar activation and inactivation kinetics (with the first one being slightly faster). This is again in contrast to $Ca_v3.3$, which is the slowest of the three subtypes (see Table 1.2 for detailed values). The deactivation time constants of $Ca_v3.1$ and $Ca_v3.2$ also have similar values (2.6 ms and 3.6 ms, respectively), whereas $Ca_v3.3$ displays significantly faster deactivation time constant of 1.12 ms. The variety of the biophysical properties of the three subtypes can have striking consequences. It is best illustrated with the differences in burst firing between thalamic reticular (NRT) and thalamocortical (TC) relay neurons. In brief, burst firing occurs when membrane potential depolarisation activates T-type Ca^{2+} channels to the point of sodium channels activation. This in turn leads to high frequency of action potentials to be generated. The process ends when potassium channels are activated and neuron repolarization occurs (for review see Cain and Snutch 2010). The part of the process with no action potentials is called low-threshold spike (LTS, described in more details in the paragraph 1.3.5.4). Experiments using $Ca_v3.3$ $^{-/-}$ mice showed that this isoform is the one responsible for the generation of LTS in NRT neurons (Astori et al. 2011). In contrast to NRT, TC neurons were not shown to be immunopositive to $Ca_v3.3$ (Talley et al. 1999). Instead, their activity have been shown to be mainly controlled by the $Ca_v3.1$ isoform (Kim et al. 2011). These discoveries contributed towards the better understanding of how different LVA subtypes can control firing patterns of neurons. In contrast to TC neurons, NRT cells show slower activation and inactivation kinetics (Huguenard and Prince 1992) which results in broader and slowly developing bursts (Mulle et al. 1986; Steriade et al. 1986; Llinas and Geijo-Barrientons 1988). Furthermore, studies on NRT neurons of cats (Domich et al. 1986) and rats (Avanzini et al. 1989) showed that these neurons display a characteristic pattern of sodium spikes within bursts, i.e. the initial increase in frequency is always followed by a decrease (so called 'accelerando-decelerando' pattern; Figure 1.10). This is in contrast to TC neurons which show decelerating burst firing pattern resulting from fast transient $Ca_v3.1$ current (Figure 1.10; Tscherter et al. 2011).

Figure 1.10. The figure showing characteristic burst firing pattern of TC and NRT neurons. The first one display typical decelerating set of action potentials (due to $Ca_v3.1$ activity), whereas the later one is characterized by accelerating-decelerating burst firing (mainly due to the presence of $Ca_v3.3$ isoform). The figure was adapted from Tscherter et al. (2011).

Although all three subunits are widely expressed in numerous brain regions (see Table 1.3), it is important to state that no $Ca_v3.1$ was reported to be present in the EC (Huang et al. 2011). Therefore, the present study focuses on the $Ca_v3.2$ Ca^{2+} channels. I will also aim to eliminate the potential effect of $Ca_v3.3$ subtype on the results using pharmacological tools described in Chapter 4.

Table 1.2. The kinetics of different T-type Ca^{2+} channel subunits. (α1G – $Ca_v3.1$, α1H – $Ca_v3.2$, α1I – $Ca_v3.3$). Table was adapted from Chemin et al. (2007).

Table 1.3. The spread of different Ca$_v$3 isoforms across human body. The table was adapted from Iftinca (2011).

1.3.5.4 T-type Ca^{2+} channels produce LTS

Since T-type Ca^{2+} channels are active at membrane potentials close to rest and have slow recovery from inactivation, they are able to produce LTS (Perez-Reyes 2003), i.e. transient slow depolarisation of the membrane caused by the subthreshold calcium currents present at hyperpolarised membrane potentials (Llinas and Jahnsen 1982). In general, LTS can only be generated after hyperpolarisation of membrane potential and resulting recovery of T-type Ca^{2+} channels from inactivation (Perez-Reyes 2003).

The LTS have important physiological consequences in numerous neuronal types. However, the most striking example was showed in thalamic neurons. The LVA Ca^{2+} channels were shown to be sufficient to generate LTS in thalamic neurons from *in vivo* (Deschenes et al. 1984), and *in vitro* experiments (Jahnsen and Llinas 1984) as well as through computational modelling (Destexhe et al. 1998). In these neurons, LTS results in generation of characteristic burst firing (Llinas and Jahnsen 1982), which in turn was

discovered to be important in numerous physiological processes, for example rhythmic activities of thalamocortical neurons (Domich et al. 1986).

1.3.5.5 Location of T-type Ca^{2+} channels in the brain

In addition to being widely distributed across the entire human body, the Ca_v3 channels are also spread in the brain. *In situ* hybridisation experiments on rats showed that all three isoforms are distributed across the olfactory system, basal forebrain, amygdala, cerebral cortex, hippocampus, thalamus, hypothalamus, midbrain and pons as well as the cerebellum and the inferior olive (Talley et al. 1999).

Furthermore, the location of Ca_v3 channels in neurons is not limited to the cell soma. In neocortical pyramidal neurons, $Ca_v3.3$ can be found both in the soma and distal and proximal dendrites, whereas $Ca_v3.1$ channels are limited to the cell body (Molineux et al. 2006). Using a variety of techniques, including computational modelling coupled with in vitro recordings (Destexhe et al. 1998), two-photon calcium imaging with electrophysiology (Hildebrand et al. 2009; Diana et al. 2017; Egger et al. 2003) or 2-photon glutamate uncaging (Carter and Sabatini 2004), T-type Ca^{2+} channels were found to be present in dendritic spines and shafts in multiple different neurons including thalamocortical (Destexhe et al. 1998), Purkinje (Hildebrand et al. 2009), cerebellum (Diana et al. 2007), striatum cells (Carter and Sabatini 2004) and olfactory bulb granule cells (Egger et al. 2003). Properties of these channels, in particular the low-threshold activation, make the T-type Ca^{2+} channels extremely suitable for excitatory post synaptic potential (EPSP) propagation in dendrites. Indeed, studies in nucleus reticularis thalami show that T-type Ca^{2+} channels boost somatic inputs and contribute towards somatic EPSP generation (Crandall et al. 2010). Recent studies using two-photon targeted patch-clamp technique also showed that in thalamocortical and thalamic reticular nucleus neurons of rat, T-type Ca^{2+} channels are present in dendritic trees where they contribute towards an action potential backpropagation (Connelly et al. 2017). Another study using whole-cell patch clamp showed that T-type Ca^{2+}

channels are also present in dendritic spines of hippocampal Schaffer collateral synapses, where in combination with L- and R-type channels together contribute towards excitatory post synaptic current (EPSC) generation and synaptic plasticity (Tigaret et al. 2016). Additionally, T-type Ca^{2+} channels found in dendro-dendritic synapses of granule cells in the olfactory bulb were shown to participate in neurotransmitter release (Egger et al. 2003). Overall, the studies show that T-type Ca^{2+} channels are important for synaptic input amplification and somatic EPSP generation.

Using a combination of patch-clamp recordings and electron microscopy, it was shown that T-type $Ca_v3.2$ Ca^{2+} channels are also present in the axons of EC layer III cells where, by interacting with HCN channels, they regulate synaptic release (Huang et al. 2011). Additionally, experiments using whole-cell voltage clamp, supported by fluorescent confocal microscopy and optogenetics, showed that $Ca_v3.1$ channels can be found close to the presynaptic active zones in paravalbumin-positive interneurons of the CA1 region, where they modulate the activity of pyramidal cells (Tang et al. 2011). Furthermore, two-photon imaging showed that T-type Ca^{2+} channels are also found in the axon initial segment of dorsal cochlear nucleus interneurons, where they regulate action potential threshold (Bender and Trussell 2009), and mossy fibres, where they control K_v7 channel activity by regulating Ca^{2+} influx into axons (Martinello et al. 2015). Moreover, whole cell patch-clamp recordings showed that axonal T-type Ca^{2+} channels also affect the action potential threshold of olfactory receptor cells (Ohkuma et al. 2013). Finally, combination of electrophysiological recordings with optogenetics revealed that T-type Ca^{2+} channels are also found in the axon initial segment of dissociated hippocampal cultured neurons. Here, they were shown to influence axon initial segment structural plasticity and, thereby, cell excitability (Grubb and Burrone 2010).

Despite the ubiquity and the importance of different subcellular locations of T-type Ca_v3 channels in neurons across all brain structures, the processes that control the channel

distribution and membrane trafficking remain a mystery. One possibility is that $Ca_v3.1$, $Ca_v3.2$ and $Ca_v3.3$ all interact with different proteins, which could potentially result in differences of their subcellular targeting mechanisms. This however has to be investigated in the future (Zhang, Jiang, et al. 2013).

1.3.5.6 The role of T-type Ca^{2+} channels in development

T-type Ca^{2+} $Ca_v3.2$ channels were characterised to appear during development as early as E9.5 in dorsal root ganglion cells (Bernal Sierra et al. 2017) which can suggest that they significantly contribute to development processes occurring in the brain. Indeed, LVA channels were observed to be present in developing neural tissues. For example, studies from E19 rat hippocampal cultured neurons showed that LVA currents are the ones to be recorded first and that they are gradually overtaken by the presence of HVA channels (Yaari et al. 1987). Experiments on developing spinal neurons of *Xenopus* showed that T-type Ca^{2+} channels are necessary for GABAergic phenotype development of these neurons (Spitzer 1994). Furthermore, studies using NG108-15 cell line showed, that inhibition of T-type Ca^{2+} channels activity prevents neuritogenesis and additionally impairs expression of the HVA Ca^{2+} channels. The authors of the study suggested that T-type calcium channels are necessary for neuronal differentiation as they influence both morphological and electrical changes taking place during that process (Chemin et al. 2002). Recent studies on embryonic neural progenitor cells showed that T-type Ca^{2+} channels are present and play an important role at early stages of neuronal differentiation (Louhivuori et al. 2013). In this study, inhibition of these channels negatively affected the number of active migrating neuron-like cells. Another study on neuroblastoma cells showed that T-type Ca^{2+} channels may be necessary for morphological differentiation of neurons as the presence of these channels always precedes the occurrence of neurite extensions (Silver and Bolsover 1991). Furthermore, studies on rats, during the ocular dominance plasticity period, have shown that T-type Ca^{2+} currents are also necessary for synaptic

plasticity. In this experiment, it was discovered that the LTP generation in the layer II/III pyramidal cells of rat visual cortex is highly dependent on the activation of T-type Ca^{2+} channels (Yoshimura et al. 2008). Furthermore, T-type Ca^{2+} current dependent-LTP was shown to regulate the visual responses of rats (Horibe et al. 2014) and kittens (Komatsu and Iwakiri 1992) during development. Additionally, another study demonstrating *in vivo* experiments on cats, have shown that T-type Ca^{2+} channels are also critical for cortical plasticity. The results of the study have shown that infusion of a T-type Ca^{2+} channel blocker (N-(4-fluorobenzyl)-1-{3-[5-(1H-1,2,4-triazol-1-ylmethyl)-1H-indol-3-yl]propyl}-N-(2,2,2-trifluoroethyl)piperidin-4-amine) significantly decreased the cortical plasticity induced by monocular deprivation (Uebele et al. 2009). Altogether, these show that the activity of T-type Ca^{2+} channels is essential during brain development.

However, due to the ubiquitous presence of T-type Ca^{2+} channels across an entire organism, it is not surprising that they also play numerous important role in the development of tissues outside the brain structures. One example could be adrenal glands. T-type Ca^{2+} channels were shown to play an important role in the neonatal chromaffin cells of rat adrenal medulla where they participate in catecholamine release during hypoxia (Levitsky and López-Barneo 2009).

Another structure other than the brain, where T-type Ca^{2+} channels play an important role during development, is the heart. Indeed, T-type Ca^{2+} currents were found to be present in the ventricular myocytes of the rat heart in newborns and were absent in the mature cells (Leuranguer et al. 2000). Later studies showed that T-type Ca^{2+} channels are also present in the rat foetal ventricular myocytes. It was therefore suggested that T-type Ca^{2+} channels contribute towards heart development by participating in a pacemaker activity or maintaining cell division (Ferron et al. 2002; Guo et al. 1998). Altogether, these and multiple other studies show that T-type Ca^{2+} channels are

46

necessary for different developmental processess happening both within and outside the nervous system.

1.3.5.7 T-type Ca^{2+} channel associated pathologies

In order to fully appreciate the importance of T-type Ca^{2+} channels, their role in multiple pathologies should be examined. Due to a wide-spread distribution of these channels across different organs, their activity has been linked with variety of diseases. This includes cardiovascular issues such as hypertension, atrial fibrillation, or congenital heart failure (Cribbs 2010; Ono and Iijima 2010; Iftinca 2011; Belardetti and Zamponi 2008) as well as other pathologies such as cancer (Dziegielewska et al. 2014) or irritable bowel syndrome (Marger et al. 2011). However, due to the nature of my work, I will focus mainly on the role of T-type Ca^{2+} channels in neural-related diseases.

Firstly, due to their presence in thalamus and cortical structures as well as their role in neuronal excitability, T-type Ca^{2+} channels are important in the development of generalised seizures in both animals and humans (Khosravani and Zamponi 2006). A variety of point mutations in T-type Ca^{2+} channels associated with childhood absence epilepsy were discovered (Beauvais et al. 2004). This was followed by another study (Heron et al. 2004), where three missense and one nonsense mutation in T-type Ca^{2+} channels was shown to be associated with the idiopathic generalised epilepsy. Furthermore, a rat model for the generalised absence epilepsy showed 55% increase in T-type Ca^{2+} current than in control and 16 % larger Ca$_v$3.2 mRNA expression (Talley et al. 2000). Additionally, a selective T-type Ca^{2+} channel blocker (belonging to a class of 1,4-substituted piperidines) showed high efficacy absence seizure reduction in another rat model, WAG/Rij (Yang et al. 2008). Some studies also showed that knocking out Ca$_v$3.1 can have a protective effect against absence seizures (Kim et al. 2001). Overall, there is a lot of evidence linking alterations in T-type Ca^{2+} channels and seizure-related pathologies.

T-type Ca^{2+} channel mutations are also linked with inflammatory and neuropathic pain (Todorovic and Jevtovic-Todorovic 2007). For example, some *in vivo* studies using antisense targeting of $Ca_v3.2$ channel, showed that silencing of these genes reduced inflammatory and neuropathic pain (Choi et al. 2007; Bourinet et al. 2005). Most recent studies using $Ca_v3.2$ knockin/flox mice showed that these Ca^{2+} channels are also essential for the development of allodynic symptoms of neuropathic pain (Francois et al. 2015). Furthermore, missense mutations of $Ca_v3.2$ were shown to be associated with autism spectrum disorder (Splawski et al. 2006). In this study, using HEK-293T cells, specific mutations of T-type Ca^{2+} channels shifted the activation curve of $Ca_v3.2$ currents to a more depolarised potential and decreased calcium conductance. This in turn could potentially affect neuronal function and result in developmental disorders, including autism (Splawski et al. 2006). This study, together with multiple other experiments that showed the role of T-type Ca^{2+} channels in neurogenesis (Chemin, Nargeot, et al. 2002), indicate that these channels are strong candidates for further exploration of autism-associated disorders (Iftinca 2011).

Additionally, some studies suggest that 3,5-dichloro-N-[1-(2,2-dimethyl-tetrahydro-pyran-4-ylmethyl)-4-fluoro-piperidin-4-ylmethyl]-benzamide (TTA-P2), a T-type Ca^{2+} channel inhibitor, shows antipsychotic effects. Behavioural experiments on rats showed that TTA-P2 can reverse the activity of psychostimulants such as amphetamine (Uslaner et al. 2012). This in turn suggested that the blockers of T-type Ca^{2+} channels can be potentially considered as a treatment for diseases such as schizophrenia. Lastly, the T-type Ca^{2+} channels are also believed to be a good therapeutic target for both essential (Handforth et al. 2010) and Parkinsonian tremor (Miwa et al. 2011). Altogether, the literature supports the notion that T-type Ca^{2+} channels are extremely important regulators of multiple processes in the brain (and other organs). Thorough understanding of their basic physiology and their role in various structures, such as

MEC, is therefore crucial, as it will potentially allow further advancements in the fields of both the neuroscience and medicine.

1.4 The dorsal-ventral gradient in the MEC

Better understanding of identity and properties of ion channels present within MEC L II SC, can help to explain a distinctive gradual change in various integrative properties along the dorsal-ventral axes that these cells express. To-date, a variety of explanations for the gradient were proposed in the literature. This includes different ion channel composition and activity in dorsal and ventral axes of the MEC. Additional factors, such as morphology, were also proposed to contribute towards it. This, together with a detailed description of dorsal-ventral gradient in a variety of L II SC properties, will be discussed below.

1.4.1 Morphology

A contributing factor for differences in excitability between dorsal and ventral MEC L II SC is their morphological diversity. In agreement with this assumption, quantification of various morphological L II SC properties, including total dendritic surface area, cell body area, and perimeter, showed significant differences between dorsal and ventral neurons (decrease in all parameters with the increased distance from the dorsal border; Figure 1.11). Nevertheless, computational models measuring whether the morphological differences were able to explain the intrinsic excitability variability of MEC L II SC showed that, by itself, this property is insufficient to set up such a large dorsal-ventral gradient (Garden et al. 2008). Further examination of this phenomenon is therefore required.

Figure 1.11. Morphology of L II SC. Examples of A) dorsal and B) ventral cells and their neurolucida reconstructions. C) The measurements of the soma reconstructions of SC plotted as a function of the location from the dorsal border. D) Total dendritic surface area of dorsal and ventral cells plotted as a function of the location of the cell body. Circles represent the neurons recorded with (open) and without (black) synaptic blockers. Figures adapted from Garden et al. (2008).

1.4.2 Properties and expression of ion channels along the dorsal-ventral axes of the MEC

Since the morphology itself was not sufficient to explain the dorsal-ventral gradient, there is a possibility that differences in ion channel expression and function in dorsal and ventral L II SC may contribute towards it. The density of the ion channels mediating K_{leak} and I_h currents followed the dorsal-ventral gradient in the MEC (Garden et al. 2008; Giocomo and Hasselmo 2008). Garden et al. (2008) showed that the amplitude of I_h was reduced across the dorsal-ventral MEC axes but its time constant did not change. In contrast, Giocomo and Hasselmo (2008) showed that amplitude of I_h current remained constant across the dorsal-ventral axes of the MEC, whereas the time constant varied and was faster in dorsal locations in comparison to ventral cells. *In situ* hybridisation showed increased HCN1 and HCN2 mRNA-protein expression in dorsal versus ventral cells, supporting the first scenario proposed by Garden et al. (2008). It is, though, unknown if the expression and function of other ion channels may also vary along the dorsal-ventral gradient. Further work in elucidating this is required.

1.4.3 Resting membrane properties

In addition to the differential expression of ion channels, the resting membrane properties also differed along the dorsal-ventral axes. Although the RMP was reported to be similar in dorsal and ventral L II SC (Garden et al. 2008), the input resistance was found to be lower in the dorsal neurons, which were also proven to have faster membrane time constants (Garden et al. 2008; Boehlen et al. 2010). The gradient in the membrane potential sag existed as well, with dorsal cells having a bigger sag than ventral neurons. This probably corresponds to the gradient in the I_h properties along the dorsal-ventral axes of the MEC (Figure 1.12).

Figure 1.12. The dorsal-ventral gradient of the MEC L II SC. Graphs representing the gradient in A) input resistance B) membrane time constant and C) membrane potential sag. The figure was adapted from Garden et al. (2008)

1.4.4 Gradient in the action potential clustering

The characteristic clustering pattern of L II SC action potentials also followed the dorsal-ventral gradient with the frequency of the spikes decreasing with the distance from the dorsal border. In contrast, the number of action potentials per cluster remains constant (Pastoll, Ramsden, et al. 2012). Furthermore, the threshold-current relationship (the current that has to be injected to evoke an action potential) also depends on the location within the MEC with the dorsal cells having significantly higher threshold than ventral neurons (Garden et al. 2008).

1.4.5 Gradient in resonance and oscillations frequency

One of the main characteristics of L II SC are their membrane potential oscillations described above (see 1.2.5). Interestingly, the oscillations of dorsal neurons have a mean frequency between 6.42-7.18 Hz whereas the ventral cells display a range of 4.23 to 4.88 Hz, depending on the membrane voltage at which they were measured. Additionally, L II SC show a resonant frequency gradient: ventral cells have a resting resonance peak at lower frequencies than dorsal neurons (Giocomo et al. 2007). These differences may point out to a possibility that dorsal and ventral L II SC have different scales used for coding time and space (Giocomo et al. 2007). However, the precise function of the dorsal-ventral gradient in membrane oscillations and resonance has to be further investigated.

1.4.6 Synaptic integration

Various properties of the EPSP waveforms of the L II SC also differ along the dorsal-ventral axes. Dorsal neurons have shorter spontaneous non-NMDA-glutamate-receptor-mediated EPSPs (AMPA/kainite mediated). This lead to a more efficient gamma frequency summation compared to ventral neurons (Garden et al. 2008). Furthermore, Garden et al. (2008) used evoked non-NMDA glutamatergic EPSPs to show that neurons located dorsally have narrower time windows for detection of coincident inputs compared to the ventral cells. This may result in an improved temporal discrimination (Garden et al. 2008) for dorsal neurons. Noteworthy, in the study from Garden and colleagues, the EPSPs resulted from stimulation of MEC layer I, which has axons of neurons from deeper layers of MEC as well as neocortical inputs. The axons that were stimulated depended on the spread of electrical pulse applied. Such spread, however, cannot be measured given the random properties of the electrical pulse. Therefore, the specific origin of EPSPs, in the work of Garden and colleagues, is unknown (Garden et al. 2008). Furthermore, since authors were unable to recruit dendritic AMPA receptor currents in their recordings, they were not able to

rule out dorsal-ventral gradient in dendritic AMPA receptors (Garden et al. 2008). However, they observed no gradient in the half-width of layer I stimulation-evoked EPSCs, and therefore concluded that it is unlikely for the AMPA receptors gradient to be present.

Additionally, the properties of the local inhibitory microcircuits of the L II SC were shown to follow the dorsal-ventral gradient in the MEC. More specifically, the inhibitory inputs (the number of synaptic contacts) from the paravalbumin positive interneurons were shown to decrease with distance from the dorsal border of the MEC (Beed et al. 2013). This can create differences in synaptic integration of inputs, and possibly to the computation of different outputs along the dorsal-ventral axes of the MEC. Based on these findings, the dorsal-ventral differences in GABA receptors cannot be ruled out. In summary, it cannot be excluded that, in addition to gradient in intrinsic conductances, there are also gradients both in excitatory (Garden et al. 2008) and inhibitory (Beed et al. 2013) synaptic inputs as well as neurotransmitter receptors.

1.4.7 Grid cells and the dorsal-ventral gradient

Due to its anatomical position, the EC is believed to be an important interface between neocortex and hippocampus during the process of memory consolidation (Squire and Alvarez 1995). However, how the sensory inputs are represented in the EC remains unclear. Interestingly, head direction cells (that become excitable when, as the name suggests, the head of an animal is directed in a particular direction) found in layer III of the MEC, are much more sharply tuned in dorsal than ventral neurons (Giocomo et al. 2014). Another cell group that has shown a dorsal-ventral gradient is the so-called grid cells, which are principally located in L II of the MEC. Fyhn et al. (2004) showed that EC neurons fire action potentials in precisely localised groups and form firing fields to allow an animal to encode its location in the environment with high precision. The key component of this neural map is the grid cell. When an animal explores its environment, these cells fire action potentials at particular positions in regards to an

animal's spatial location. Representation of these firing patterns forms a characteristic grid structure (Figure 1.13; Hafting et al. 2005). Interestingly, the spatial resolution of grid fields and the size of the fields increases proportionally with distance from the dorsal border of the MEC (Fyhn et al. 2004). This organisation mirrors the above mentioned gradients in L II SC: intrinsic theta-frequency, resonance and various other integrative properties. These observations suggest that L II SC of the MEC can indeed contribute to grid cell activity and SC can play an important role in the generation of the cellular computations crucial for grid fields formation (O'Donnell and Nolan 2011). Therefore, further and more detailed investigation of the L II SC properties is essential.

Figure 1.13. Graphical representations of grid cell firing fields. A) Trajectory map B) rate map and C) spatial autocorrelogram of the recorded cells (red spots) D) The spacing of the grid firing fields plotted as a function of the distance from the dorsal boarder of the MEC. Figures were adapted from Hafting et al. (2005)

1.5 Aims

The dorsal-ventral differences in K_{leak} and the I_h kinetics and density of the HCN channels along the MEC axes (Garden et al. 2008) can partially explain the gradient in L II SC intrinsic membrane excitability along the dorsal-ventral axes. It is, though, unknown if other channels may also contribute to this. Considering the ubiquity of T-type Ca^{2+} channels across different neuronal locations, including the MEC layer III pyramidal cells, and the important role they play in regulating cell excitability in other cell types, in my work I will aim to understand whether T-type Ca^{2+} channels and the currents they mediate also contribute towards the dorsal-ventral gradient in the MEC L II SC. I will investigate whether the $Ca_v3.2$ subtype in particular contributes towards the gradient in input resistance, RMP, excitability, single action potential properties as well as the EPSPs summation and intrinsic membrane oscillations. Using a combination of electrophysiology, pharmacology and genetic tools (global knock out), I will investigate whether the amount of $Ca_v3.2$ current differs when measured in dorsal and ventral ends of the MEC.

2. Materials and methods

2.1 Mouse Breeding

All work involving animal experimentation was performed in accordance to local UCL ethics and United Kingdom regulations (Animal Scientific Procedures Act 1986). The experimenter was a personal license holder and the work has been done under an approved Home Office project license.

The $Ca_v3.2$ global knock out mice were a gift from Professor H. Beck (University of Bonn Medical Centre) and were generated using homologous gene targeting (Chen, Lamping, et al. 2003). In brief, a construct designed to specifically target and globally delete $Ca_v3.2$ gene (*Cacna1h*) was transfected into embryonic stem cells via electroporation. It was followed by polymerase chain reaction (PCR) that allowed to select the cells with appropriate deletion. Next, chimeric mice were created by blastocyst injection. The male and female mice containing one mutant and one wild type allele of the $Ca_v3.2$ subunit, known as heterozygotes, were bred together to generate $Ca_v3.2$ wild type and null littermates. The colony was kept in individually ventilated cages. At P21, the tail tissue from mice were obtained by the experimenter and the genotyping procedure was performed by Mr Martin Stuart in Biosciences Huxley Building Molecular Biology Facilities, University College London. In brief, DNA was extracted from the tissue using a standard extraction protocol (Truett et al. 2000). The PCR was performed using the following primers: a1H FWD, 5'-ATTCAAGGGCTTCCACAGGGT-3'; a1H RVS, 5'-CATCTCAGGGCCTCTGGACCAC-3'; a1H(1277), 5'-GCTAAAGCGCATGCTCCAGACTG-3'. PCR reactions were resolved on a 1.5% TAE gel. The products of interest were expected to be following sizes: Wt allele 480 bp, mutant allele 330 bp. The PCR conditions varied, and were adjusted depending on the enzymes used. The results were reported back to the experimenter, the mice were weaned and $Ca_v3.2$ wild type and null animals were kept for the

experiments. All of the voltage-clamp and part of the current-clamp experiments were performed blindly. It was not possible to hide the mice genotype during some of the current-clamp recordings due to the ongoing training of the experimenter.

2.2 Slice Preparation

2.2.1 Equipment used for slicing procedures

All the slicing procedures were performed using the Leica VT1200S vibratome. The Feather 0.1 mm blades have been broken in half to fit the holder, wiped with acetone and water prior to slicing. The vibro-check was performed to minimise the vibrations in the z-direction using following settings: 0.14 mm/s blade feed rate, 0.40 mm amplitude vibrations and the 350-400 µm thickness.

2.2.2 Solutions and Materials used for Slicing

The modified artificial cerebral spinal fluid (ACSF) of the following composition was used during the slicing procedure (mM): 2.5 KCl, 1.25 NaH_2PO_4, 25 $NaHCO_3$, 0.5 $CaCl_2$, 7 $MgCl_2$, 7 dextrose and 110 choline chloride. All surgical tools, including silver scissors, forceps and spatulas, were cleaned prior to surgery with a detergent and distilled water.

2.2.3 Intra-cardiac perfusion

Intra-cardiac perfusion was carried out using ice-cold ACSF to rapidly cool the brain, thereby allowing optimal preservation of all cellular properties. P 35-56 adult mice were anaesthetised with ketamine/xylazine (1:2 ratio) solution. After 5-10 min, a toe reflex was tested to assess the depth of anaesthesia. When no reflex was observed, the lateral incision through the abdominal wall was made with small surgical scissors, followed by cutting through the diaphragm, the rib cage and sternum in order to expose the heart while holding the remaining skin with the surgical forceps. A sterile needle was then inserted into a left ventricle and cold (4-8°C) modified ACSF was perfused at a rate of approximately 10 ml per min. A small incision was also made in the right

chamber of the heart to facilitate the flow rate. After 2-3 min, when the colour of the liver changed from red to grey, indicating the successful perfusion, the animal was decapitated and the brain was rapidly (<60 s) removed.

2.2.4 Parasagittal slice preparation

Following decapitation, the brain was instantly submerged in a cold (4°C) ACSF solution. It was then placed onto a filter paper in an upright position, hemisected along the midline (sagittal axis) and orientated so that the MEC of the two hemispheres was facing upwards (Figure 2.1). The hemispheres were then mounted onto the vibratome cutting plate using 3M Vetbond tissue glue and submerged in the cold ACSF gassed with 95% oxygen/ 5% carbon dioxide mix to maintain the pH of 7.2. The glued hemispheres were then placed in the vibratome tray. The blade was horizontally angled at 20 degrees. The vibratome was programmed at exactly the same settings as for the vibro-check.

2.2.5 Identification of slices containing MEC

Slices containing the MEC were identified by the change in the shape of the rostral boundary of the hippocampus from round to linear (Pastoll, White, et al. (2012)). Therefore, the shape of the hippocampus changed from round to bean-like when moving from lateral to medial part of the entorhinal cortex (Figure 2.1).

Figure 2.1. The differences between MEC and LEC. **Ai)** and **ii**) show a typical appearance of the LEC. **Bi)** and **ii**) represents lateral part of the MEC. Blue and yellow arrows indicate dorsal and ventral borders, respectively. **Ci)** and **ii**) show a typical MEC appearance (with the change in the shape of the hippocampus). The schematics represent typical anatomical landmarks allowing the identification of MEC and LEC. C – Cerebellum, L-LEC, M-MEC, H-hippocampus. The orange colour indicates the external capsule of the hippocampus, blue is corpus callosum, CA3 and CA1 are marked with green whereas cyan colour represents DG. The picture was adapted from (Pastoll, White, et al. 2012).

Typically, 1 to 2 top slices from each hemisphere were classified as lateral and rejected, whereas 3 following slices containing MEC were collected and used for the experiments. The slices were then transferred into a chamber filled with the oxygenated ACSF and submerged in a 35°C water bath for 20 min incubation period. Lastly, slices were removed from the water bath and left in the oxygenated chamber at a room temperature for approximately 45 min prior to the patching procedures.

2.3 Data acquisition

2.3.1 Electrophysiology

2.3.1.1 Equipment used for electrophysiological recordings

The cells were visualised using Olympus BX51W1 microscope (Microscope Service and Sales, UK) situated on a Newport RG Breadboard vibration isolation table inside a

custom-made Faraday Cage at low and high magnification using x10 and x60 objective, respectively. The Faraday cage reduced electrical interference noise from the external environment. The microscope was attached to the Photonix VX55 Camera that was transmitting the image onto a monitor (Hitachi TV). A Luigs and Newmann SM7 manipulator was used to control the position and movement of the patch pipettes throughout the recording procedures.

The slices were placed in a recording chamber composed of a glass coverslip glued at the bottom of the plastic ring using silicon adhesive (Sylgard). The chamber was approximately 5 mm deep and had 1.5 cm in diameter. It was attached to a centre of a metal holder where two magnetic perfusion cannulae were placed. The solution was perfused through the recording chamber with a flow system installed inside the faraday cage. It was placed approximately 50 cm above the recording level and used gravity force enabling the solution to flow at a rate of approximately 2 ml per min. A surgical drip (Baxter) was installed along the tubing to allow more accurate control of the solution flow. Additionally, a thermometer, attached to the inflow canula tubing, was sending a feedback information to a Warner Instruments heater, allowing precise control of the temperature inside the recording chamber.

Current-clamp recordings were performed using an AxoClamp 2B amplifier (Molecular Devices Ltd). Voltage-clamp recordings were obtained using AxoClamp 200B amplifier. The head stage of both amplifiers was situated on the Luigs and Newmann manipulator. Both amplifiers were also connected to a Digitiser 1440A (Molecular Devices Ltd). Analog signals acquired using the Axoclamp 2B were additionally filtered with a Cyberamp 320 signal conditioner before converted to digital signals via the Digidata 1440B. The Digidata was connected to a computer and data were acquired using pClamp 10.4 acquisition software.

2.3.1.2 Patch Pipettes

Borosilicate glass capillaries (1.5 mm and 0.86 mm outer and inner diameters respectively; Harvard Apparatus) were fire polished and pulled using vertical Narishige puller (PC-10 model, Intra Cell). The patch pipettes (used for voltage and current clamp recordings), which were 5-7 MΩ resistance when filled with an appropriate intracellular solution, were used to form a gigaseal (resistance > 1 GΩ) on the cell membrane.

2.3.1.3 Identification of MEC and SC under microscope

Following 45 min room temperature incubation, slices were placed in a recording chamber and perfused with the extracellular solution maintained at a temperature of approximately 33°C. Using x10 microscope, the MEC, together with its dorsal and ventral borders, was identified. The parasubiculum allowed establishment of the dorsal border, whereas the ventral border was estimated based on the general shape of the slice. Following the identification of the appropriate region of interest, the objective was switched to x60 for better visualization of the MEC laminar organization. L II of the MEC is described to be thinner than layer III with the visible cells being organized in groups (van Groen 2001). Three criteria were then used to identify SC. Firstly, they are known to be the most abundant in the superficial or middle parts of L II, therefore SC inter-laminar location was used as an indicator. Secondly, their distinctive morphological characteristics were used for identification. Typical SC were characterized by the oval or trapezoid shape of the soma perpendicularly elongated in the pial surface direction and the presence of multiple primary dendrites (Figure 2.2) (Klink and Alonso 1997a). Thirdly, the electrophysiological properties were used to definitively assess the identity of patched cells. This includes the appropriate input resistance, action potential firing pattern, the presence of bi-phasic AHP and depolarising after potential (DAP) as well as characteristic sag arising due to the activity of the I_h current (Alonso and Klink 1993). Additionally, in comparison to other major excitatory neuronal type found within MEC L II, pyramidal neurons, SC have

been shown to have shorter action potential duration (Alonso and Klink 1993) and a tendency to create so called clustered firing patters (burst firing) (Alonso and Klink 1993; Fuchs et al. 2016; Pastoll, Ramsden, et al. 2012). Only the cells fulfilling all of the above-mentioned conditions were positively identified as SC.

Figure 2.2. A typical SC of L II of the MEC. The soma of the cells can be usually found in the upper part of L II. The picture was adapted from Alonso and Klink (1997).

2.3.1.4 Current-clamp recordings

2.3.3.4.1 Solutions

Whole-cell current-clamp recordings were performed using ACSF composed of (mM): 125 NaCl, 2.5 KCl, 1.25 NaH_2PO_4, 25 $NaHCO_3$, 2 $CaCl_2$, 2 $MgCl_2$, 10 dextrose and synaptic blockers (1 µM of CGP55845, 10 µM of CNQX and bicuculline and 50 µM of DL-AP5). Patch pipettes were filled with an intracellular solution composed of (mM): 120 $KMeSO_4$, 15 KCl, 10 HEPES, 0.2 EGTA, 2 $MgCl_2$, 4 Na_2ATP, 0.3 Tris-GTP, 14 Tris-phosphocreatine and Neurobiotin (0.2 % w/V), 295 mOsm/l. The intracellular

solution has been calibrated to 7.3 pH using approximately 200 µl of KOH solution (VWR SB70P pH meter).

2.3.3.4.2 Recording procedures

2.3.3.4.2.1 Recording procedures at RMP

All the current-clamp recordings were performed in a whole-cell mode. The RMP was continually monitored throughout the recording procedures and the values were reported in a digital form and saved for further analysis. Intrinsic membrane properties of SC were measured using 5 s current injections (from -200 pA to 300 pA, at 50 pA intervals). These data allowed measuring the input resistance and the excitability of the cells (number of action potentials evoked during each current injection). All the hyper-excitable cells (firing upon +50 or +100 pA current injections), or the neurons with the RMP below – 60 mV, have been classified as unhealthy and were discarded from the data set.

2.3.3.4.2.2 Recording procedures at fixed membrane potentials

The intrinsic membrane properties, such as cell excitability, are dependent on the changes in the membrane potential. Therefore, following the measurement at the RMP, all of the cells were clamped at fixed membrane potentials of – 70 mV. This allowed more accurate cell to cell comparison. As for the RMP, 5 s current injections were applied at the – 70 mV and both, the cell excitability and the input resistance, were monitored.

To measure the amplitude, threshold and half-width of action potentials, single action potentials were elicited from a fixed potential of -70 mV using a 10 ms depolarising current injection ranging from 0.5 to 1.5 nA followed by 810 ms resting period. The protocol was repeated three times and the mean values were used for further analysis. This method was chosen to be more accurate as it did not contain any interference of

additional SC membrane properties, such as AHP, that appear during long 5 s recordings and can affect the shape of action potentials.

To assess the involvement of $Ca_v3.2$ channels in EPSP integration, a single alpha wave stimulation protocol (αEPSP) was applied. αEPSPs were generated using the equation below (Huang et al. 2011).

$$A = \left(\frac{t}{T}\right) * \exp(1 - \left(\frac{t}{T}\right))$$

Equation 2.1. The equation used to generate αEPSPs. T and A represents the rise time constant and amplitude respectively

The equation parameters were designed to mimic EPSPs elicited by extracellular stimulation onto entorhinal cortical neurons. The amplitude of the αEPSPs were adjusted to be less than or equal to 2 mV. 20 Hz and 50 Hz aEPSP summation protocols were also generated by eliciting 5 waveforms consecutively at intervals of 50 ms and 20 ms apart, respectively.

2.3.3.4.2.3 Estimation of the Ca_v3 contribution

Stock solutions of Ca_V3 pharmacological inhibitors, $NiCl_2$ (Sigma-Aldrich, UK) and TTA-P2 (Merck Research Labs, USA), were made at concentrations of 1 mM and 100 µM in water and DMSO, respectively. These were then diluted to obtain final concentrations of 50 µM $NiCl_2$ and 100 nM TTA-P2, that selectively inhibit Ca_V3 channels. To understand the contribution of Ca_V3 currents to changes in intrinsic membrane excitability, recordings were obtained under control conditions and following 20 min extracellular perfusion of these inhibitors onto wild type and $Ca_V3.2$ null stellate neurons. The inhibitors were washed off for a period of 20-30 min during which recordings were made as well.

### 2.3.1.5 Voltage-clamp recordings

2.3.1.5.1 Solutions

Whole-cell voltage-clamp recordings were performed using previously described ACSF with synaptic blockers (1 µM of CGP55845, 10 µM of CNQX and bicuculline and 50 µM of DL-AP5). To obtain clear recording of T-type $Ca_v3.2$ channels, additional blockers of sodium, potassium and calcium (L, R, N, P/Q – type) were added: 0.001 mM TTX, 2 mM $CsCl_2$, 10 mM TEA, 0.1 mM 4-AP, 0.02 mM Nifedipine, 0.0002 mM ω-agotoxin, 0.0002 ω-conotoxin and 0.0002 mM SNX. All blockers were pre-prepared, diluted in distilled water, aliquoted and stored in the − 20°C with the exception of nifedipine that was diluted in DMSO and prepared fresh on the day. Following addition of nifedipine, all beakers containing ACSF were kept in the darkness. Patch pipettes were filled with an intracellular solution composed of: 120 mM $CsCl_2$, 1 mM $CaCl_2$, 5 mM $MgCl_2$, 10 mM EGTA, 10 mM HEPES, 2 mM Na_2ATP, 0.3 mM Tris-GTP and 14 mM phosphocreatine and Neurobiotion (0.4 % w/V). The pH of the internal solution was adjusted to 7.3 using KOH and the final osmolarity was ranging from 295 – 300 mOsm/l.

2.3.1.5.2.1 Voltage-clamp recordings

The slices for voltage-clamp were obtained using the same method as used for the current-clamp recordings. Following the 45 min incubation at room temperature, the slices were placed in the recording chamber in the ACSF.

SC were voltage-clamped at − 70 mV. To activate T-type Ca^{2+} currents, the previously described protocol allowing to produce reasonable activation curve, was used (Martinello et al. 2015). It consisted of 1 s pre-pulse applied to -100 mV followed by 1 s pulses spanning from -90 to -45 mV at 5 mV intervals (Figure 2.3 A). The inactivation protocol consisted of ten 1 s pulses ranging from -100 mV to − 55 mV followed by 1 s after pulse at − 50 mV (Figure 2.3 C). Both activation and inactivation protocols were followed by a leak subtraction protocol consisting of a 1 s pre-pulse to − 100 mV

followed by 1 s pulse to − 110 mV (Figure 2.3 B). All of the protocols were repeated at least 3 times and the mean value was saved for further analysis.
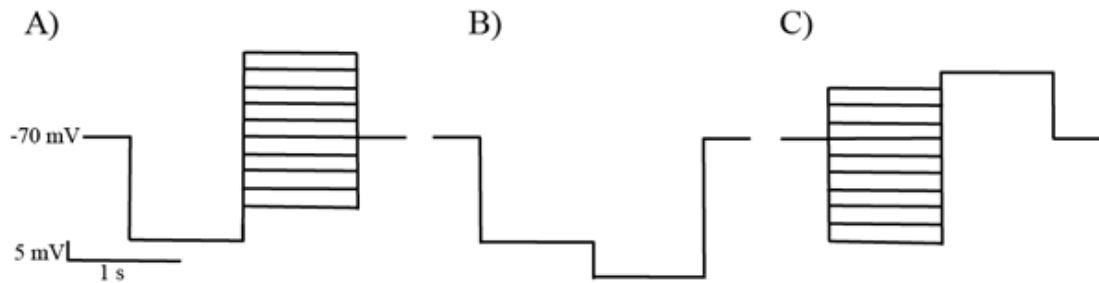
Figure 2.3. The T-type current protocols. A) Activation protocol: the cell was held at − 70 mV and hyperpolarised to -100 mV for 1 s. This was followed by 1 s current injection bringing the cell membrane to voltages ranging from -90 to -45 mV in 5 mV steps. B) Leak current protocol: 1 s pre-pulse at − 100 mV followed by 1 s pulse at − 110 mV. C) Inactivation protocol: ten 1 s pulses (-100 mV to − 55 mV), each followed by 1 s after pulse at − 50 mV

Following the control recordings, the above-mentioned ACSF with blockers was supplemented with TTA-P2 (100 nM). After the minimum of 7-10 min of the drug perfusion, the activation, inactivation and leak protocols were repeated and saved for the analysis. Only the recordings from cells that had a holding potential <200 pA and, series resistance <35 MΩ, which could be compensated for by at least 70%, were included in the analysis. Additionally, neurons that had a change in the series resistance greater than 20% throughout the drug infusion were excluded from the data set. Furthermore, the presence of Na^+, K^+, HCN and HVA Ca^{2+} blockers helped to improve the quality of voltage-clamp.

2.3.2 Confocal Microscopy

2.3.2.1 Slice fixing

In all experiments, neurobiotin was included in the patch pipette solution and was dialysed into the cells during recordings to allow accurate assessment of the cell morphology and position. Once the recordings were completed, the patch pipette was gently removed and the brain slice was left in ACSF for approximately 10 min in the

recording chamber. The slice was then transferred into 0.4 % paraformaldehyde (PFA) solution and incubated overnight. The following day, it was washed three times in phosphate buffered saline (PBS) solution to remove any residuals of PFA.

2.3.2.2 Immunohistochemistry staining

The slices were incubated in the PBS for up to three weeks. This was followed by two hours incubation with Triton X-100 (0.5 % in PBS, Sigma). Slices were then washed three times in PBS and incubated for two hours with Alexa Fluor 488 streptavidin conjugate dye (0.2 % in PBS, Life Technologies). The conjugate is composed of the protein streptavidin, which binds to neurobiotin. The fluorescent label, Alexa Fluor dye that is covalently attached to streptavidin, allowed identification and accurate visualization of the neurons that were previously filled with neurobiotin. Lastly, the slices were washed three times in PBS and mounted on microscope slides using Vectashield mounting medium (Vector Laboratories Inc.) to protect fluorescence. Slices were stored in the dark at 4°C.

2.3.2.3 Identification of cell position within MEC

The brain sections were visualized using a confocal microscope (LSM 710) at x10 magnification and Zen Software (Zeiss). The Lasos (Zeiss) RMC 7812Z2 laser was set to read the AlexaFluor488 dye at 494-551 nm range. It was possible to clearly view the fluorescent cell against the background staining of the whole slice (dark green, Figure 2.4). In order to establish the position of the neuron of interest (bright green spot), the dorsal (close to parasubiculum) and ventral (based on the slice shape) borders of MEC were determined (Figure 2.4). The total length of the MEC, which has changed in accordance to the depth of the cut varying between around 2500-4000 µm, was measured. The position of the neuron of interest was then established.
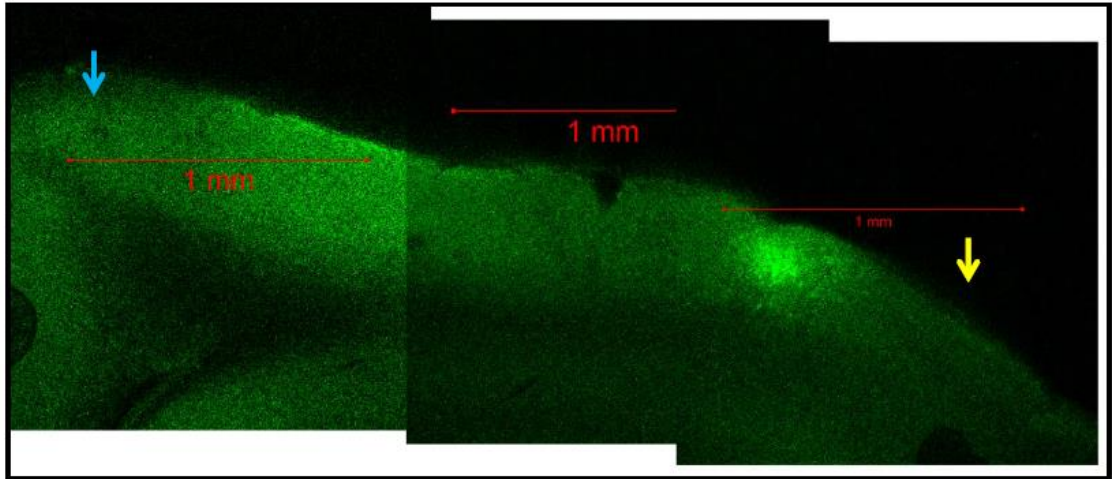
Figure 2.4. An example of the confocal picture of the parasagittal brain section that was used to establish the position of patched neurons. The Alexa Fluor®488 dye was used to visualize the slice (dark green background staining) and cells (bright green). The total length of the slice was established (from dorsal – blue arrow, to ventral – yellow arrow, border), followed by the measurement of the position of the neuron of interest from the dorsal border. This procedure allowed classifying cells as dorsal or ventral.

2.3.2.4 Assessment of cell morphology

Following the establishment of the cell position, the magnification was increased to x40 or x60. To obtain high quality images of the cell body and dendritic processes, the Z stack image of the cell was taken. Each Z stack consisted of 1.32 µm thick, 60 to 120 slices, depending on the size of the cell. Additionally, each slice was composed of 4 (2X2) individual images (tile scan 2833.97 µm x 2833.97 µm) in order to assure a high--quality image of each neuronal section. The channel gain and offset were adjusted individually for each cell, at the values of approximately 686 and 11, respectively.

2.4 Data Analysis

2.4.1 Electrophysiology

2.4.1.1 Programmes used for data analysis

All electrophysiological data were analysed using Clampfit 10.4 software (Molecular Devices, UK). All the graphs and figures were prepared using OriginPro 9.0 (OriginLab) programme and Adobe Illustrator CS3 (Adobe Systems) software. Confocal images

were acquired using Zen (Zeiss) software. The position of the neurons of interest, visualized on the confocal pictures, was calculated using ImageJ (Java) software.

2.4.1.2 Analysis of SC membrane properties

2.4.1.2.1 Membrane Potential

The RMP is an important indicator of cell health. It is determined by different ionic conductances present in the cell membrane and is therefore an important feature for cell identification. The RMP of SC was therefore recorded in a digital form during current-clamp recordings. It was measured at the first 500 ms of recording prior to each current injection starting from -200 pA untill +300 pA, at 50 pA intervals. The average RMP value of each cell was then calculated.

2.4.1.2.2 Cell Excitability

The activity and density of various ion channels present in the SC membrane can affect its excitability. The number of the action potentials evoked upon the current stimulation was therefore measured for each step (from -200 pA to 300 pA, at 50 pA intervals) using the Clampfit 10.4 software that automatically measures the number of spikes at the particular sweeps. The cell excitability was analysed and reported for both RMP and at -70 mV fixed membrane potential.

2.4.1.2.3 Input Resistance

Acquired data were also used to calculate the intrinsic membrane properties such as input resistance. Using Ohm's Law (Equation 2.2), the steady-state input resistance was calculated at -100 pA and +100 pA current injections steps. As it is depended upon the changes in the membrane potential, the input resistance was analysed and reported for both RMP and at -70 mV fixed membrane potential.

$$R = \frac{V}{I}$$

Equation 2.2. The Ohm's law. It was used to calculate the input resistance, R = resistance, V = voltage, I = current.

2.4.1.2.4 Latency

Using the Clampfit 10.4 software, the time required to evoke first action potential was calculated. The current injections required for an action potential generation varied between cells therefore both the current injections and the time were taken into consideration when comparing groups of cells.

2.4.1.2.5 Sag

A typical feature of the electrophysiological recordings obtained from the SC is the presence of the so-called membrane potential sag. This is due to the hyperpolarisation activated I_h current which opposes the small membrane potential perturbations of the SC (Alonso and Llinas 1989). In my study I tested whether the sag was affected by the T-type Ca^{2+} channel blockers in both $Ca_v3.2$ null and wild type neurons. Sag amplitude was calculated, following previously described method (Nolan et al. 2004). The amplitude was expressed as the ratio of the value measured at the hyperpolarization peak at – 100 pA step (where the sag appeared to be the most prominent) and steady state hyperpolarization. The long, 5 s recordings were used for these measurments.

2.4.1.2.6 Oscillatory activity

SC were observed to display characteristic subthreshold membrane potential oscillations (sMPOs) (Alonso and Klink 1993). To verify whether there was any difference in the frequency and magnitude of the oscillations between SC obtained from $Ca_v3.2$ null and wild type animals, the data were further analysed using MATLAB (MathWorks Inc.) in collaboration with Mr Talfan Evans and Professor Neil Burgess (Institute of Cognitive Neuroscience, University College London).

To analyse the sMPOs in the theta range, the traces were low-pass filtered (100 Hz). To exclude the effects of action potential and their AHP on the sMPOs, the parts of the

recording where the spikes occurs, together with 400 ms after the action potential, were artificially removed. The spikes were then linearly interpolated (Figure 2.5)
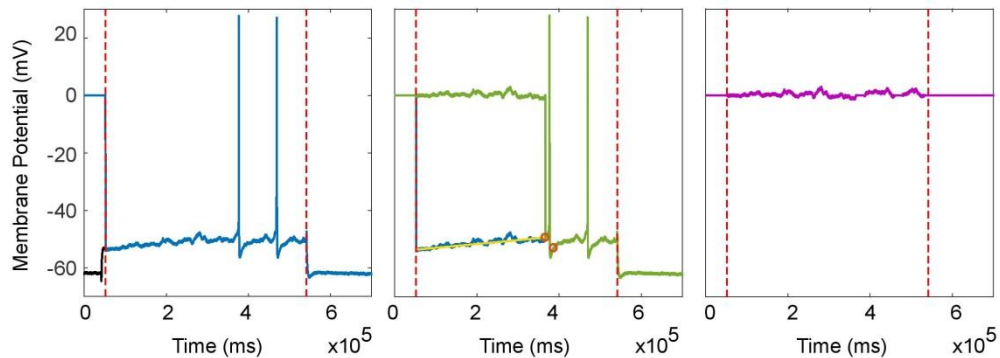

Figure 2.5. The process of spike removal. The panel show trace before (blue) during (green) and after (purple) deletion of the action potentials. Red circles on the middle panel represent the time points at which the data were removed and replaced with a straight line.

It is important to note however, that some of the cells were highly excitable, particularly at the -50 mV to -45 mV membrane potential. In these cells, it was not possible to remove the spikes effectively. Therefore, to minimise the bias, for the recordings with high excitability, only the traces were there was a minimum 2 s space between minimum one pair of spikes were included into analysis (Figure 2.6). Additionally, only the traces with the mean membrane potential exceeding – 55 mV, which is when majority of sMPOs manifested, were analysed.

To measure the power of sMPOs, a sliding window analysis method was used (Giocomo et al. 2007). Spectograms in a sliding window (1s width at 0.1 s intervals, 0.9 s overlap between windows) were analysed (with the exclusion of the part of the traces were spikes were previously removed). Next, the mean power of three bands (1-4 Hz, 4-8 Hz and 8-12 Hz, (Garden et al. 2008)) was measured for each spectrogram. The highest average power was then calculated for each band. It is important to note however, that rather than averaging multiple trials for each cell, the maximum power values (of each of the bands) for individual recording trials were reported, resulting in the sample size higher than the number of cells.
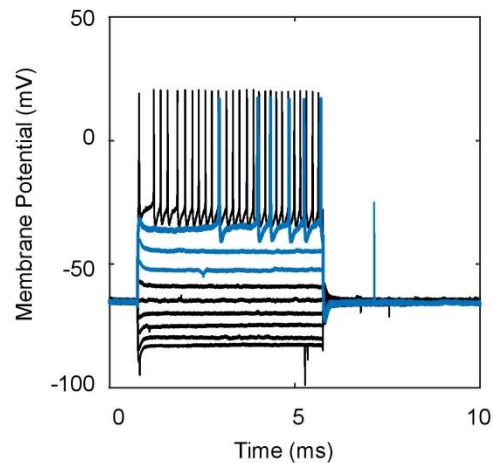
Figure 2.6. The criteria used for trace inclusion. Dark lines represent all of the recorded traces. Blue lines show the traces that were chosen to be included into the analysis. The blue trace with action potentials was included as it had a minimum of 2 s space between a spike pair.

2.4.1.2.7 Action potential amplitude

The amplitude of single action potentials elicited using a 10 ms pulse (short protocol) when SC were hold at fixed – 70 mV membrane potential was analysed. This allowed more accurate comparison between different cells (dorsal and ventral, $Ca_v3.2$ wild type and null neurons). The amplitude was measured manually as mV difference between the spike threshold and its peak value using the ClampFit 10.4 software.

2.4.1.2.8 Action potential threshold

The spike threshold of single action potentials elicited by a 10 ms pulse was also measured. The phase-plane plots (dv/dt plotted as a function of the voltage change) were constructed and the threshold was measured by setting cursors at a point at which the initial upstroke begins.

2.4.1.2.9 Action potential half-width

Finally, the half-width of the single action potentials was measured. The half width was calculated at half-maximal value of the action potential amplitude.

2.4.1.3 Alpha wave stimulation

2.4.1.3.1 Single alpha wave stimulation

To evaluate the potential involvement of T-type Ca^{2+} currents in the post-synaptic activity of SC, the single alpha wave stimulation, αEPSPs, were applied to the patch neurons held at the membrane potential of -70 mV. Data were then collected and imported into Clampfit 10.4 software. Due to the issues with access resistance, some of the cells had to be excluded from the data set. Next, the half-width of the αEPSPs recorded from the SC was measured at the half-maximal value of the waveform. Obtained data were then compared between different sets of cells.

2.4.1.3.2 Stimulation at 20 and 50 Hz

Using the above-mentioned αEPSPs protocol (Huang et al. 2011) the SC response to 20 and 50 Hz stimulation was measured at – 70 mV. The data were then collected and analysed using ClampFit10.4 software. To calculate the summation ratio, the maximum amplitude of the last (fifth) peak was divided by the maximum amplitude of the first peak.

2.4.1.4 Pharmacology

The cells were held at fixed -70 mV membrane potential by injecting positive or negative current. This allowed to minimize the interfering effects of changes in the RMP and different voltage activated ion channels. Such changes would otherwise affect the measured intrinsic membrane properties, input resistance and excitability. These were measured using same method as for the control recordings. The input resistance was measured at -100 pA and +100 pA current injections steps and the number of the action potentials evoked upon the current stimulation for each step (from -200 pA to 300 pA, at 50 pA intervals) were calculated. The data used to calculate the effects of the drug were taken at the 10-15 min time point from the bath application of appropriate compound, when there was maximal effect of the pharmacological agent. It was followed by 20-30 min washout, when the cells were placed in the ACSF. A full

washout did not occur in all neurons. Therefore, the data where the maximum washout occurred was analysed. It was typically 20 – 30 min from the beginning of the washout procedure, when no further change in the membrane properties was observed.

2.4.1.4 Voltage-clamp measurements of T-type Ca^{2+} current

To accurately measure the T-type Ca_v3 currents, the control recordings (Figure 2.7 A) and data obtained in the presence of TTA-P2 (Figure 2.7 B), activation and inactivation protocols, were leak subtracted using ClampFit10.4 software. The recordings in the presence of TTA-P2 were then subtracted from the leak-subtracted control data (Figure 2.7 C). The T-type Ca^{2+} currents were calculated from these traces as the difference between the baseline and the peak of the current. These were measured as a mean of roughly 200 ms obtained from approximately 1.9 s and 1.3 s time points, respectively.

A

B

C
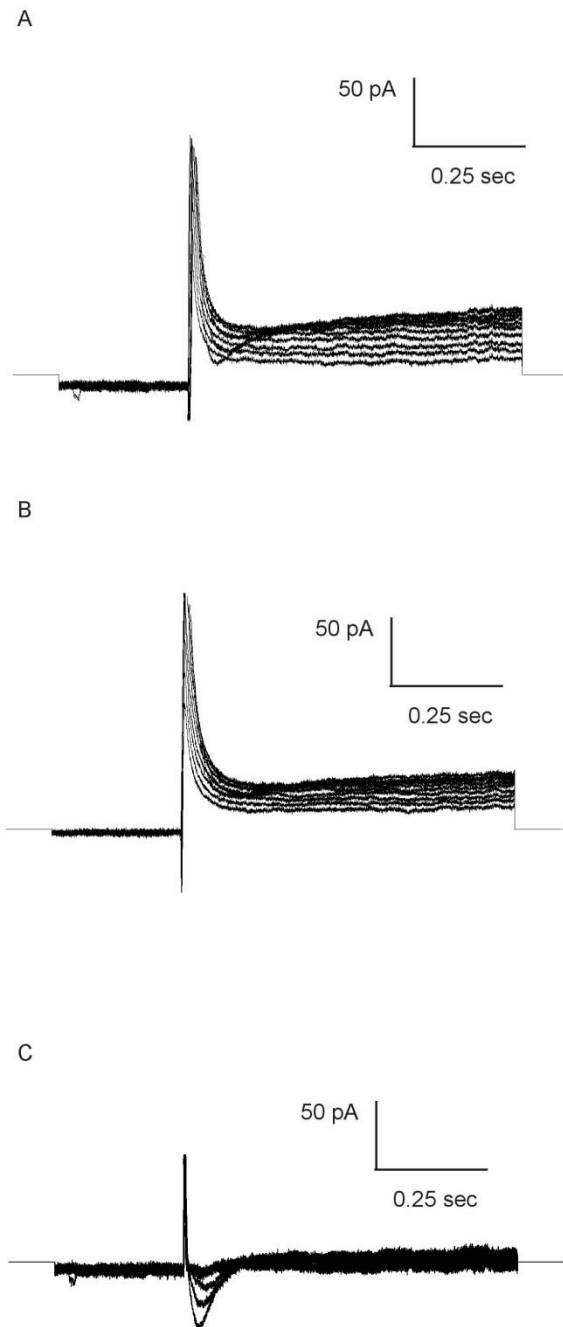
Figure 2.7. Example showing the subtraction protocol. A) Control recording B) and in the presence of drug after the leak subtraction. C) The trace showing leak subtracted control minus drug condition (A-B) that was used to evaluate the amplitude of T-type Ca_v3 Ca^{2+} current.

When there was no obvious current visible, the measurements were set at the same time point as where the first T-type Ca^{2+} current appeared. The same method was used for the inactivation protocol. For cells obtained from the $Ca_v3.2$ null mice, where there was no obvious T-type Ca^{2+} current visible, a set time point was used for measurements. This time point was set to overlap with a time point where the peak T-type Ca^{2+} current typically appears in wild type neurons and was consistent across all $Ca_v3.2$ null cells.

Furthermore, the maximal current from the wild type dorsal and ventral cells, obtained at -45 mV and at – 100 mV for activation and inactivation protocols, respectively, was fitted into single exponential equation using OriginPro (Equation 2.3).

$$y = y_0 + A_1 e^{-x/\tau}$$

Equation 2.3. Exponential Decay equation. y_o stands for the offset, A_1 is an amplitude and τ is a decay time constant.

From there, the inactivation Tau (τ_1) values were obtained. It was not possible to accurately fit the activation part of the current. Due to the small current values it was not possible to obtain a consistent fit from the null neurons.

2.4.2 Analysis of a position of the cells

The position of neurons within the MEC was measured as a percentage of the total length of the MEC using ImageJ software. The total length of the MEC was calculated as the distance from dorsal to ventral border. All the cells that were found to be present below 30 % of the total length of the slice have been classified as dorsal, whereas all the neurons above the 70 % of the total distance were classified as ventral. All other neurons, including the cells located closely to midline of the MEC, were classified as middle. Input resistance and RMP of 'middle' neurons were presented in some graphs. All other data obtained from these neurons were, however, excluded when comparing other characteristics.

2.4.3 Analysis of the cell morphology

2.4.3.1 Cell soma

Typical SC has a trapezoid, ovoid or circular soma that is elongated in a perpendicular direction to the pia and has dimensions of 23±4.4 μm x 12.9±2.2 μm (Klink and Alonso 1997a). Furthermore, the size of the cell soma decreases towards the ventral end of the MEC (Garden et al. 2008). To confirm the identity of the patched cells the confocal images of the cells filled with the neurobiotin were used. Then, ImageJ software was used to directly measure the soma size. In order to achieve this, the confocal images (volume Z-stack) were exported into the programme, the scale was calibrated accordingly and the 'freehand selection' tool was used to draw a frame along the soma borders. ImageJ then automatically calculated the area size of the soma (μm) which was then exported to Excel and the comparison between the cell groups was performed.

2.4.3.2 Dendritic processes and Sholl analysis

SC typically have five to eight primary dendrites radiating from the cell body in the multiple directions (Klink and Alonso 1997a). To compare the dendritic complexity of the patched cells, Sholl analysis was performed. In Adobe Illustrator, the image of concentric circles, progressively increasing their radius by 10 μm, was superimposed with Z-stack confocal images in a way that the centre of the circles was overlapping with the middle part of the cell body. The image was then transferred to ImageJ software and the number of intersections of the individual dendrites at each circle (corresponding to a particular distance) was calculated. The data were then compared between different cell sets using OriginPro software.

2.4.4 Statistical analysis

All the statistical analysis was performed using the SPSS, Origin and R software. Unless stated otherwise, all mean values are ±SEM. Student's t-test, ANOVA and Multiple Regression Analysis were used to test the statistical significance of the data.

# 3. Dorsal-ventral gradient of $Ca_v3.2$ channels in MEC L II SC

3.1 Introduction

SC are distributed along the dorsal-ventral axes of the MEC L II. It has been previously shown that their intrinsic membrane properties differ depending on their location in the MEC (Pastoll, Ramsden, et al. 2012; Giocomo and Hasselmo 2008; Giocomo et al. 2007; Nolan et al. 2007; Garden et al. 2008; Dodson et al. 2011). A variety of ion channels have been shown to contribute towards these differences, including HCN1 and potassium conductances (Garden et al. 2008; Giocomo and Hasselmo 2008), however the role of the T-type $Ca_v3.2$ Ca^{2+} channels, and their potential contribution towards the dorsal-ventral gradient of the MEC L II SC, has not been investigated in the past. The unique properties of T-type Ca^{2+} channels, i.e. their activity at subthreshold membrane potentials, made them an interesting target when investigating dorsal-ventral gradient in L II SC. Additionally, T-type $Ca_v3.2$ Ca^{2+} channels have been previously shown to be expressed and colocalised with HCN1 channels at the mature asymmetric presynaptic terminals active zone where they synapse onto pyramidal neurons of layer III entorhinal cortex (Huang et al. 2011). Therefore, in the following chapter I evaluated whether T-type $Ca_v3.2$ Ca^{2+} are present in the MEC L II SC and whether they influence their membrane properties.

To evaluate the contribution of the T-type $Ca_v3.2$ Ca^{2+} currents in mediating SC activity, I used a combination of $Ca_V3.2$ null mice and their wild type littermates. The mice did not exhibit any overt phenotype, however the Western and Northern blot analyses have both confirmed a complete and global loss of $Ca_v3.2$ subunit (Chen, Lamping, et al. 2003). Furthermore, two pharmacological agents, TTA-P2 and $NiCl_2$, were also used to pharmacologically block $Ca_v3.2$ activity and therefore to confirm the results obtained with null animals.

3.2 MEC L II SC exhibit dorsal-ventral gradient in their intrinsic membrane properties

Current-clamp recordings from MEC L II SC were performed. Traces from $Ca_V3.2$ wild type dorsal (within 30 % of the presubiculum border; (Figure 3.1 A and C) and ventral (within 30 % of the periamygdaloid cortex border; Figure 3.1 B and D) neurons revealed typical SC properties. These include the presence of a characteristic sag induced upon hyperpolarisation, subthreshold voltage oscillations and a clear visible bi-phasic AHP (Alonso and Klink 1993), an input resistance of approximately 50-170 MΩ (depending on the location), and the RMP at around -66 mV (Garden et al. 2008).
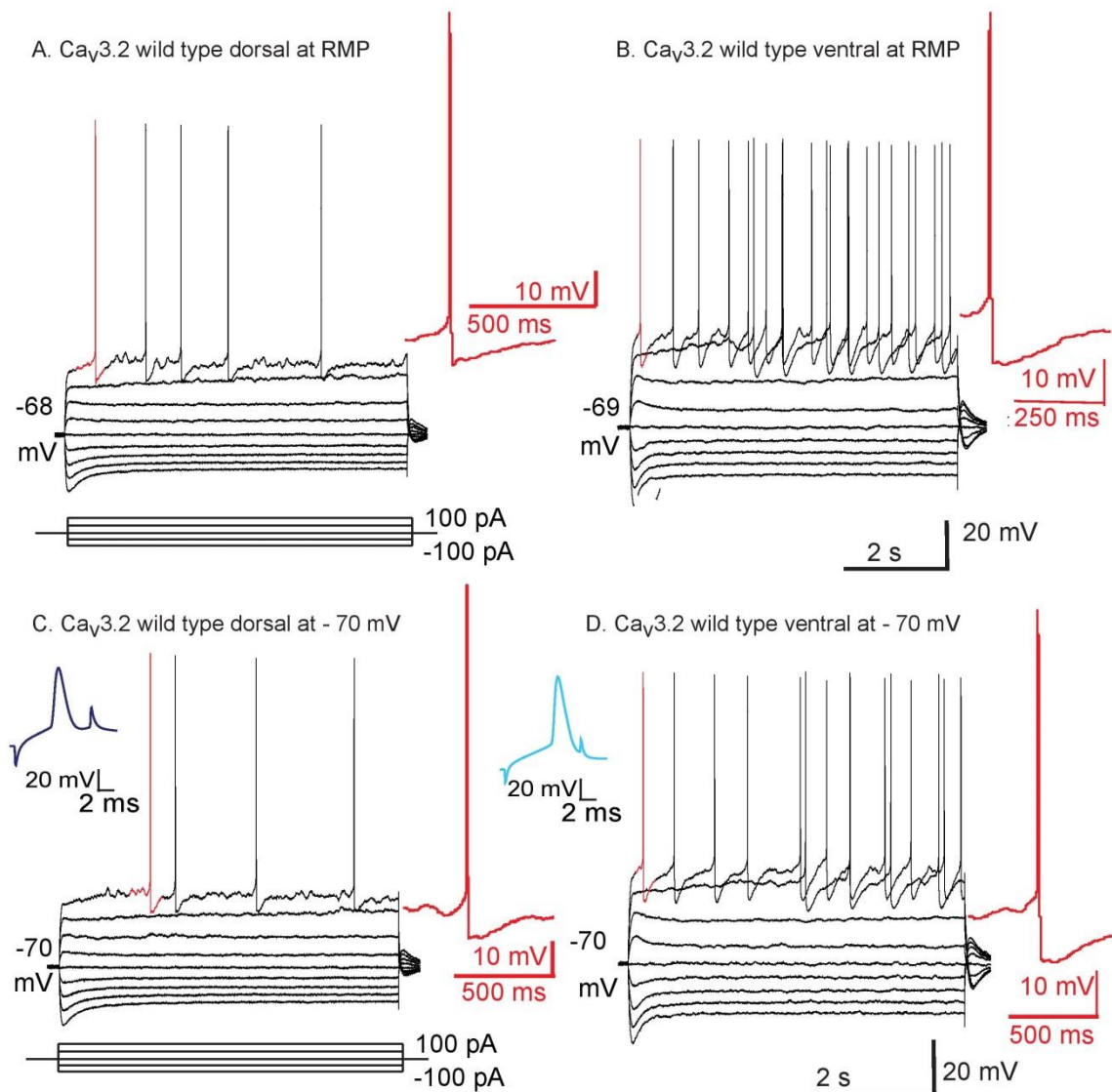
Figure 3.1. Example traces of MEC L II dorsal (A and C) and ventral (B and D) cells. The recordings were performed at RMP (A and B) and a fixed potential of – 70 mV (C and D). Single action potentials were also elicited by applying a 10 ms pulse from a potential of -70 mV. Representative action potential traces of dorsal (C, dark blue line) and ventral (D, light blue line) are shown. Additionally, enlarged single action potentials from dorsal and ventral cells at RMP and -70 mV are shown in red to illustrate the biphasic AHP.

In agreement with the previous findings, the RMP of the L II SC varied between -60 mV and – 70 mV (Alonso and Llinas 1989). However, in contrast to previous reports (Garden et al. 2008), a significant difference in the RMP (Figure 3.2 A) was observed with ventral cells (-70.2±0.4 mV; n=26) having more hyperpolarized RMP than dorsal neurons (-68.2±0.7 mV, n=28, $p<0.01$, t-test).

Furthermore, the input resistance of the L II SC has been previously reported to vary along the dorsal-ventral axes of the MEC (Garden et al. 2008). To determine if this is the case in the $Ca_v3.2$ wild type neurons, -100 pA and +100 pA current injections were applied to the cells. The input resistance was measured at RMP and a holding potential of – 70 mV (Figure 3.2 B, E and C, F respectively). Consistent with previous findings (Garden et al., 2008), the input resistance was significantly greater in ventral cells compared with dorsal cells when measured using a +100 pA current injection step at RMP (dorsal and ventral cells: 80.6±5 MΩ, (n=28) and 112.2±7.9 MΩ (n=26), respectively, $p=0.001$, t-test, Figure 3.2 C). The input resistance values were not different between dorsal and ventral cells when measured using a –100 pA current injection steps at RMP (dorsal and ventral cells: 46.7±3.2 MΩ (n=28) and 55.3±4.2 MΩ (n=26), respectively, $p=0.1$, t-test, Figure 3.2 B). The dorsal-ventral gradient at +100 pA current injection was even more prominent when measured at a set membrane potential of – 70 mV (dorsal and ventral: 66.5±4 MΩ (n=28) and 106.6±7.9 MΩ (n=26), respectively, $p<0.001$, t-test, Figure 3.2 F). Interestingly, the gradient was still present when measured at – 100 pA current injection at the fixed membrane potential (dorsal

and ventral: 43.1±2.9 MΩ (n=28) and 55.2±4.1 MΩ (n=26), respectively, p<0.02, t-test; Figure 3.2 E).

The above-described dorsal-ventral gradient in the RMP, input resistance and cell excitability was established for MEC L II SC by comparing the neurons found exclusively with 30 % of the dorsal and ventral borders. I also investigated if this gradient existed if wild type SC outside these borders were included in the analysis. To achieve this, all of the recorded neurons were added into the data set, including the middle L II SC. Using this approach, a small (R^2=0.0874, n=59) gradient in the RMP was observed with the dorsal neurons being more depolarised in comparison to ventral cells (Figure 3.3 A). Furthermore, a gradient in the input resistance at both RMP (R^2=0.0891 and R^2=0.2297 at -100 pA and +100 pA current injections respectively, Figure 3.3 B and C) and at fixed membrane potential of − 70 mV (R^2=0.1355 and R^2=0.3119 at -100 pA and +100 pA current injections respectively, Figure 3.3 D and E) was observed. Under both conditions, dorsal cells had a lower input resistance than ventral neurons. As expected, the gradient was clearly more prominent at the +100 than -100 pA current injection step, when more $Ca_v3.2$ channels are active (Bruehl and Wadman 1999).

A. Resting Membrane Potential
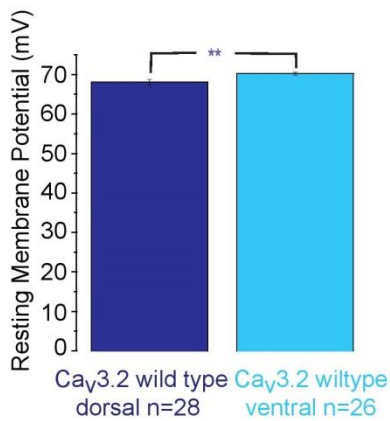
Figure 3.2 Intrinsic membrane properties of Ca$_v$3.2 wild type cells. Dark and light blue colour represents dorsal and ventral cells, respectively. A) Mean RMP values of dorsal and ventral neurons B) and C) Individual (squares) and average (lines) input resistance values measured at RMP with steps of -100 pA and +100 pA current injections, respectively D) Mean number of action potentials obtained with varying current injections in dorsal and ventral neurons at RMP E) and F) Individual (dots) and average input resistance measured at the set membrane potential of – 70 mV at -100 and + 100 pA current injections, respectively G) Average action potential numbers in dorsal and ventral neurons at the set membrane potential of – 70 mV. Single (*) and two (**) denote significance at $p<0.05$ and $p<0.01$ respectively.
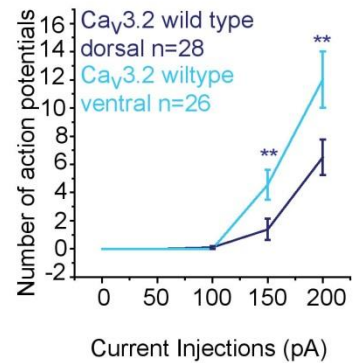
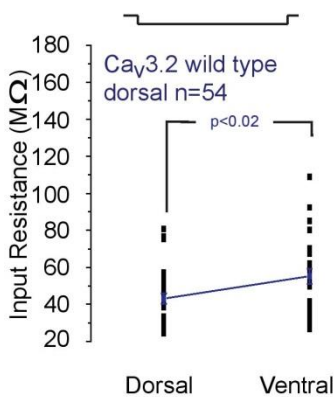B. Input Resistance at - 100 pA at RMP
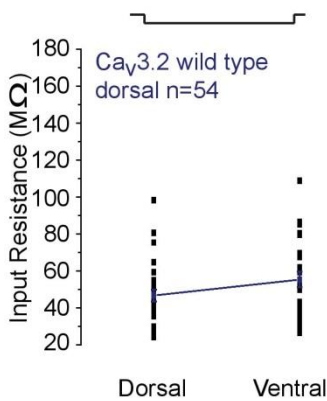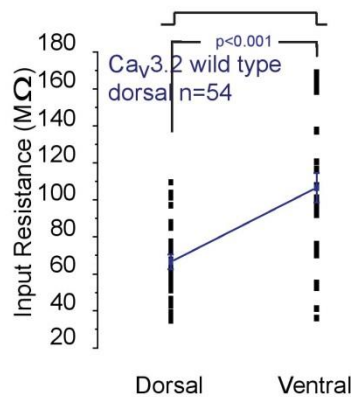
C. Input Resistance at + 100 pA at RMP
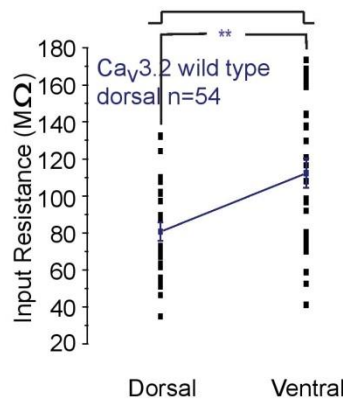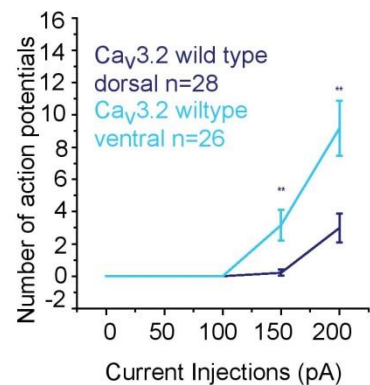
D. Excitability at RMP

E. Input Resistance at - 100 pA at - 70 mV

F. Input Resistance at + 100 pA at - 70 mV

G. Excitability at - 70 m

3.3 The excitability of MEC L II SC also follows the dorsal-ventral gradient
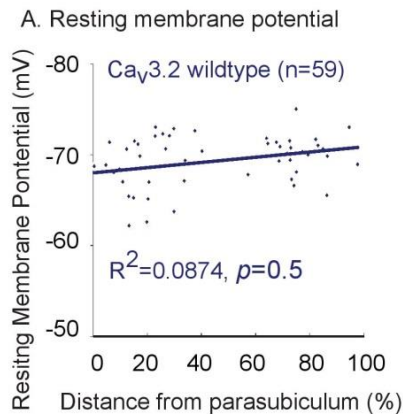
The dorsal-ventral gradient in the input resistance of the MEC L II SC is likely to affect their excitability. To investigate this, gradually increasing current steps (from +50 pA to +200 pA) were injected into the cells during the current-clamp recordings. As predicted, at RMP, the average number of action potentials elicited using 5 s depolarizing steps in ventral neurons (4.6±1.1 (n=26) and 12±2 (n=26) action potentials at +150 pA and +200 pA current injection, respectively) were significantly greater than in dorsal cells (1.38±0.8 (n=28 , p=0.002) and 6.5±1.3 (n= 28, p=0.005) action potentials at +150 pA and +200 pA current injection, respectively, Figure 3.2 D, Figure 3.1)

A similar effect was observed at fixed membrane potential of − 70 mV (Figure 3.2 G, Figure 3.1) with the mean number of spikes in ventral neurons (3.2±1 (n=26) and 9.2±1.7 (n=26) action potentials at +150 pA and +200 pA current injection, respectively) being significantly greater than in dorsal cells (0.2±0.2 (n=28 , p=0.005) and 3±0.9 (n=28 , p=0.003) at +150 pA and +200 pA current injection, respectively). The changes in the firing along the dorsal-ventral gradient could have been purely a result of the input resistance differences.

To investigate potential differences in the axonal properties between dorsal and ventral L II SC, I next measured action potential's half-width, amplitude and threshold. A short 10 ms current injection was applied onto the cells and a single action potential waveform was evoked. The results showed no statistical difference between $Ca_v3.2$ wild type dorsal and ventral cells (Figure 3.1 C and D, Table 3.1).
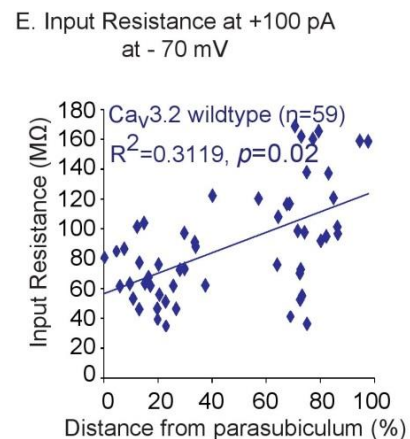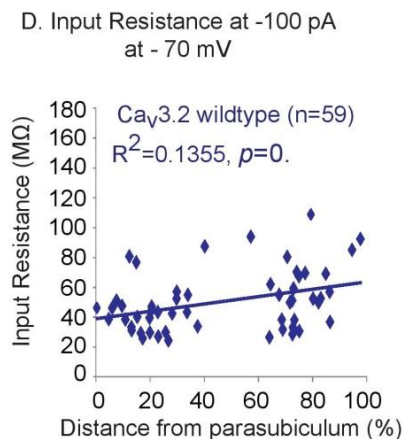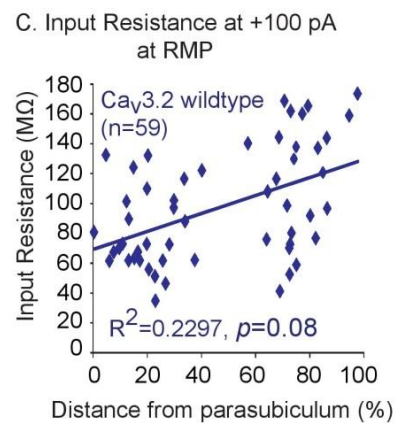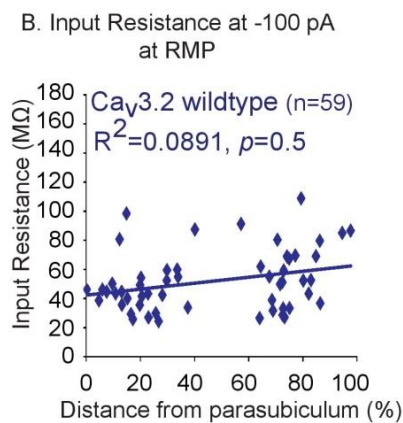
Another way of accessing the excitability of cells is to compare the latency to the first spike upon the current injection. As it has been previously described that a typical SC should exhibit a very short latency to fire an action potential with a depolarizing step (Fuchs et al. 2016; Alonso and Klink 1993), I also determined the latency to the first

spike with a given depolarizing step in the stellate neurons that I made recordings from. The results shown that, on average, dorsal and ventral L II SC display similar latency, with the average value of 182±0.2 ms (n=28) and 161±0.24 ms (n=26) for dorsal and ventral neurons, respectively, at -70 mV membrane potential (Table 3.1).

A. Resting membrane potential

Figure 3.3. Overall dorsal-ventral gradient in wild type stellate neurons. A) RMP gradient B) and C) input resistance values measured at RMP for – 100 pA and +100 pA current injections, respectively and D) and E) input resistance values recorded at – 70 V fixed membrane potential at -100 pA and +100 pA current steps, respectively. The neurons found in the middle parts of the MEC were included into data set (n=59).

B. Input Resistance at -100 pA at RMP

C. Input Resistance at +100 pA at RMP

D. Input Resistance at -100 pA at - 70 mV

E. Input Resistance at +100 pA at - 70 mV

3.4 Dorsal and ventral L II SC have similar I_h sag amplitude

It has been previously reported that HCN induced current, I_h, found within MEC L II stellate neurons, also follows the dorsal-ventral gradient (Garden et al. 2008). Since HCN1 channels have been shown to be colocalised and interact with T-type $Ca_v3.2$ Ca^{2+} channels in synaptic terminals synapsing onto layer III entorhinal cortex pyramidal cells (Huang et al. 2011), the potential influence of the latter on the membrane potential sag in the L II SC was investigated. In agreement with previous findings (Giocomo and Hasselmo 2008), no difference in the sag amplitude ratio between dorsal and ventral cells was found (Table 3.1, Figure 3.12).

3.5 Subthreshold activity of MEC L II SC follows dorsal-ventral gradient

In vivo, neurons receive EPSPs which then sum to initiate action potentials. Previous studies have shown that both spontaneous and evoked EPSPs follow a dorsal-ventral gradient (Garden et al. 2008) in the MEC L II SC. Although the amplitude and the rise-time of EPSPs have remained stable across the dorsal-ventral axes of the MEC, the half width of both, evoked and spontaneous EPSPs, was greater in ventral neurons.

To assess, whether the T-type $Ca_v3.2$ Ca^{2+} channels affect the dorsal-ventral synaptic integration gradient in MEC L II SC, EPSPs were artificially evoked using current injections directly into cell soma and the half-width was measured. Using this approach, no differences were observed in αEPSP half-widths between ventral neurons (13.9±1.5 ms, n=5) and dorsal neurons (12.7±0.9 ms, n=4) cells.

Additionally, previous studies have shown that also a summation of EPSPs at gamma frequency (>40 Hz) exhibits a dorsal-ventral gradient. The difference was particularly prominent at 80 Hz stimulation (Garden et al. 2008) with EPSP summation in ventral neurons being substantially greater than in dorsal neurons. I also wanted to test whether,αEPSPs at frequencies of 20 Hz and 50 Hz current were different when

elicited in Ca$_v$3.2 wild type dorsal and ventral neurons. As in Garden *et* al. (2008), 50 Hz αEPSP summation ratios were significantly higher in Ca$_v$3.2 wild type ventral neurons (2±0.12, n=5) than dorsal neurons (1.7±0.1, n=4, *p*=0.054). In contrast, the summation ratios for 20 Hz αEPSPs were very similar between Ca$_v$3.2 wild type dorsal (1.12±0.06, n=4), and ventral (1.26±0.1, n=5) cells.

3.6 Morphology of typical wild type SC

During the whole cell current-clamp recordings from wild type Ca$_V$3.2 cells, neurobiotin tracer was incorporated in the intracellular solution. This allowed for subsequent identification of the location of the cells within the MEC in the slice and detailed analysis of the size of the cell soma and the number of dendritic processes radiating from the soma. A neuron was classified to be a SC if it was located in MEC L II and the morphology of the cell matched previously described criteria (Klink and Alonso 1997a):

(1) a trapezoid, ovoid or circular soma that is elongated in the direction perpendicular to the pia;

(2) soma dimensions of approximately 23±4.4 µm x 12.9±2.2 µm (296.7 µm^2 total soma size);

(3) multiple primary dendrites radiating from the cell body in numerous directions.

Examples of cells that fulfilled these criteria are shown (Figure 3.4 A and B). Detailed morphological analysis of all patched neurons was not possible as in some cases they were not fully filled (possibly due to the dye not being able to sufficiently penetrate into dendrites), or I was not able to see the cell body at all. In the later scenario, I used the remaining dendritic staining or a mark left by the patching pipette to assess the position of the neuron of interest.

Since previous reports have shown that the SC soma size (perimeter and cell body cross sectional area) becomes smaller with increased distance from the dorsal border

of the MEC (Garden et al. 2008), I performed similar measurements. My results confirmed that soma size was significantly (p=0.012) larger in dorsal (216.8±20.2 μm^2 (n=7)) compared with ventral (143.6±10.8 μm^2, (n=6)) MEC L II SC (Figure 3.4 D).

Additionally, Garden et al. (2008) showed a decrease in the total dendritic surface area across the dorsal-ventral axes of the MEC, with dorsal stellate neurons having a larger number of primary dendrites than ventral cells. My results, however, showed no difference in the number of a primary dendrites between dorsal (7.7±0.5 dendrites, n=7) and ventral (6.8±0.7 dendrites, n=6, non-significant) MEC L II SC.
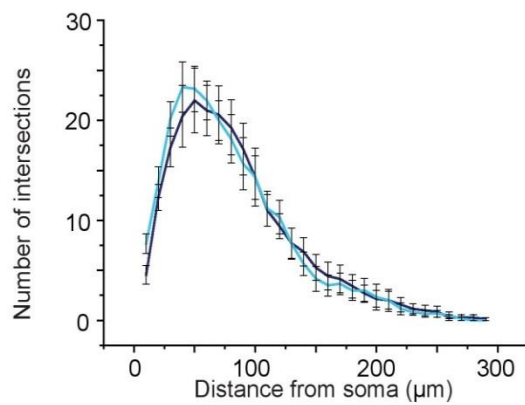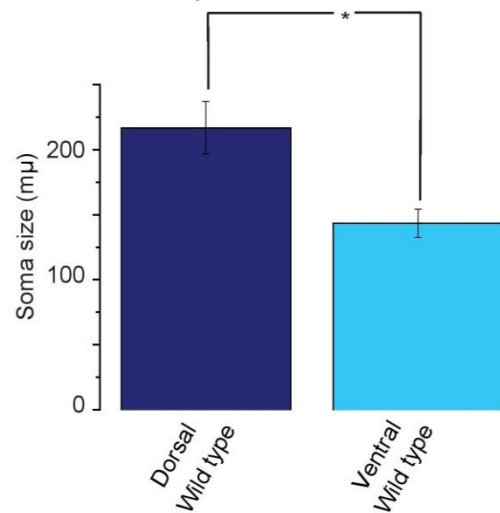
A. Ca$_V$3.2 wild type dorsal
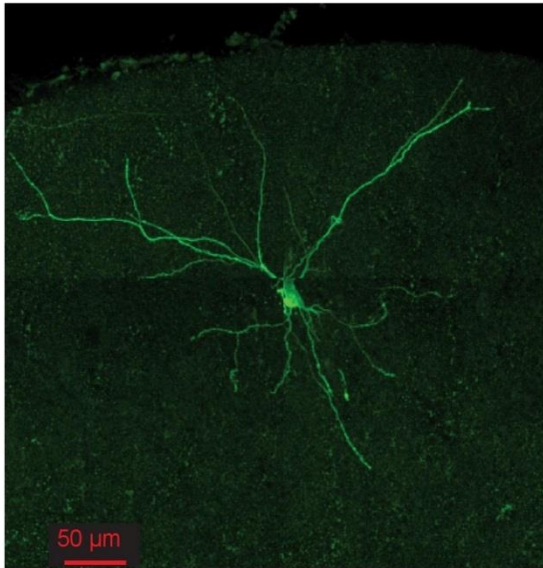
B. Ca$_V$3.2 wild type ventral
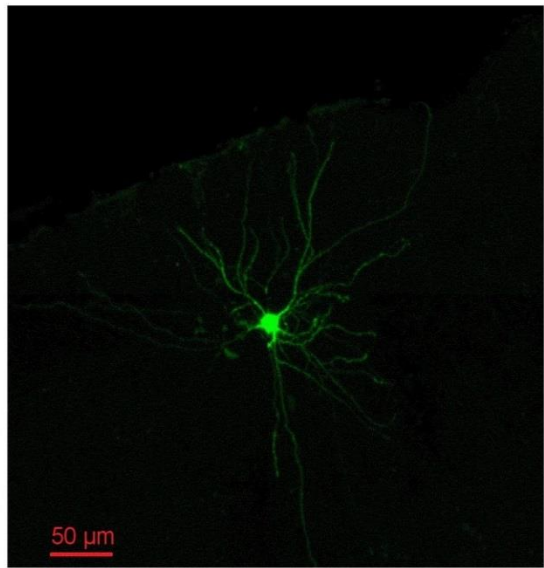
C. Sholl analysis

D. Cell soma analysis

Figure 3.4. Ca$_v$3.2 wild type SC. A) and B) Confocal images of a typical dorsal and ventral L II SC obtained from parasagittal slices containing MEC. C) Sholl analysis of dorsal (dark blue, n=7) and ventral (light blue, n=6) cells D) Soma size comparison between dorsal (216.8±20.2 µm^2, n=7) and ventral (143.6±10.8 µm^2, n=6) neurons, p=0.01.

Finally, it has been demonstrated that ventral neurons have significantly smaller number of branching points in comparison to the dorsal cells (Garden et al. 2008). To test this, a Sholl analysis was performed. The number of dendritic intersections with increasing distance from the cell body were counted (one-way ANOVA, Tukey *Post-Hoc* test). No significant differences were found between dorsal and ventral SC .

## 3.7 Comparison of Ca$_v$3.2 null and wild type SC properties

Next, I compared the basic electrophysiological properties of Ca$_V$3.2 null and wild type dorsal and ventral stellate neurons. Whole cell current-clamp recordings from Ca$_v$3.2 null dorsal (Figure 3.5 A and C) and ventral (Figure 3.5 B and D) showed typical SC properties such as sag, bi-phasic AHP and subthreshold membrane potential oscillations. These observations were followed by more detailed analysis of the intrinsic properties of the MEC L II Ca$_v$3.2 null SC.

In contrast to the Ca$_v$3.2 wild type neurons, the Ca$_V$3.2 null cells had no significant differences in their RMP (dorsal and ventral neuron RMP = -69.1±0.4 mV (n=24) and -69.6±0.7 mV, (n=15), p=0.57, respectively). In addition, no significant differences were observed between the RMP of Ca$_v$3.2 wild type and null dorsal (-69.1±0.4 mV (n= 28) and -68.2±0.7 mV (n=24), respectively, p=0.25) and ventral (-69.6±0.7 mV (n=26) and -70.2±0.4 mV (n=15), respectively, p=0.39) neurons (Figure 3.6 A).

As with Ca$_V$3.2 wild type neurons, there were no differences in input resistance of Ca$_v$3.2 null dorsal and ventral stellate neurons at - 100 pA or current injection steps at RMP (Ca$_v$3.2 null dorsal and ventral input resistance = 45.5±3.3 MΩ (n=24) and 42.7±3.4 MΩ (n=15), p=0.56, Figure 3.6 B). However, the Ca$_v$3.2 null ventral neuron input resistance was significantly reduced compared with that of wild type neurons (55.3±4.2 MΩ, n=26, p=0.02).

Interestingly, a significant difference between Ca$_v$3.2 null dorsal and ventral neurons was observed when the input resistance was measured at +100 pA current injection

steps at RMP (dorsal and ventral input resistance = 71±5.2 MΩ (n=24) and 91.8±7.2

MΩ (n=15), p=0.03, t-test, Figure 3.6 C).
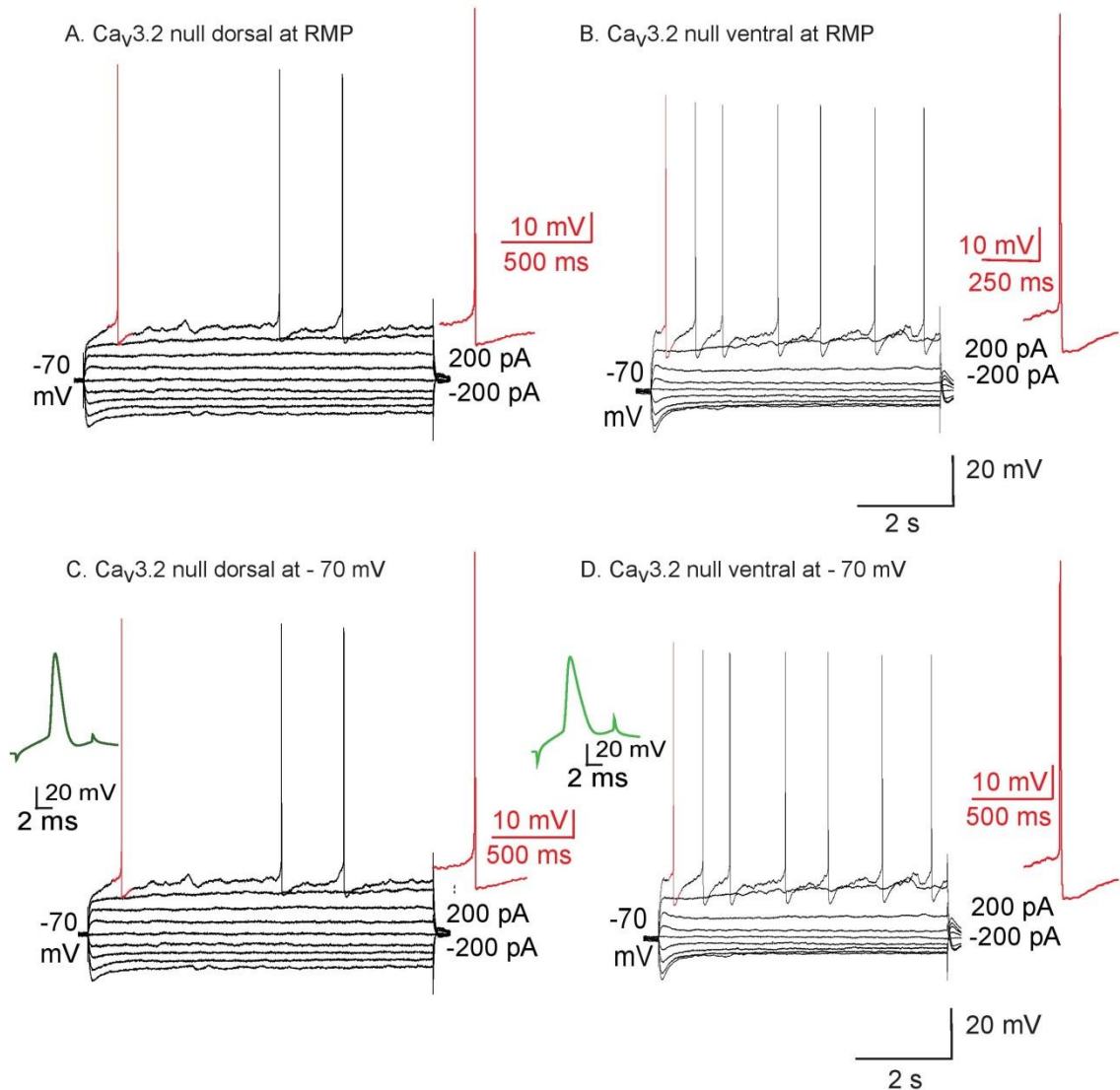
Figure 3.5. Whole cell current-clamp recordings obtained from Ca$_v$3.2 null mice.
Dorsal (A and C), and ventral (C and D) MEC L II stellate neurons at RMP (A and B)
and at -70 mV fixed membrane potential (C and D). The recordings at – 70 mV are
additionally enriched with single action potential traces of a typical dorsal (dark green)
and ventral (light green) Ca$_v$3.2 null cell. Enlarged (red) action potentials are shown to
illustrate the biphasic AHP.

It is however important to note that the significance (p=0.03) was decreased in

comparison to the Ca$_v$3.2 wild type neurons (p=0.001). Further, whilst no difference in

input resistance were observed between Ca$_v$3.2 null and wild type dorsal neurons, the input resistance when measured using a +100 pA step was greater in Ca$_V$3.2 null ventral neurons compared with wild type ventral neurons (112.2±7.9 MΩ (n=26), p=0.03, Figure 3.6 B).
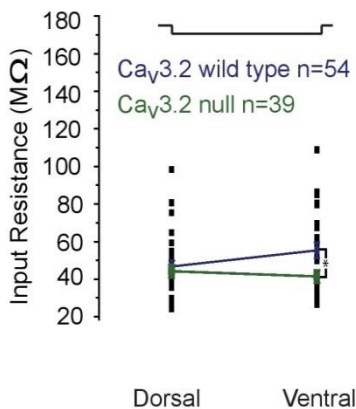
Furthermore, the reduction of the dorsal-ventral gradient in the input resistance of the Ca$_v$3.2 null neurons was even more striking when measured at fixed membrane potential of − 70 mV. Similar to that observed at RMP, with a −100 pA current injection there was no significant difference in input resistance between Ca$_v$3.2 null dorsal (43.4±2.9 MΩ, (n=24)) and ventral (43±3.8 MΩ, (n=15)) neurons (p=0.9, Figure 3.6 E). There was, though, a significant difference in input resistance between dorsal (66.3±4.3 MΩ, (n=24)) and ventral (81.8±5.8 MΩ, (n=15)) cells (p=0.04) when measured using a +100 pA step (Figure 3.6 F). However, it is important to note that it has been strikingly smaller that the difference reported for the wild type neurons (p<0.001). Additionally, when the comparison have been made exclusively between the Ca$_v$3.2 wild type and null ventral neurons, a significant difference in input resistance was observed at both −100 pA and +100 pA current injections (p=0.03 and p=0.02, respectively). Altogether these clearly indicated that deleting T-type Ca$_v$3.2 Ca^{2+} subunits resulted in decrease of the input resistance dorsal-ventral gradient found in the MEC L II SC.
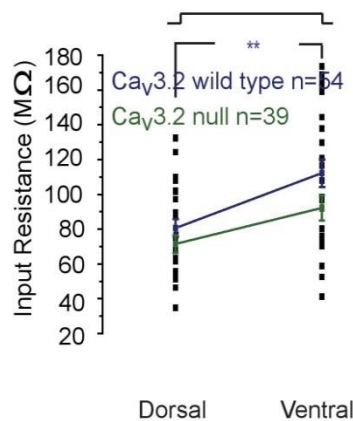
A. Resting Membrane Potential

Ca$_v$3.2 wild type dorsal n=28
Ca$_v$3.2 wild type ventral n=26
Ca$_v$3.2 null dorsal n=24
Ca$_v$3.2 null ventral n= 15
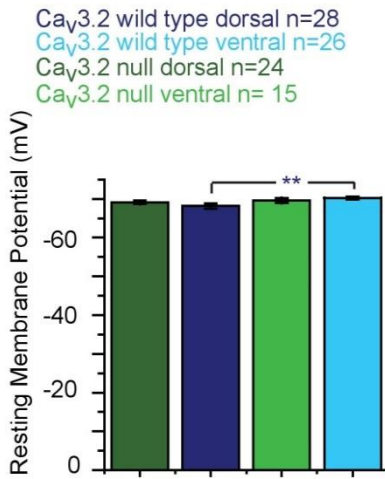
Figure 3.6. Intrinsic properties of Ca$_v$3.2 null SC A) RMP comparison between Ca$_v$3.2 wild type dorsal and ventral with null dorsal (-69.1±0.4 mV) and ventral (-69.6±0.7 mV) SC. B) and C) input resistance at rest of Ca$_v$3.2 wild type dorsal and ventral neurons compared with Ca$_v$3.2 null SC at – 100 pA and +100 pA current injection, respectively. E) and F) -70 mV input resistance of Ca$_v$3.2 wild type and null dorsal and ventral cells at – 100 pA and +100 pA current injection, respectively. Black squares show individual points obtained from Ca$_v$3.2 null SC. The dark green and blue (superimposed) lines connect points representing average values of Ca$_v$3.2 null and wild type SC, respectively. A comparison of the number of action potential recorded at D) RMP and G) set membrane potential of – 70 mV, between the four groups.

B. Input Resistance at -100 pA at RMP
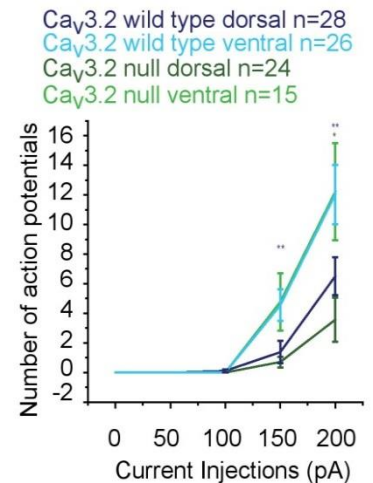
Ca$_v$3.2 wild type n=54
Ca$_v$3.2 null n=39

C. Input Resistance at +100 pA at RMP

Ca$_v$3.2 wild type n=54
Ca$_v$3.2 null n=39

D. Excitability at RMP

Ca$_v$3.2 wild type dorsal n=28
Ca$_v$3.2 wild type ventral n=26
Ca$_v$3.2 null dorsal n=24
Ca$_v$3.2 null ventral n=15

E. Input Resistance at -100 pA at - 70 mV

Ca$_v$3.2 wild type n=54
Ca$_v$3.2 null n=39

$p<0.02$

F. Input Resistance at +100 pA at - 70 mV

Ca$_v$3.2 wild type n=54
Ca$_v$3.2 null n=39

$p<0.001$

G. Excitability at - 70 mV

Ca$_v$3.2 wild type dorsal n=28
Ca$_v$3.2 wild type ventral n=26
Ca$_v$3.2 null dorsal n=24
Ca$_v$3.2 null ventral n=15
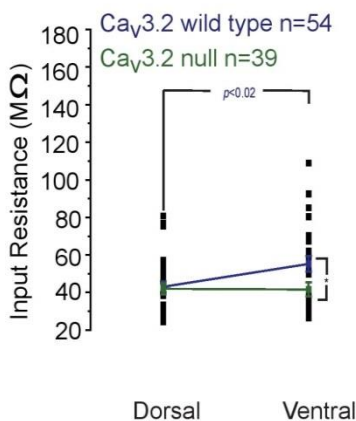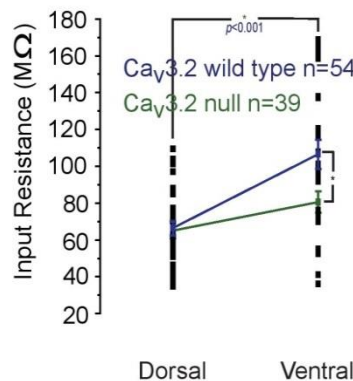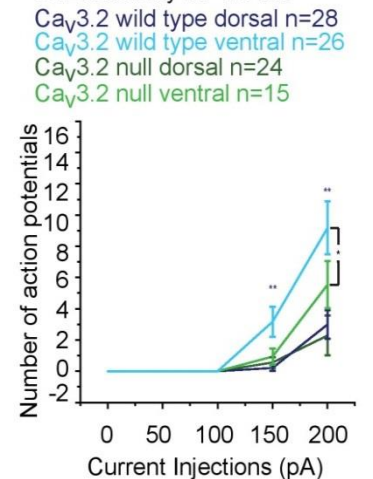
As for wild type neurons, I also determined the dorsal ventral gradient in RMP and input resistance of all SC found within MEC L II, including those that did not fall within 30 % of the ventral and dorsal borders. Using this approach, it was observed that $Ca_v3.2$ null neurons have smaller gradient ($R^2=0.0153$, n=42) in the RMP compared to $Ca_v3.2$ wild type cells ($R^2=0.0874$, n=59, Figure 3.7 A). Furthermore, at RMP, it was determined that the gradients in input resistance measured at both -100 pA step ($Ca_V3.2$ wild type and null = $R^2=0.0134$ and $R^2=0.0891$, respectively) and +100 pA step ($Ca_V3.2$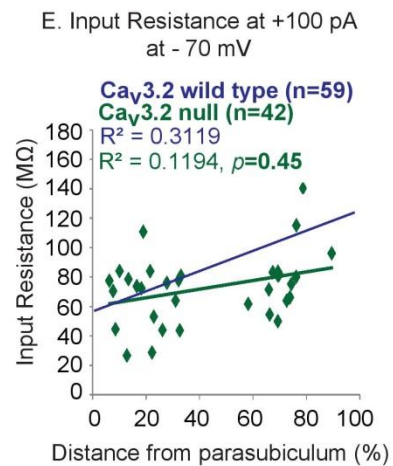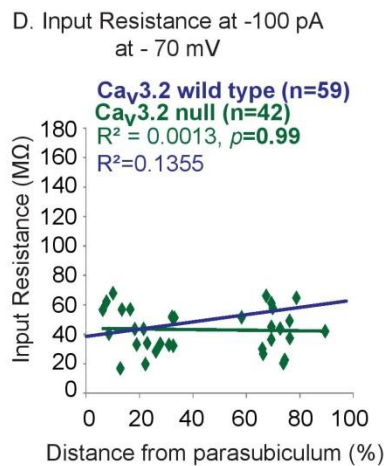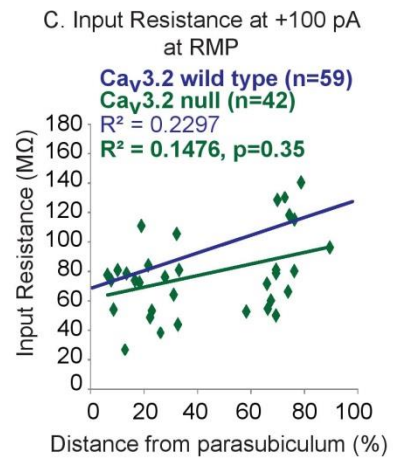 wild type and null = $R^2=0.2297$ and $R^2=1476$, respectively) were reduced in $Ca_v3.2$ null than wild type neurons (Figure 3.7 B and C). A similar effect was found at if the same current pulses were elicited from a fixed membrane potential of -70 mV (-100 pA pulse in $Ca_V3.2$ wild type and null = $R^2=0.1355$ and $R^2=0.0013$, respectively and +100 pA in $Ca_V3.2$ wild type and null = $R^2=0.3119$ and $R^2=0.1194$, respectively; Figure 3.7 D and E).

Overall, the data presented above suggest that the T-type $Ca_v3.2$ Ca^{2+} channels can potentially influence the RMP of the MEC L II SC. Importantly, the dorsal-ventral gradient present in these cells could be affected by significantly decreasing input resistance in the $Ca_v3.2$ null ventral neurons.

A. Resting membrane potential

Ca$_V$3.2 wild type (n=59)
Ca$_V$3.2 null (n=42)

R² = 0.0874
R² =0.0153, p=0.92
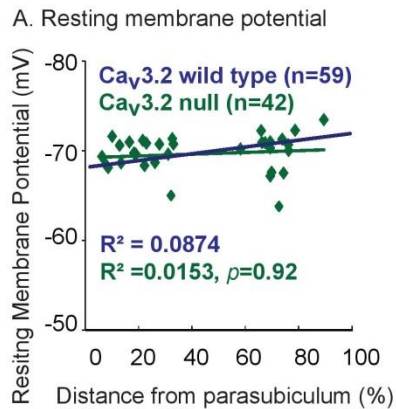
Figure 3.7. A comparison of the overall dorsal-ventral gradient between T-type Ca$_v$3.2 wild type and null cells. A) RMP values B) and C) input resistance measured at RMP for – 100 pA and +100 pA current injections, respectively D) and E) input resistance (at – 70 mV) with -100 pA and +100 pA current steps, respectively. The individual points (green) are displayed for Cav3.2 null only, the wild type line (blue) was superimposed from the data presented in the Fig 3.3

B. Input Resistance at -100 pA at RMP

Ca$_V$3.2 wild type (n=59)
Ca$_V$3.2 null (n=42)
R²=0.0891
R² = 0.0134, p=**0.93**

C. Input Resistance at +100 pA at RMP

Ca$_V$3.2 wild type (n=59)
Ca$_V$3.2 null (n=42)
R² = 0.2297
R² = 0.1476, p=0.35

D. Input Resistance at -100 pA at - 70 mV

Ca$_V$3.2 wild type (n=59)
Ca$_V$3.2 null (n=42)
R² = 0.0013, p=**0.99**
R²=0.1355

E. Input Resistance at +100 pA at - 70 mV

Ca$_V$3.2 wild type (n=59)
Ca$_V$3.2 null (n=42)
R² = 0.3119
R² = 0.1194, p=**0.45**

95
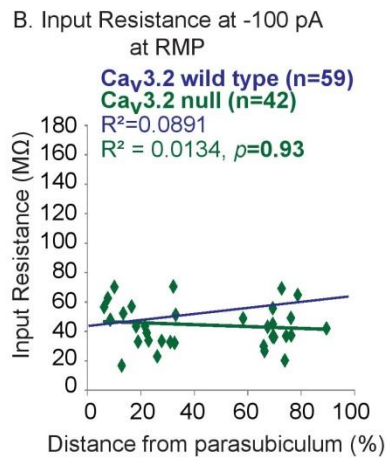
3.8 Excitability of the $Ca_v3.2$ null neurons showed decreased dorsal-ventral gradient in comparison to wild type littermates

As for the wild type neurons, I also determined if the number of action potentials evoked with increasing current steps (from +50 pA to +200 pA) were different between dorsal and ventral $Ca_v3.2$ null SC. Fewer action potentials were elicited in dorsal SC with a 5 s, +200 pA current pulse than in ventral cells (dorsal and ventral action potentials numbers = 3.6±1.5 spikes (n=24) and 12.2±3.3 spikes (n=15), p=0.03, Figure 3.6 D). However, when measured at a fixed membrane potential of – 70 mV, no significant differences in the numbers of action potentials existed between dorsal and ventral stellate neurons (Figure 3.6 G). Further, at – 70 mV membrane potential, significant differences in the number of action potentials elicited using a 5 s, +200 pA current pulse were detected between $Ca_v3.2$ null (5.5±1.5 spikes, n=15) and wild type (9.2±1.7 spikes, n=26) ventral neurons (Figure 3.6 G, p=0.05).

The reason for such a prominent difference in firing between $Ca_v3.2$ null ventral cells at RMP and at -70 mV, was the significant contribution of 3 neurons included in the dataset. Even though they did not affect the RMP average (approximately – 70mV), they were particularly depolarised in comparison to the rest of the cells in this group (RMP between -63 mV and - 66 mV). This affected the $Ca_v3.2$ null ventral SC firing properties measured at RMP.

The difference in the cell excitability could be explained by the changes in the kinetics of the action potential. Therefore, the properties of action potential waveform elicited by short (10 ms) current injection of $Ca_v3.2$ null neurons (Figure 3.5 C and D) were tested. As for the wild type, $Ca_v3.2$ null stellate dorsal and ventral neurons had similar action potential threshold, half width and amplitude properties to wild type neurons. These results suggest no apparent contribution of T-type $Ca_v3.2$ Ca^{2+} channels towards the action potential characteristics. Furthermore, there were little differences in the latency

for the 1st spike to be initiated with a given depolarization between Ca$_v$3.2 wild type and null dorsal and ventral neurons (Table 3.1). These findings have clearly shown that latency of the 1st spike also does not follow a dorsal-ventral gradient.

3.9 T-type Ca^{2+} Ca$_v$3.2 channels do not influence the amplitude of membrane potential sag

To test whether Ca$_v$3.2 null animals exhibited differences in the membrane potential sag, the comparison between null dorsal and ventral SC was performed. No difference was found between Ca$_v$3.2 wild type dorsal and ventral neurons (Table 3.1, Figure 3.12). Interestingly, the membrane sag amplitude ratio was significantly greater in Ca$_v$3.2 null dorsal neurons than ventral neurons at RMP (sag ratio amplitude in dorsal and ventral cells = 0.57±0.03, (n=28) and 0.47±0.03 (n=26), p=0.04, Table 3.1, Figure 3.12). The sag ratio amplitudes, though, were similar between dorsal Ca$_v$3.2 null and wild type neurons or between ventral Ca$_v$3.2 null and wild type neurons at RMP (Table 3.1, Figure 3.12). Furthermore, no significant difference in the sag (ratio) amplitude between all four groups was present when measured at fixed membrane potential of – 70 mV (Table 3.1, Figure 3.12).

3.10 Dorsal-ventral gradient in subthreshold activity of L II SC

Finally, the activity of Ca$_v$3.2 null SC at subthreshold membrane potentials was investigated. The half-width of αEPSPs of Ca$_v$3.2 null dorsal (11.8±1.1 ms, n=3) and ventral (12±1.3 ms, n=3) neurons were very similar and not different from wild type neurons (Figure 3.8 A and D). Interestingly, the Ca$_v$3.2 null ventral 50 Hz αEPSP summation ratio (1.6±0.04, n=3, (p=0.03)) was significantly lower than in ventral wild type neurons (2±0.12, n=5, Figure 3.8 C and F). Consequently, there was little difference in 50 Hz αEPSP summation ratios between Ca$_v$3.2 null ventral and dorsal (1.55±0.25, n=3, p=0.75, Figure 3.8 C and F) neurons.

In contrast, the summation ratios for 20 Hz αEPSPs were very similar between $Ca_v3.2$ wild type dorsal (1.12±0.06, n=4), wild type ventral (1.26±0.1, n=5), $Ca_v3.2$ null dorsal (1.1±0.04, n=3) and $Ca_V3.2$ null ventral (1±0.1, n=3) cells (Figure 3.8 B and E).
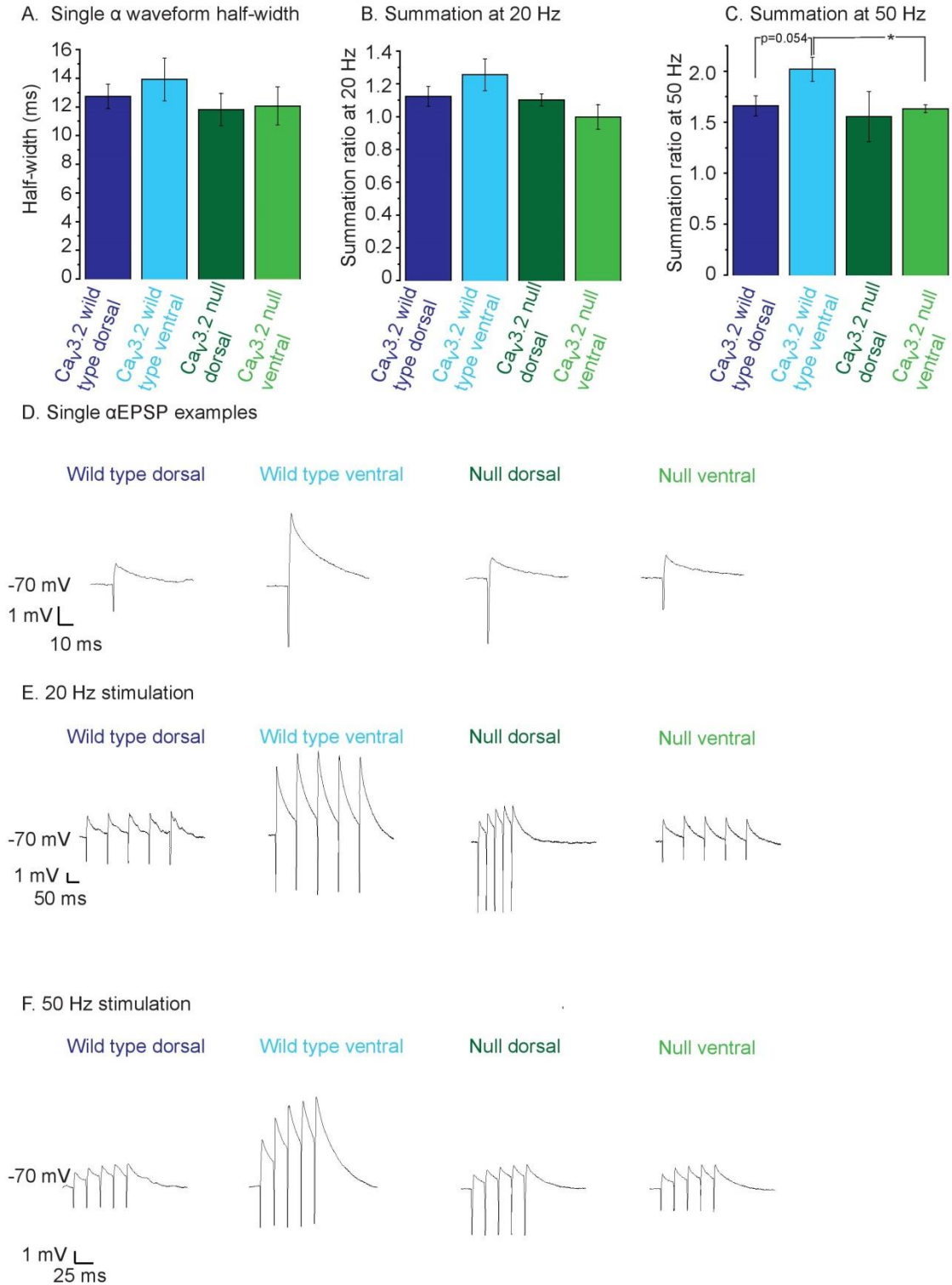
Figure 3.8. Figure showing αEPSP recordings. Summary of αEPSPs A) half-width obtained from single recordings and summation at B) 20 Hz and C) 50 Hz. D, E, and F show examples of αEPSPs recorded with single current stimulation, and at 20 Hz and 50 Hz respectively, obtained from $Ca_v3.2$ wild type dorsal (n=4) and ventral (n=5) as well as and null dorsal (n=3) and ventral (n=3) cells.

3.11 Oscillatory activity of L II SC

It has been previously shown, that the mean frequency of L II SC subthreshold membrane potential oscillation is higher in dorsal than in ventral neurons (Giocomo et al. 2007). Different ion channels, such as Na_p (Alonso and Llinas 1989) have been hypothesised to affect these oscillations. To determine whether T-type Ca^{2+} channels also affect the membrane oscillations, the mean power of sMPOs in the SC obtained from dorsal and ventral $Ca_v3.2$ wild type and null mice was measured. The analysis of current-clamp recordings showed that the SC have the largest sMPOs at the frequencies of 1-4 Hz. The oscillations were gradually decreasing at 4-8 Hz, followed by 8-12 Hz at both RMP and at membrane potential of – 70 mV (Figure 3.9 and Figure 3.10) .

However, no significant difference in the sMPOs power between $Ca_v3.2$ wild type dorsal and ventral cells was observed at both RMP (Figure 3.9, Appendix 6), and at a set membrane potential of – 70 mV (Figure 3.10, Appendix 6). More importantly, no significant difference between $Ca_v3.2$ null and wild type cells was present (Figure 3.9 and Figure 3.10, Appendix 6). These results suggest, that T-type $Ca_v3.2$ Ca^{2+} channels do not contribute towards the sMPOs activity in the MEC L II SC.
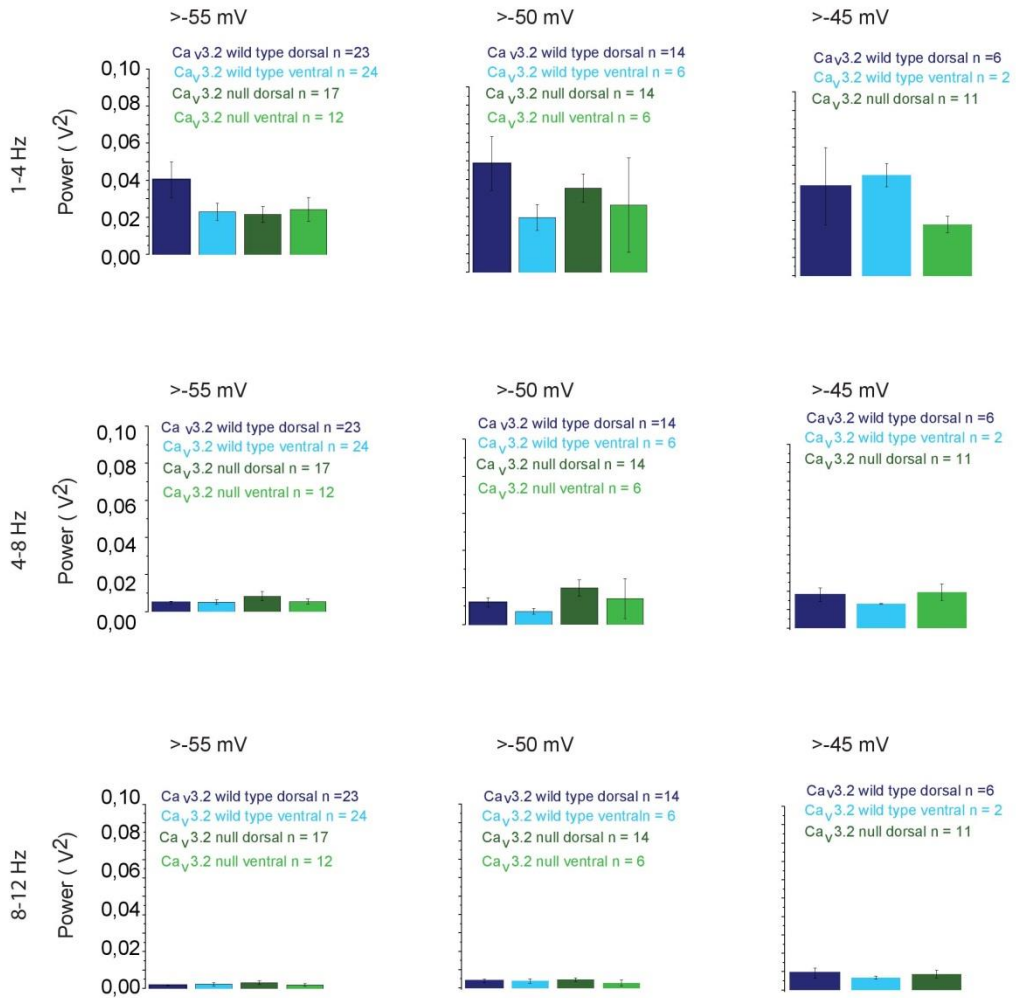
Figure 3.9. The mean power of sMPOs of L II SC recorded at RMP. The data were collected using current-clamp recordings.
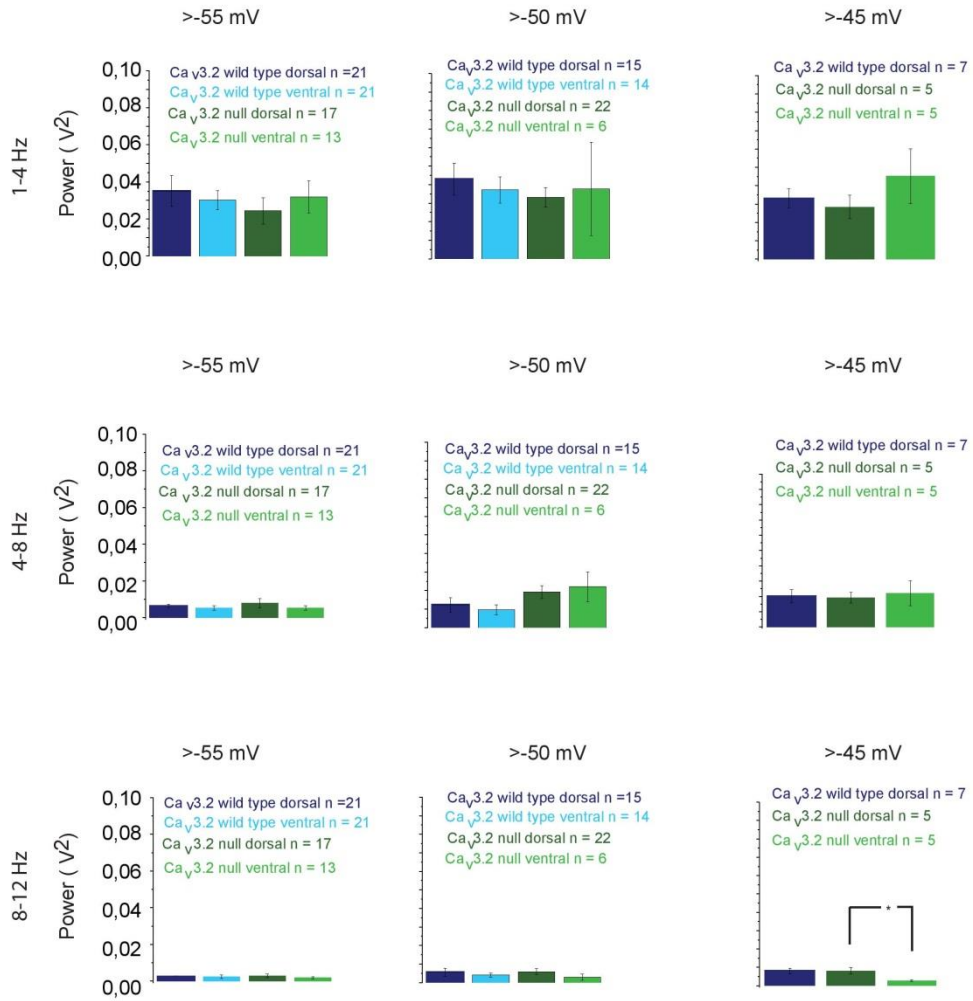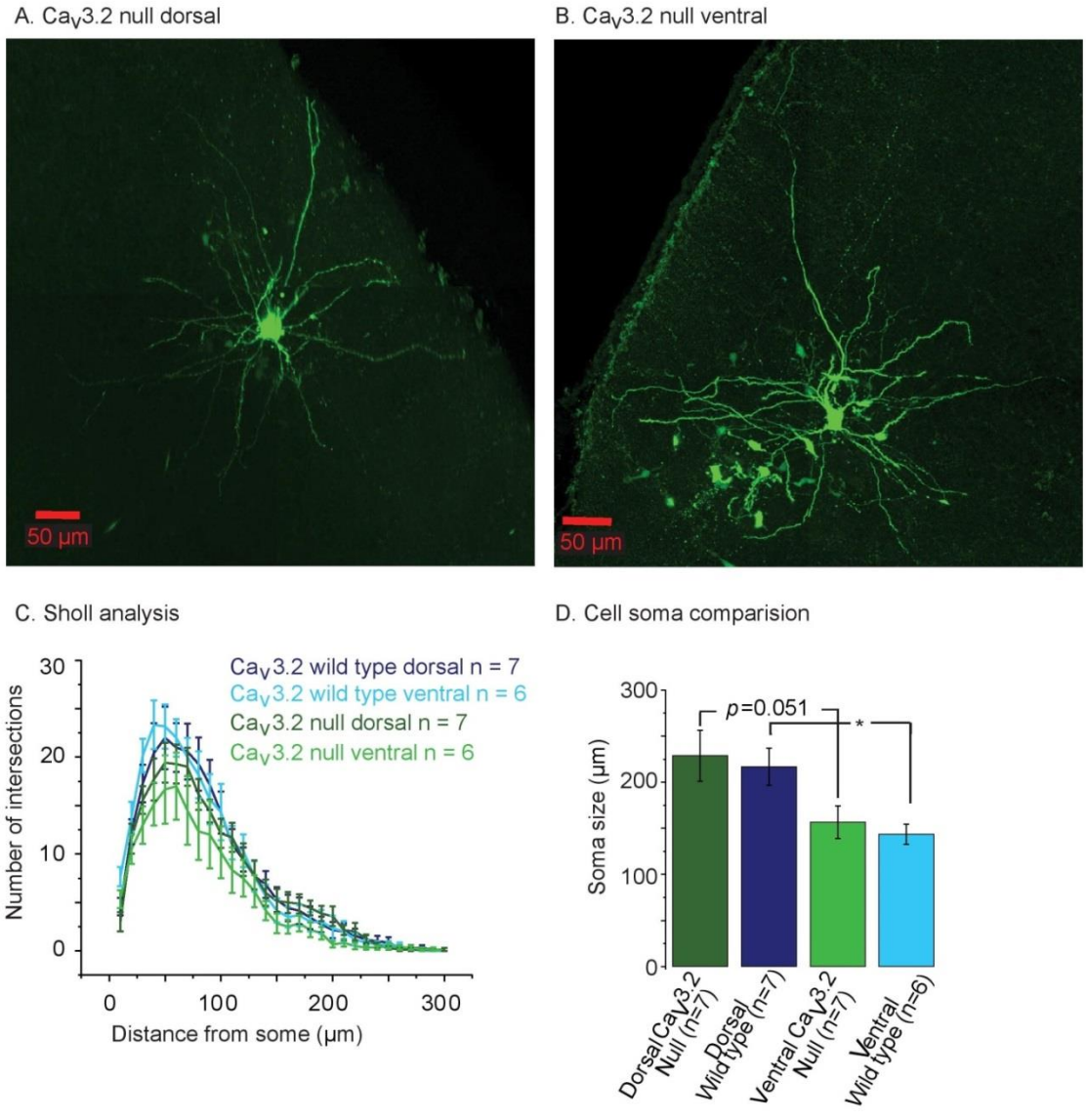
Figure 3.10. The mean power of sMPOs recorded at a set membrane potential of – 70 mV. Single (*) denote significance at p<0.05.

3.12 Morphological properties of the $Ca_v3.2$ null cells

To test whether knocking out of the $Ca_v3.2$ gene had an effect on the cell morphology and confirm the identity of the patched neurons, the morphological analysis of $Ca_v3.2$ null SC was performed (Figure 3.11 A and B). The dorsal and ventral $Ca_v3.2$ null SC soma size was similar to wild type cells (dorsal and ventral cell soma area = 228.7 ± 27.5 μm^2, n=7 and 156.6 ± 17.7 μm^2, n=7, $p=0.051$, respectively, Figure 3.11 D). Additionally, the dorsal and ventral cell somata of $Ca_v3.2$ null and wild type stellate neurons were very similar (dorsal $Ca_v3.2$ null and wild type somata = 228.7 ± 27.5 μm^2 (n=7) and 216.8 ± 20.2 μm^2 (n=7), $p=0.73$, respectively; ventral $Ca_v3.2$ null and wild type soma = 156.6 ± 17.7 μm^2 (n=7) and 143.6 ± 10.8 μm^2 (n=6), $p=0.55$, respectively).
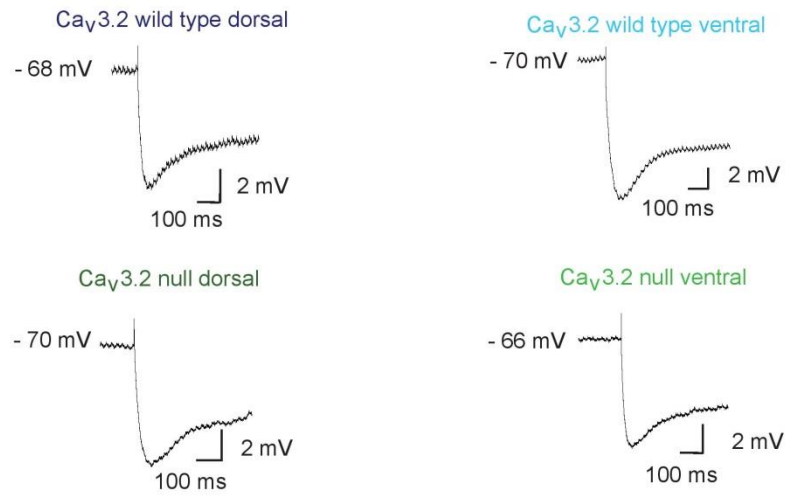
I also investigated the dendritic complexity of the $Ca_v3.2$ null dorsal and ventral neurons. To compare all four cell types and to assess whether they differ in their dendritic complexity at any particular radius (10-290 µm), the data were analysed in R software using mixed (between 2-way ANOVA and repeated measured ANOVA) statistical model. No significant differences in the number of dendritic intersections between the four groups was found ($p=0.637$). Furthermore, there was no interaction between the effect of the radius and the cell type ($p=0.368$, Figure 3.11 C). Additionally, there was no difference in the number of primary dendrites between $Ca_v3.2$ null dorsal (7.9 ± 0.7 dendrites, (n=7)) and ventral (6.7 ± 0.6, (n=6), $p=0.23$) cells. Finally, no difference between wild type and null dorsal (7.7 ± 0.5 dendrites, (n=7) and 7.9 ± 0.7 dendrites, (n=7), respectively, $p=0.87$) and ventral (6.8 ± 0.7 dendrites, (n=6) and 6.7 ± 0.6 dendrites, (n=6), respectively, $p=0.86$) neurons was observed. Overall, these results confirmed that a global deletion of T-type $Ca_v3.2$ Ca^{2+} channels did not have any major effect on the morphological properties of the MEC L II SC.

A. Ca$_V$3.2 null dorsal

B. Ca$_V$3.2 null ventral

C. Sholl analysis

Ca$_V$3.2 wild type dorsal n = 7
Ca$_V$3.2 wild type ventral n = 6
Ca$_V$3.2 null dorsal n = 7
Ca$_V$3.2 null ventral n = 6
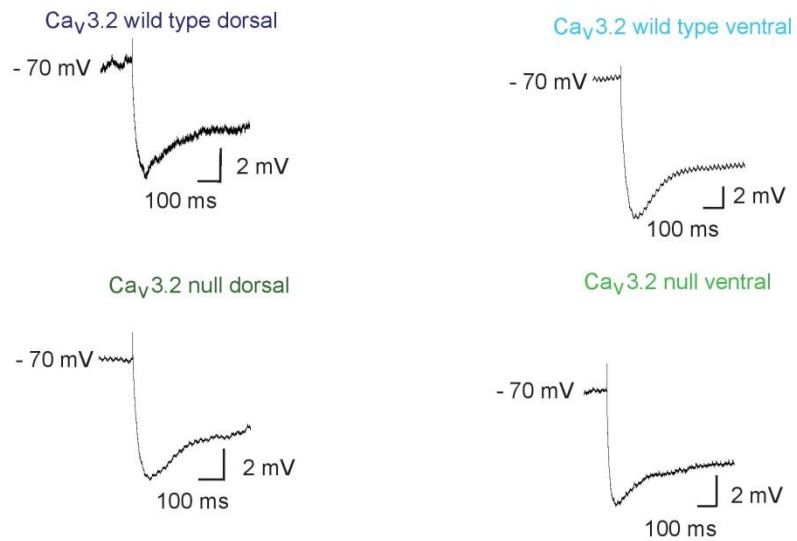
D. Cell soma comparision

p=0.051

*

Figure 3.11. Morphology of Ca$_v$3.2 null cells. A confocal image of a typical T-type Ca$_v$3.2 Ca^{2+} null dorsal (A) and ventral (B) neuron. The Sholl analysis (C) and soma size comparison (D) of Ca$_v$3.2 wild type dorsal (dark blue), ventral (light blue) and Ca$_v$3.2 null dorsal (dark green) and ventral (light green) MEC L II SC.

1) Membrane Potential Sag at RMP

Ca$_V$3.2 wild type dorsal

- 68 mV

2 mV

100 ms

Ca$_V$3.2 wild type ventral

- 70 mV

2 mV

100 ms

Ca$_V$3.2 null dorsal

- 70 mV

2 mV

100 ms

Ca$_V$3.2 null ventral

- 66 mV

2 mV

100 ms

2) Membrane Potential Sag at - 70 mV

Ca$_V$3.2 wild type dorsal

- 70 mV

2 mV

100 ms

Ca$_V$3.2 wild type ventral

- 70 mV

2 mV

100 ms

Ca$_V$3.2 null dorsal

- 70 mV

2 mV

100 ms

Ca$_V$3.2 null ventral

- 70 mV

2 mV

100 ms

Figure 3.12. **Examples of membrane potential sags recorded at – 100 pA.** The recordings were made at both RMP (1) and the membrane potential of – 70 mV (2).

Cell types				
	Wild type dorsal	**Wild type ventral**	**Null Dorsal**	**Null Ventral**
Action potential amplitude	69.4±1.5 mV (n=23)	72.8±1.4 mV (n=22)	70.4±1.5 mV (n=22)	73±2.3 mV (n=14)
Action potential half width	1.57±0.05 ms (n=23)	1.7±0.06 ms (n=22)	1.5±0.04 ms (n=22)	1.52±0.05 ms (n=14)
Action potential threshold	-53.3±1.1 mV (n=23)	-46.2±5.1 mV (n=22)	-53.9±1.4 mV (n=22)	-51.7±1.4 mV (n=14)
Sag ratio amplitude at RMP	0.58±0.03 (n=28)	0.55±0.03 (n=26)	0.57±0.03 (n=24)	0.47±0.03 (n=15)
Sag ratio amplitude at - 70 mV	0.56±0.02 (n=28)	0.57±0.03 (n=26)	0.56±0.03 (n=24)	0.49±0.04 (n=15)
Latency to 1st spike	182±0.2 ms (n=28)	161±0.24 ms (n=26)	176±0.26 ms (n=24)	175±0.31 ms (n=15)
T-test (*p* values)				
	Wild type dorsal vs ventral	**Null dorsal vs ventral**	**Dorsal wild type vs null**	**Ventral wild type vs null**
Action potential amplitude (mV)	0.10	0.35	0.65	0.95
Action potential half width (ms)	0.25	0.73	0.25	0.10
Action potential threshold (mV)	0.19	0.26	0.70	0.31
Sag ratio amplitude at RMP	0.44	0.04	0.72	0.05
Sag ratio amplitude at - 70 mV	0.89	0.11	0.97	0.11
Latency to 1st spike (ms)	0.53	0.99	0.85	0.74

Table 3.1. A summary of different properties of Ca$_v$3.2 null and wild type neurons.
The sag was as a ratio between peak hyperpolarisation at at – 100 pA step and peak steady state hyperpolarization. No difference in single action potential properties between Ca$_v$3.2 wild type dorsal and ventral with Ca$_v$3.2 null dorsal and ventral was observed. Furthermore, no significant difference for the 1[st] spike latency and sag measured at -70 mV fixed membrane potential was reported between Ca$_v$3.2 null and wild type dorsal and ventral SC. A significant difference in sag between Ca$_v$3.2 null dorsal and ventral neurons has been observed at RMP.

3.13 Summary

In agreement with previous findings, a dorsal-ventral gradient in the intrinsic properties of the MEC L II SC was observed. The gradient was present when comparing RMP, the input resistance and excitability. Not surprisingly, the differences in both input resistance and excitability were more prominent when measured at a set membrane potential (-70 mV) than when measured at RMP. Interestingly, the difference in input resistance was particularly prominent at the +100 pA current injection step, which has been shown to result in the membrane potential of approximately – 50 mV, at which T-type $Ca_v3.2$ channels are active (Bruehl and Wadman 1999). Indeed, the recordings obtained from $Ca_v3.2$ null mice showed a significantly reduced gradient in the RMP, input resistance and the excitability. Their apparent reduction in the $Ca_v3.2$ null neurons has arisen due to a decrease in action potential number and the input resistance exclusively in the ventral neurons, rather than an overall shift in the cell properties across the whole MEC L II. These results highlight the importance of T-type $Ca_v3.2$ channels in establishing dorsal-ventral gradient of intrinsic membrane properties in MEC L II SC.

In my report, the overall values of input resistance have been observed to range from approximately 50 to 170 MΩ at RMP, depending on the location of the cell within the MEC. In comparison, it has been previously reported that, at RMP, L II SC input resistance vary from 20 to 80 MΩ (Alonso and Llinas 1989; Garden et al. 2008; Nolan et al. 2007). The observed disparity has most likely resulted from the differences of the intracellular solution composition. Most importantly, it has not affected the dorsal-ventral gradient of the intrinsic properties of the MEC L II SC.

Furthermore, no differences in action potential kinetics, latency to the first spike or sag amplitude were found between $Ca_v3.2$ wild type dorsal and ventral neurons. These

results are different from previous reports. The discrepancies are likely to be the results of differences in protocols used. In particular, for the latency measurements:

1) Both, Alonso and Klink (1993) and Fuchs, Neitz et al. (2016) use relatively short pulses (300 ms to 500 ms) to initiate action potentials, whereas I use a 5 s pulse.

2) The amount of current injected to elicit the action potentials. I measured the latency to the 1st spike irrespective of the current injection which spanned from +150 pA to + 300 pA. The magnitude of the depolarizing current pulse used to elicit the action potentials by Alonso and Klink (1983) and Fuchs et al. (2016) is not reported.

It is therefore likely, that the differences in the dorsal-ventral SC excitability is purely an effect of the input resistant gradient or that other (than Ca$_v$3.2) ion channels had an effect on the firing. Additionally, no difference in the single action potential properties, the sag and the latency were found between Ca$_v$3.2 wild type and null neurons. Together, the data suggest that T-type Ca$_v$3.2 Ca^{2+} channels do not influence these properties.

Furthermore, the data suggest that T-type Ca^{2+} channels do not contribute to membrane oscillations of L II SC. Next, no difference in the αEPSPs half-width between dorsal and ventral Ca$_v$3.2 wild type cells was observed. It is important to note that the potential effect could have been masked due the access resistance issues. Interestingly, in agreement with previous studies (Garden et al. 2008), my results show a trend towards the dorsal-ventral gradient in the αEPSPs and summation ratio at 50 Hz stimulation. More importantly, no difference was observed between the Ca$_v$3.2 null neurons, and a significant difference between Ca$_v$3.2 null and wild type ventral cells was observed suggesting a possibility of T-type Ca$_v$3.2 Ca^{2+} channels contribution in shaping the SC synaptic integration gradient across dorsal-ventral axes of MEC L II.

However, to draw any further conclusions the sample number for these experiments has to be significantly increased, as it is possible that the significance values between $Ca_v3.2$ null and wild type ventral was caused by particularly low sample number of the first group (n=3, SEM=0.04).

4. The dorsal-ventral gradient was affected by pharmacological agents, TTA-P2 and NiCl₂.

4.1 Introduction

Using T-type $Ca_v3.2$ Ca^{2+} global knock-out mice, I established that $Ca_v3.2$ channels contribute towards the dorsal-ventral gradient of the SC intrinsic properties. The results showed that $Ca_v3.2$ channels contribute significantly more prominently to ventral, rather than dorsal, L II MEC SC activity. To confirm these observations, in this chapter, I used two pharmacological agents, $NiCl_2$ and TTA-P2, to inhibit Ca_v3 T-type channels.

To-date, three subtypes of these channels have been described. Using molecular cloning techniques, it has been possible to characterise $Ca_v3.1$ (Perez-Reyes et al. 1998), $Ca_v3.2$ (Cribbs et al. 1998) and $Ca_v3.3$ (Lee, Daud, et al. 1999) isoforms. Importantly, $Ca_v3.2$ subunit has been shown to be sensitive to low concentrations of $NiCl_2$ (IC_{50}=13 µM), whereas both $Ca_v3.3$ and $Ca_v3.1$ have required much higher dose of the drug to be inactivated (IC_{50}=216 µM and IC_{50}=250 µM, respectively, (Lee, Gomora, et al. 1999)). Further studies have revealed that this is due to the unique properties of S3-S4 loop, which contains His-191, that makes $Ca_v3.2$ sensitive to low $NiCl_2$ concentrations (Kang et al. 2006). This property of $NiCl_2$ made it a better pharmacological tool to investigate the role of $Ca_v3.2$ channels than for example mibefradil (Martin et al. 2000) or other ions such as La^{3+}, Cd^2+, Zn^{2+}, Co^{2+} (Kaneda and Akaike 1989) which does not have subtype selectivity.

The vast majority of previously used pharmacological blockers of T-type Ca^{2+} channels, such as ethosuximide, also displayed constrained usability due to their selectivity and potency (McGivern 2006; Leresche et al. 1998), or required relatively high concentrations to be effective such as D-600 (Kaneda and Akaike 1989) or diltiazem (Kaneda et al. 1990) with the inhibition IC_{50} values of 4.4 x10^{-5} M and 8.2 x 10^{-5} M, respectively. I therefore decided to use another T-type Ca^{2+} channel antagonist, TTA-

P2 (Shipe et al. 2008). This compound has been shown to be a selective and potent blocker of Ca_v3 T-type Ca^{2+} channels (Dreyfus et al. 2010; Choe et al. 2011). This use of two independent pharmacological agents allowed me to examine the reliability of the knock-out model and whether any remaining $Ca_v3.3$ current (no $Ca_v3.1$ has been previously observed to be present in the EC (Huang et al. 2011)) exists in MEC L II SC. Thus, in this chapter, I compared the intrinsic membrane properties, including the input resistance, and excitability, before and after treatment with each drug under whole-cell current-clamp recordings from $Ca_v3.2$ wild type and null mice.

4.2 The $Ca_v3.2$ pharmacological inhibitor, $NiCl_2$, affects the intrinsic membrane properties of wild type ventral but not dorsal neurons.

Taking advantage of the unique selectivity of $NiCl_2$ at low concentrations, 50 µM of the drug was bath applied whilst recording from MEC L II SC under current-clamp conditions. 5 s current injection steps (from -200 pA to 300 pA, at 50 pA intervals) were applied onto the cells to record the intrinsic membrane properties at RMP and a set membrane potential of – 70 mV under control conditions (for approximately 15-20 min each), in the presence of the drug (10-20 min) and during washout (15-20 min).

Application of $NiCl_2$ caused a significant reduction in input resistance, measured using a +100 pA current step, and numbers of action potentials elicited by depolarizing current steps in $Ca_v3.2$ wild type ventral neurons at a holding potential of -70 mV. The changes were partially reversible during washout (Figure 4.1 B). In contrast, no differences in input resistance measured using +100 pA step or action potential firing was observed in wild type dorsal cells (Figure 4.1 A).

I quantified the changes in input resistance. When measured at +100 pA step, I found that the input resistance was significantly reduced in the presence of $NiCl_2$ (93.5±13.5 MΩ, n=6) compared with under control conditions (119±15.1 MΩ, n=6, $p<0.002$, Figure 4.2 C, Appendix 1) in wild type ventral cells. The decrease in input resistance

recovered after approximately 20 min during washout (110±11.9 MΩ, n=6). In contrast, no difference in input resistance was observed at the -100 pA current injection step (65.8±10.7 MΩ, 66.2±9.4 MΩ, 75.2±8.7 MΩ for control, $NiCl_2$ and washout conditions, respectively, Appendix 1).

Interestingly, $NiCl_2$ had no effect on input resistance in wild type dorsal neurons when measured at either +100 pA (Figure 4.2 A) or – 100 pA current injections (Appendix 1).
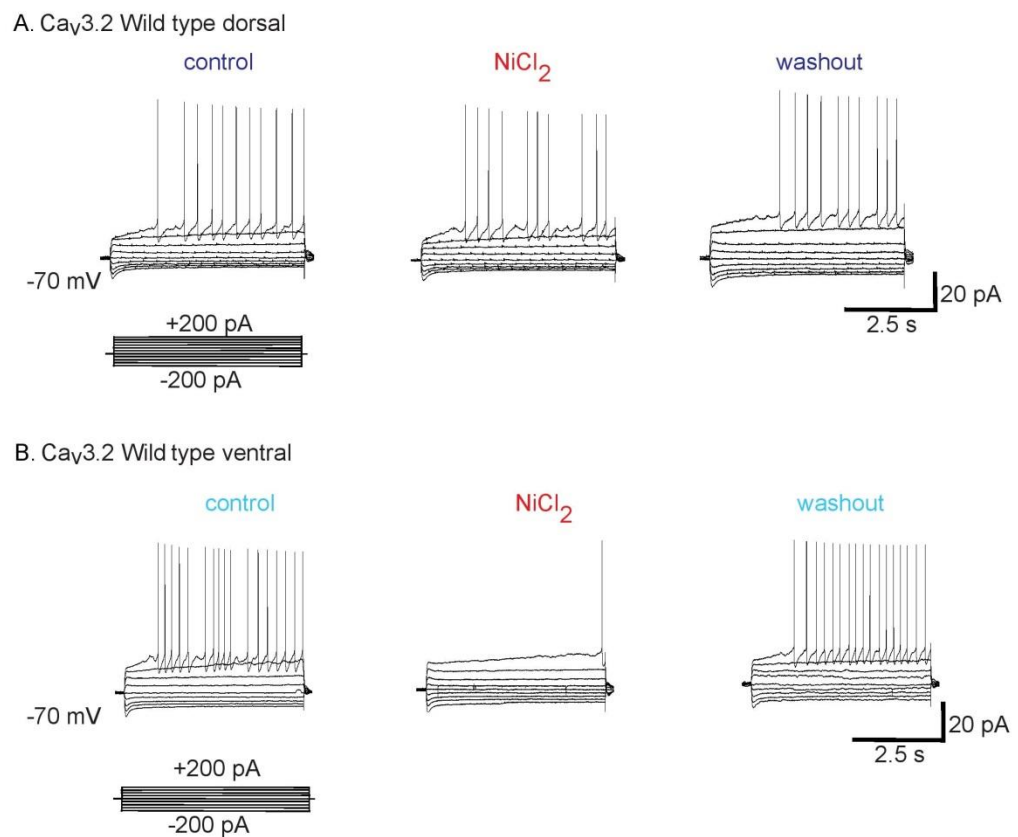
Figure 4.1. Example recordings from $Ca_V3.2$ wild type cells. Traces show A) dorsal and B) ventral neurons. The traces were obtained in response to hyperpolarising and depolarising current pulses before (left), during (middle) and after washout (right) of 50 µM $NiCl_2$.

Additionally, the number of the action potentials elicited with specific current injections were decreased during $NiCl_2$ application compared with control conditions in wild type

ventral neurons (Figure 4.2 D, Appendix 1). The effect partially recovered with washout of $NiCl_2$. As expected from the input resistance data, no significant difference in the number of action potentials were observed in the absence and presence of $NiCl_2$ in wild type dorsal neurons. There was no change in cell excitability during washout either (Figure 4.2 B, Appendix 1).

To investigate whether a decrease of excitability of $Ca_v3.2$ wild type ventral neurons was a result of changes in the action potential properties, I used short single current injection protocol to test the effects of $NiCl_2$ on the threshold, amplitude and half-width of single action potentials. The measurements were taken before, during and after bath application of $NiCl_2$. No significant differences in action potential properties were observed in $Ca_v3.2$ wild type dorsal (n=5) or wild type ventral (n=5) cells between control conditions and in the presence of $NiCl_2$ (Table 4.1).
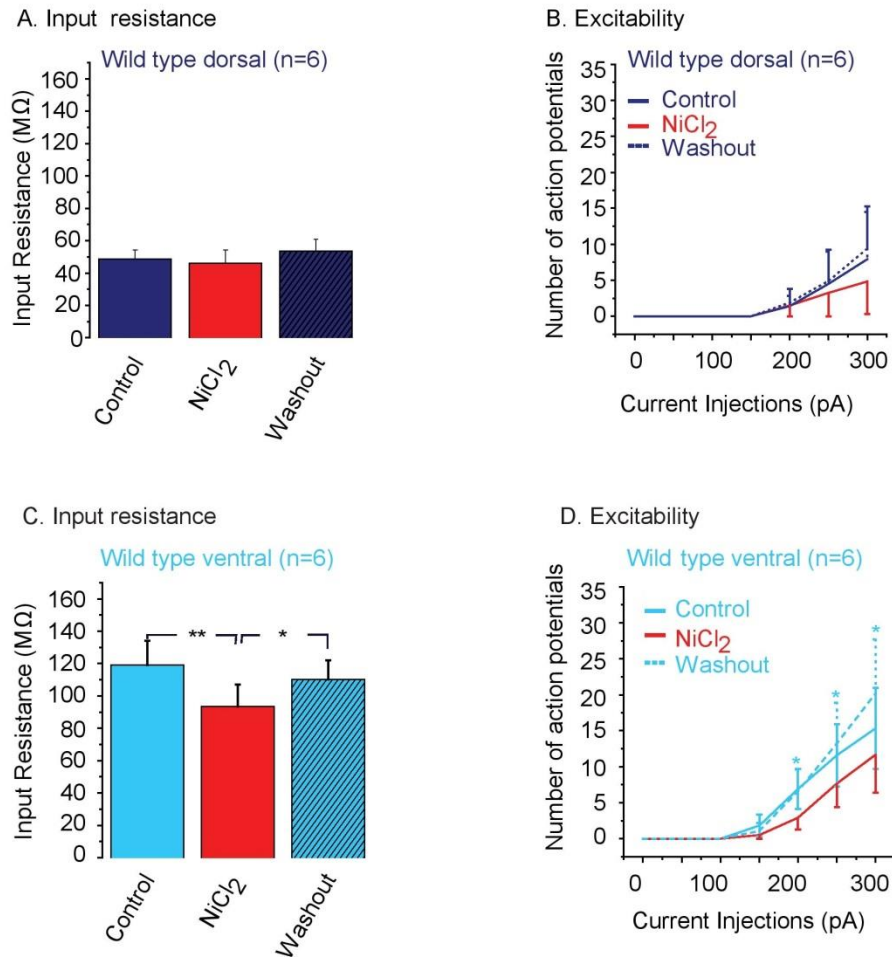
Figure 4.2. Graphs illustrating the input resistance and the excitability of the wild type neurons. Data obtained from in wild type dorsal (A and B) and ventral (C and D) cells before (dark and light blue, respectively), during (red) and after (shaded area/ dotted line) treatment with 50 µM NiCl$_2$. The input resistance was recorded at +100 pA and action potential number was measured at a set membrane potential of -70 mV (detailed numerical values can be found in the Appendix 1).

4.3 The Ca$_v$3 pharmacological inhibitor, TTA-P2, also preferentially affected the intrinsic membrane properties of wild type ventral neurons.

I also used a second selective T-type Ca$_v$3 channel inhibitor, TTA-P2, IC$_{50}$=100 nM, (Dreyfus et al. 2010; Choe et al. 2011) to confirm my NiCl$_2$ observations. Current-clamp recordings at a fixed membrane potential of -70 mV were once again obtained from dorsal and ventral L II SC. Recordings were obtained in the absence, presence and during washout of TTA-P2 (100 nM).

Bath-application of TTA-P2 resulted in a clear decrease in the input resistance and number of action potentials elicited with depolarization in wild type ventral (Figure 4.3 C), but not dorsal (Figure 4.3 A) neurons.
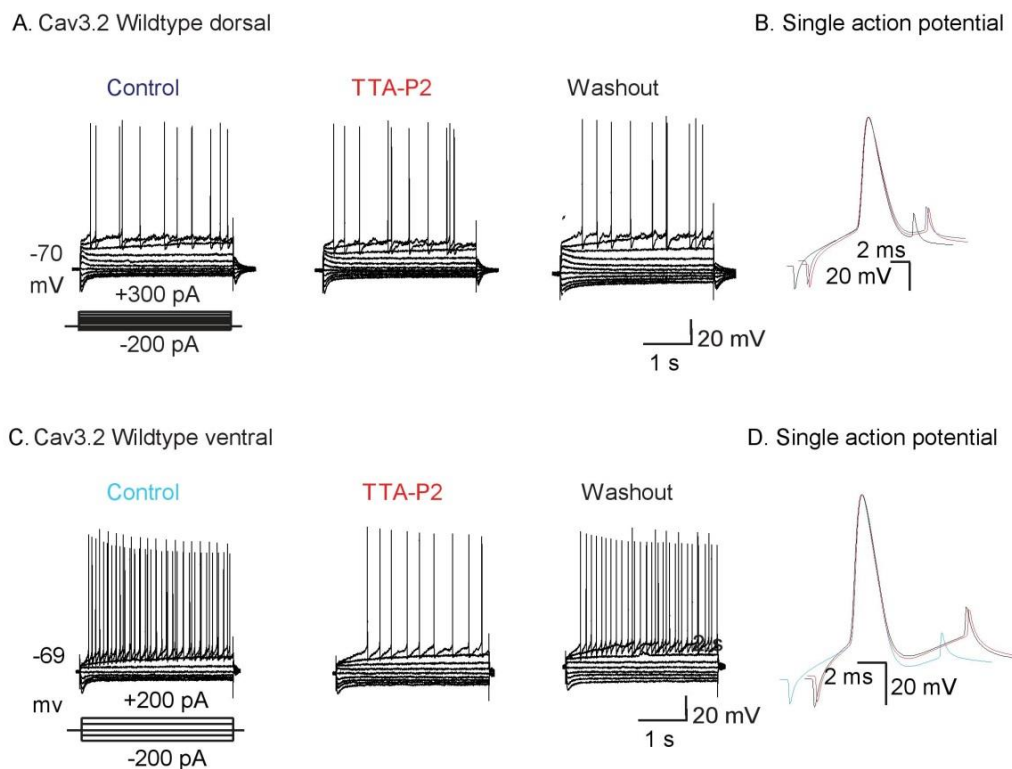
Figure 4.3. Example recordings from wild type neurons. The traces were obtained from A) dorsal and C) ventral cells in response to hyperpolarising and depolarising current pulses before (left), during (middle) and after washout (right) of 100 nM TTA-P2. Superimposed traces of single action potentials recorded from Ca$_v$3.2 wild type B) dorsal (dark blue) and D) ventral (light blue) neurons. Red lines represents TTA-P2 and black washout traces.

I then quantified the effects of TTA-P2 on input resistance at the – 100 pA and +100 pA current injection steps. The data showed a significant decrease in input resistance measured at +100 pA between control conditions (96.7±11.3 MΩ, n=8) and in the presence of TTA-P2 (78.5±8.5 MΩ, n=8, $p<0.003$, Figure 4.4 C, Appendix 2) in wild type ventral neurons. The input resistance recovered after approximately 20 min of washout of TTA-P2 (88.9±10.1 MΩ, n=8). In contrast, no difference in the input resistance ($p=0.98$ for control versus TTA-P2) was observed when measured at -100 pA current injection step (input resistance = 49.2±5.2 MΩ (n=8), 49.2±6 MΩ (n=8), 62±7.8 MΩ (n=8) for control, TTA-P2 and washout conditions, respectively, Appendix 2).

Similar to my findings with NiCl$_2$, TTA-P2 had no effect on the input resistance of wild type dorsal neurons measured with either -100 pA (38.7±4.2 MΩ (n=6), 36.7±4.5 MΩ (n=6), 47.2±6.6 MΩ (n=6) for control, TTA-P2 and washout conditions, respectively, $p=0.67$ for control versus TTA-P2, Appendix 2) or +100 pA (62.7±7.6 MΩ (n=6), 58.9±7.4 MΩ (n=6), 67.8±7.7 MΩ (n=6) for control, TTA-P2 and washout conditions, respectively, Figure 4.4 A, p=0.13 for control versus TTA-P2 current injections. See Appendix 2 for detailed numerical values).

Consistent with my findings with NiCl$_2$, application of 100 nM of TTA-P2 also decreased the number of the action potentials evoked with depolarizing current injections in the presence of TTA-P2, compared with that in the absence, in Ca$_v$3.2 wild type ventral neurons (Figure 4.4 D, Appendix 2). The effect partially recovered during washout. Similarly to NICl$_2$ data, wild type dorsal neurons showed no significant differences in the number of action potentials elicited with depolarizing steps between control condition, with TTA-P2 and during washout (Figure 4.4 B, Appendix 2). As with the NiCl$_2$, application of TTA-P2 onto Ca$_v$3.2 wild type dorsal (n=4, Figure 4.4 B) and ventral (n=6, Figure 4.4 D) cells did not affect action potential threshold, amplitude and half width (Table 4.2)
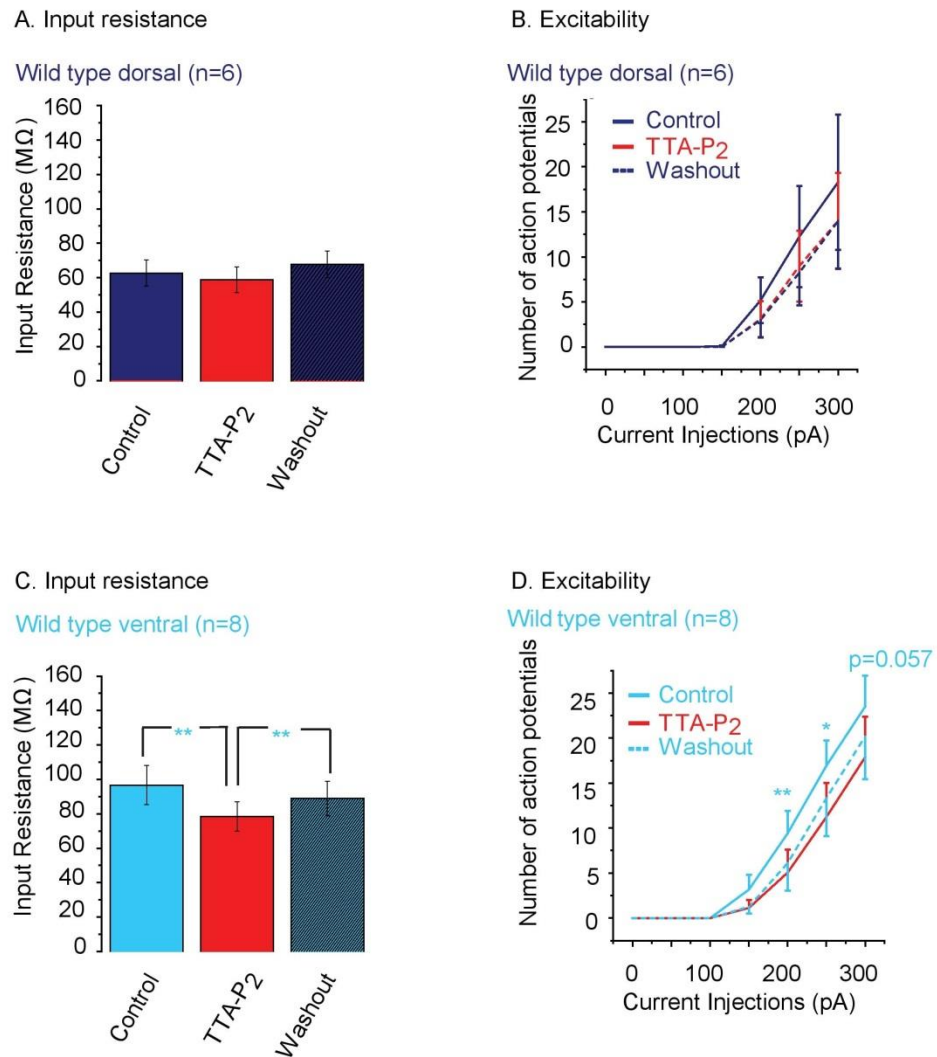
Figure 4.4. Graphs illustrating the changes in the excitability and the input resistance of wild type neurons upon TTA-P2 application. Dorsal (A and B) and ventral (C and D) neurons before (dark and light blue, respectively), during (red) and after (shaded area/dotted line) treatment with 100 nM TTA-P2. The reported input resistance was measured at +100 pA whereas action potential number was recorded at set membrane potential of -70 mV (see Appendix 2 for detailed values).

4.4 The intrinsic properties of Ca$_v$3.2 null neurons were not affected by application of the pharmacological inhibitor, NiCl$_2$.

Using a global Ca$_v$3.2 knock-out mouse model, I have shown that the dorsal-ventral gradient in the intrinsic properties of the L II SC present in the Ca$_v$3.2 wild type littermates, is significantly diminished in the null neurons, indicating that Ca$_v$3.2 channels contribute towards the dorsal-ventral gradient. In order to confirm these results and to determine whether the effects of NiCl$_2$ above were due to inhibition of Ca$_V$3.2 channels, current-clamp recordings were obtained from Ca$_V$3.2 null neurons in the absence and presence of NiCl$_2$ (50 µM). This compound had little effect on either input resistance or excitability of Ca$_v$3.2 null dorsal (Figure 4.5 A) and ventral (Figure 4.5. B) neurons.

A. Ca$_V$3.2 null dorsal

B. Ca$_V$3.2 null ventral
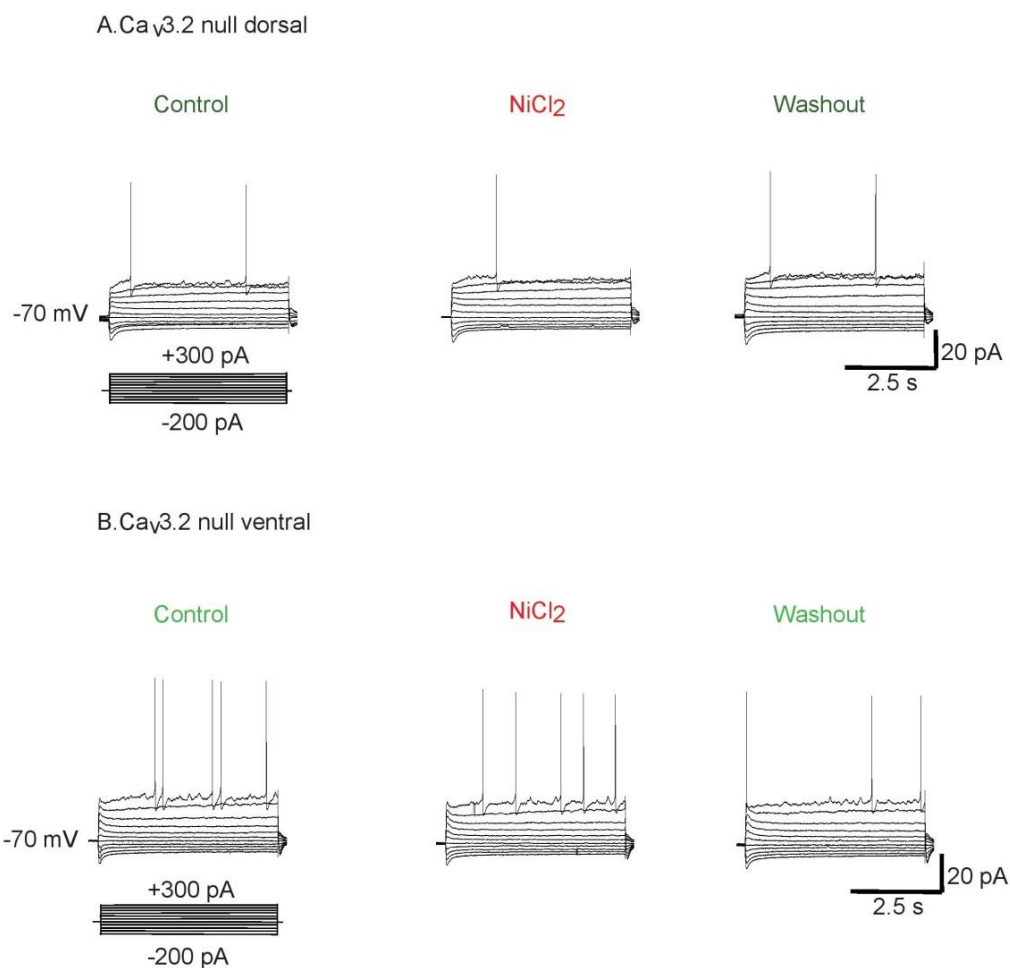
Figure 4.5. Example recordings from Ca$_v$3.2 null L II SC. The traces were obtained from A) dorsal and B) ventral in response to hyperpolarising and depolarising current pulses before (left), during (middle) and after washout (right) of 50 µM NiCl$_2$.

Quantification confirmed that there were no significant differences in input resistance measured using either -100 pA or +100 pA current steps and excitability of Ca$_v$3.2 null dorsal (Figure 4.6 A and B, Appendix 3) and ventral (Figure 4.6 C and D, Appendix 3) neurons in the absence, presence of NiCl$_2$ and during washout. As expected, no changes in the single action potential properties (amplitude, half-width and threshold) were observed in Ca$_v$3.2 null dorsal (n=5) or ventral (n=3) cells between control conditions and in the presence of NiCl$_2$ (Table 4.1).

A. Input resistance

Ca$_V$3.2 null dorsal (n=5)
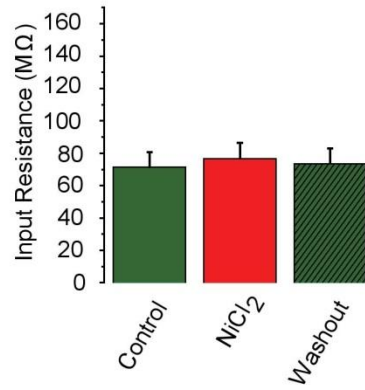
B. Excitability

Ca$_V$3.2 null dorsal (n=5)
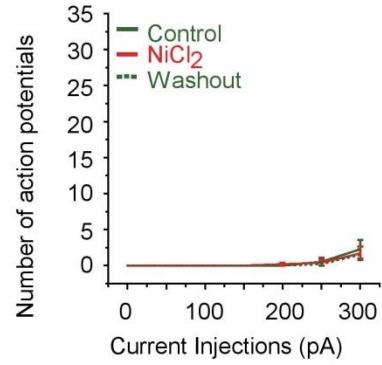
C. Input resistance

Ca$_V$3.2 null ventral (n=6)
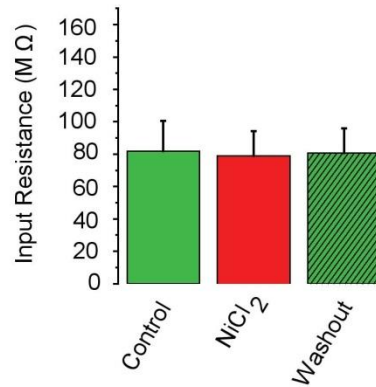
D. Excitability

Ca$_V$3.2 null ventral (n=6)
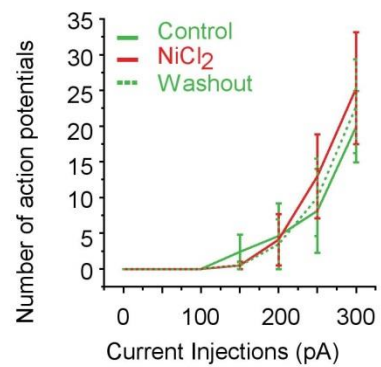
Figure 4.6. Graphs illustrating the changes in the Ca$_v$3.2 null cells upon the 50 μM NiCl$_2$ application. The input resistance was measured at +100 pA and action potential number at set membrane potential of -70 mV. Null dorsal (A and B) and ventral (C and D) neurons before (dark and light green, respectively), during (red) and after (shaded area/dotted line) treatment with NiCl$_2$ (see Appendix 3 for supplementary numbers).

4.5 The intrinsic properties of $Ca_v3.2$ null neurons were also not affected by the pharmacological inhibitor, TTA-P2.

The effects of a second pharmacological blocker of Ca_v3 channels, TTA-P2 were also investigated on $Ca_V3.2$ null neurons. 15-20 min application of TTA-P2 caused no apparent differences in input resistance or excitability of $Ca_v3.2$ null dorsal (Figure 4.7 A) and ventral (Figure 4.7 C) neurons.
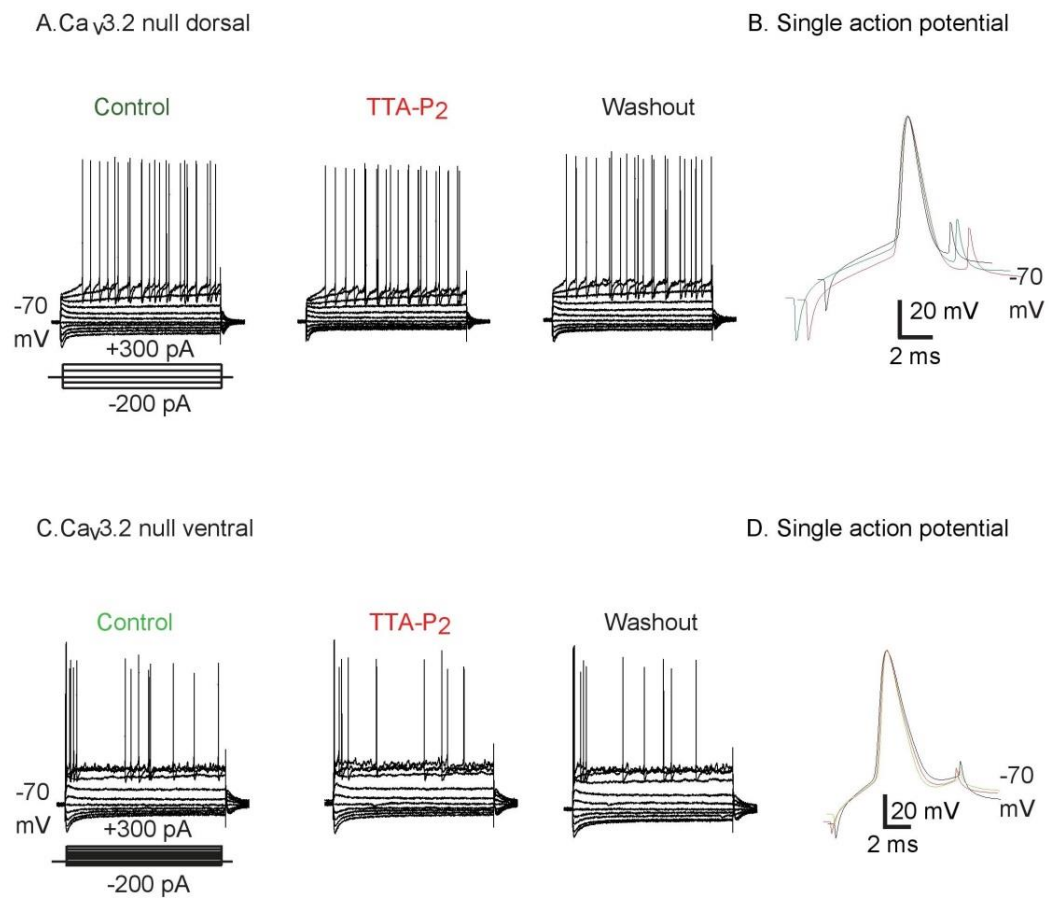
Figure 4.7. Example recordings from $Ca_v3.2$ null neurons upon 100 nM TTA-P2 application. Traces from A) dorsal and C) ventral neurons were obtained in response to hyperpolarising and depolarising current pulses before (left), during (middle) and after washout (right) of TTA-P2. Superimposed traces of single action potentials recorded from $Ca_v3.2$ null B) dorsal (dark green) and D) ventral (light green) neurons. Red lines represents TTA-P2 and black washout traces.

Quantification confirmed that bath application of TTA-P2 had no effect on input resistance or numbers of action potentials elicited with depolarizing current pulses in $Ca_v3.2$ dorsal (Figure 4.8 A and B, Appendix 4) and ventral (Figure 4.8 C and D, Appendix 4) neurons.

Furthermore, $Ca_v3.2$ null dorsal (n=5, Figure 4.7 B) and ventral (n=4, Figure 4.7 D) neurons showed similar action potential threshold, amplitude and half-width values before and after the application of TTA-P2 (Table 4.2). These data, therefore, strongly support the notion that T-type $Ca_v3.2$ channels do not affect action potential properties in MEC L II SC. Additionally, they confirmed that there are no additional $NiCl_2$ or TTA-P2 sensitive Ca_v3 currents in $Ca_v3.2$ null MEC L II SC.
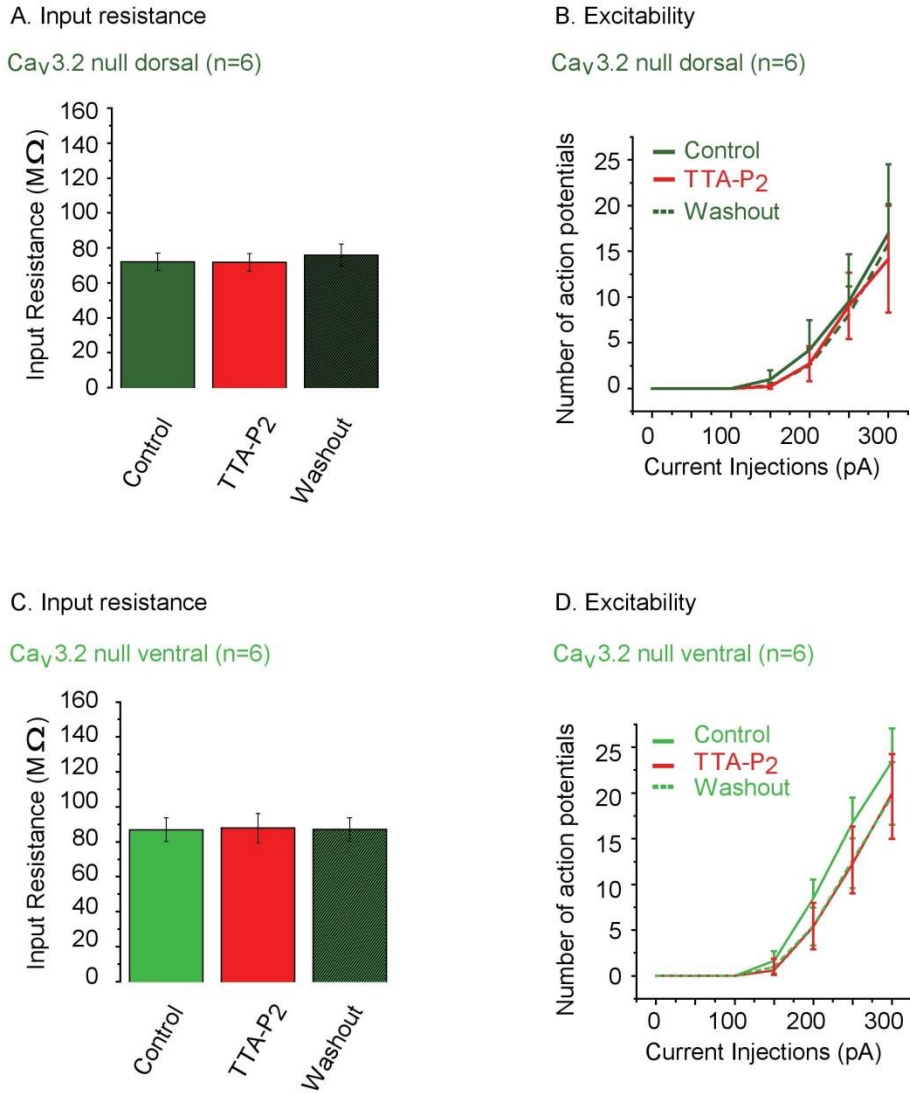
Figure 4.8. Quantification of input resistance and excitability changes upon 100 nM TTA-P2 application in Ca$_v$3.2 null neurons. Dorsal (A and B) and ventral (C and D) cells before (dark and light green, respectively), during (red) and after (shaded area/ dotted line) treatment with TTA-P2. The input resistance was measured at +100 pA and action potential number at set membrane potential of -70 mV (see Appendix 4 for supplementary numerical data).

		Control	NiCl$_2$	Washout	Control vs NiCl2, significance (*p*) value
Latency (sec)	WT Dorsal	1.95±0.6 (n=6)	1.36±0.8 (n=6)	1.66±0.6 (n=6)	0.56
	WT Ventral	1.11±0.6 (n=6)	1.27±0.7 (n=6)	0.44±0.2 (n=6)	0.86
	Null Dorsal	2.06±0.8 (n=5)	2.5±0.8 (n=5)	1.9±0.6 (n=5)	0.72
	Null Ventral	2.65±0.6 (n=5)	2.11±0.6 (n=5)	1.58±0.8 (n=5)	0.58
Sag ratio	WT Dorsal	0.59±0.04 (n=6)	0.56±0.05 (n=6)	0.58±0.03 (n=6)	0.57
	WT Ventral	0.64±0.07 (n=6)	0.61±0.06 (n=6)	0.61±0.05 (n=6)	0.66
	Null Dorsal	0.62±0.04 (n=5)	0.59±0.03 (n=5)	0.62±0.03 (n=5)	0.43
	Null Ventral	0.54±0.06 (n=5)	0.59±0.03 (n=5)	0.6±0.03 (n=5)	0.17
Action potential ampitude (mV)	WT Dorsal	72.2±1 (n=5)	72.7±0.7 (n=4)	71.1±2.6 (n=4)	0.69
	WT Ventral	73±2.2 (n=5)	71.8±3.4 (n=4)	71.6±5.7 (n=4)	0.76
	Null Dorsal	68.9±2.8 (n=5)	69.4±4.1 (n=4)	66.±3.8 (n=4)	0.93
	Null Ventral	72.2±3.7 (n=3)	68.9±7.4 (n=3)	66.7±5.9 (n=3)	0.23
Action potential half-width (ms)	WT Dorsal	1.62±0.1 (n=5)	1.73±0.1 (n=4)	1.8±0.2 (n=4)	0.57
	WT Ventral	1.7±2.2 (n=5)	1.9±0.1 (n=4)	1.93±0.2 (n=4)	0.05
	Null Dorsal	1.48±0.04 (n=5)	1.56±0.03 (n=4)	1.56±0.1 (n=4)	0.19
	Null Ventral	1.57±0.1 (n=3)	1.77±0.2 (n=3)	1.82±0.2 (n=3)	0.06
Action potential threshold (mV)	WT Dorsal	-50.6±1.9 (n=5)	-53.7±1.4 (n=4)	-55.4±0.9 (n=4)	0.23
	WT Ventral	-49.1±3.5 (n=5)	-49.6±2.5 (n=4)	-53.7±3.8 (n=4)	0.91
	Null Dorsal	-48.5±1.7 (n=5)	-48±2.4 (n=4)	-49.3±2.4 (n=4)	0.87
	Null Ventral	-47.7±1.1 (n=3)	-51±1.6 (n=3)	-54±1.5 (n=3)	0.08

Table 4.1. The table showing the effects of 50 µM NiCl$_2$ application onto Ca$_v$3.2 wild type (WT) and null neurons. This includes the properties of single action potential (amplitude, half-width and threshold) as well as the latency to the first spike and the sag ratio in the control conditions, upon the NICl$_2$ application and in a washout. The most right column represents significance values of student *t*-test between control and NiCl$_2$ condition.

		Control	TTA-P2	Washout	Control vs TTA-P2
Latency (ms)	WT Dorsal	1.66±0.4 (n=6)	1.3±0.5 (n=6)	1.26±0.3 (n=6)	0.43
	WT Ventral	1.94±0.3 (n=8)	1.97±0.4 (n=8)	2.24±0.4 (n=8)	0.96
	Null Dorsal	1.42±0.5 (n=6)	1.48±0.6 (n=6)	1.38±0.5 (n=6)	0.94
	Null Ventral	1.19±0.4 (n=6)	1.73±0.4 (n=6)	2.29±0.6 (n=6)	0.15
Sag ratio	WT Dorsal	0.52±0.06 (n=6)	0.51±0.04 (n=6)	0.55±0.04 (n=6)	0.91
	WT Ventral	0.55±0.04 (n=8)	0.57±0.04 (n=8)	0.63±0.04 (n=8)	0.67
	Null Dorsal	0.53±0.07 (n=6)	0.59±0.06 (n=6)	0.58±0.05 (n=6)	0.12
	Null Ventral	0.43±0.04 (n=6)	0.47±0.06 (n=6)	0.54±0.06 (n=6)	0.48
Action potential ampitude (mV)	WT Dorsal	72.3±1.1 (n=4)	73.3±1.6 (n=4)	73.7±2 (n=4)	0.62
	WT Ventral	76±3.4 (n=6)	75.6±3.6 (n=6)	78.1±4.1 (n=5)	0.93
	Null Dorsal	74.3±1.8 (n=5)	74.5±1.5 (n=5)	72.9±2.1 (n=5)	0.93
	Null Ventral	76.4±4.2 (n=4)	76.5±4.6 (n=4)	76.8±4.4 (n=4)	0.99
Action potential half-width (ms)	WT Dorsal	1.52±1.4 (n=4)	1.5±0.1 (n=4)	1.48±0.1 (n=4)	0.86
	WT Ventral	1.54±0.1 (n=6)	1.62±0.1 (n=6)	1.51±0.1 (n=5)	0.56
	Null Dorsal	1.48±0.1 (n=5)	1.62±0.1 (n=5)	1.7±0.2 (n=5)	0.32
	Null Ventral	1.62±0.1 (n=4)	1.8±0.2 (n=4)	1.8±0.2 (n=4)	0.39
Action potential threshold (mV)	WT Dorsal	-50.5±1.2 (n=4)	-50.6±1 (n=4)	-49.6±1.9 (n=4)	0.94
	WT Ventral	-46.8±1.7 (n=6)	-51.4±1.9 (n=6)	-49.4±2.2 (n=5)	0.1
	Null Dorsal	-50.4±1.6 (n=5)	-50.6±1.6 (n=5)	-52.3±1.9 (n=5)	0.93
	Null Ventral	-47.1±1.7 (n=4)	-49.3±2.1 (n=4)	-50.4±2.8 (n=4)	0.45

Table 4.2. The table illustrating the changes in various properties of Ca$_v$3.2 null and wild type (WT) neurons in response to application of 100 nM TTA-P2. The action potential amplitude, half width and threshold as well as the sag ratio and the latency were compared in the control, TTA-P2 and washout condition. The right column shows the significance *p* value obtained from the *t*-test when comparing control and TTA-P2 conditions.

4.6 TTA-P2 and NiCl$_2$ had no effect on the sag ratio and the spiking latency

To confirm that Ca$_v$3 channels do not affect the latency to spike or the sag ratio, I measured these parameters in Ca$_v$3.2 wild type dorsal, wild type ventral, Ca$_v$3.2 null dorsal and Ca$_v$3.2 null ventral (n=6, n=6, n=5, n=5, respectively) in the absence, presence and during washout of NiCl$_2$. The data showed no significant differences between the groups (Table 4.1).

Similarly, also application of TTA-P2 had little effect on the latency and sag ratio of Ca$_v$3.2 wild type dorsal, wild type ventral, Ca$_v$3.2 null dorsal and Ca$_v$3.2 null ventral (n=6, n=8, n=6, n=6, respectively, Table 4.2). Together, these data suggest that T-type Ca$_v$3 channels do not affect the spiking latency or the sag ratio in the MEC L II SC.

4.7 Summary

In this chapter, I have confirmed the notion that T-type $Ca_v3.2$ Ca^{2+} channels contribute towards dorsal-ventral gradient in the MEC L II SC intrinsic properties by selectively influencing ventral neurons. T-type $Ca_v3.2$ Ca^{2+} channels are responsible for the cell depolarisation. I therefore expected that the introduction of a Ca_v3 antagonist would reduce the overall input resistance of L II SC. Indeed, after 10-20 min of bath application, both drugs decreased the input resistance, measured using a +100 pA step, and number of action potentials elicited with depolarizing steps in $Ca_v3.2$ wild type ventral, but not dorsal, neurons. No differences in the action potential threshold, amplitude and half-width were observed with $NiCl_2$ and TTA-P2 perfusion, suggesting that the changes in action potential firing are likely to be due to changes in the input resistance.

My results are in agreement with previous studies showing $NiCl_2$ at low concentrations (50 μM) to be an effective and selective blocker of Ca_v3 channels (sensory neurons, dorsal root ganglion cells, CA3 pyramidal and cultured neurons (Dubreuil et al. 2004; Todorovic and Lingle 1998; Reid et al. 2008; Autret et al. 2005)). Furthermore, in agreement with previous studies (Autret et al. 2005; Martinello et al. 2015), my results show that 20-30 min of washout is sufficient to reverse the changes in input resistance and numbers of action potentials that occur in the presence of $NiCl_2$.

In contrast, after application of TTA-P2 only a partial recovery in some of the L II SC action potential firing was observed. Although some literature (e.g. Martinello et al. (2015)) shows full recovery, the differences in the methods used should be taken into consideration. This includes:

a) The type of the cells and brain region where the recordings take place

b) The depth of patched neurons

c) Total washout time

d) The perfusion velocity

Indeed, it was previously shown that the effects of TTA-P2 on the T-type Ca^{2+} currents can be either only partially reversible (Choe et al. 2011) or extremely slow (55 min in thalamocortical neurons (Dreyfus et al. 2010)).

Interestingly, both drugs affected the input resistance when measured using a +100 pA step of wild type ventral neurons to a similar degree, i.e. decreased it by 20-30 MΩ. Since $NiCl_2$ at 50 µM concentration is expected to be selective for $Ca_v3.2$ (Lee, Gomora, et al. 1999), it would suggest that it is mainly this subtype which affects the intrinsic membrane properties of L II SC ventral neurons. The lack of TTA-P2 or $NiCl_2$ effect on $Ca_V3.2$ null neurons supports this hypothesis.

Lastly, the application of the Ca_v3 antagonists did not have any effect on spike latency or the sag, suggesting no contribution of these channels towards these properties and supporting my previous conclusions (comparison of the $Ca_v3.2$ wild type and null data, Chapter 3).

Altogether the pharmacological data support my findings obtained from wild type and $Ca_V3.2$ null dorsal and ventral L II SC. Together, they strongly suggest that T-type $Ca_v3.2$ Ca^{2+} contribute towards the activity of ventral SC selectively and therefore influence the dorsal-ventral gradient of MEC L II SC intrinsic properties.

5.   L II SC display differences in the T-type Ca^{2+} currents across dorsal-ventral axes of the MEC

5.1 Introduction

Since their discovery in 1980s (Llinas and Yarom 1981), the low-voltage activated Ca^{2+} channels, known as T-type Ca^{2+} channels, were shown to play numerous important functions in different cell types, such as thalamic (Llinas and Janhsen 1982) or sensory (Carbone and Lux 1984) neurons. Furthermore, T-type Ca^{2+} channels were shown to be present in different subcellular locations, including dendritic spines and shafts (Chausson et al. 2013; Destexhe et al. 1998; Egger et al. 2003; Hildebrand et al. 2009) orpresynaptic terminals (Huang et al. 2011; Tang et al. 2011) and have diverse biophysical properties and molecular identity depending on their subtype (Ca$_v$3.1, Ca$_v$3.2 and Ca$_v$3.3).

As my results have shown that Ca$_V$3 pharmacological inhibitors differentially affect the excitability and input resistance of dorsal and ventral SC neurons and because there are significant differences in intrinsic membrane properties between wild type and Ca$_V$3.2 null ventral neurons, I decided to investigate whether dorsal and ventral SC have different amplitudes of the Ca$_v$3.2 currents.

As discussed in detail in chapter 1.3.5 on the example of thalamic neurons, any modifications in the biophysical properties of the T-type Ca^{2+} channels (including differences between various isoforms) can have major consequences on the neuronal firing patterns (Tscherter et al. 2011). Since dorsal and ventral SC displayed differences in their excitability, I decided to investigate whether the inactivation kinetics of the recorded current differs between dorsal and ventral SC.

The voltage-clamp experiments were performed on the MEC L II SC obtained from Ca$_v$3.2 wild type and null littermates. The T-type Ca^{2+} current was pharmacologically

isolated and the selected biophysical properties were measured and compared between dorsal and ventral neurons.

5.2 Wild type ventral neurons have more prominent T-type Ca^{2+} current than dorsal cells

I first decided to investigate whether $Ca_v3.2$ wild type dorsal and ventral cells have any variability in the amount of T-type Ca^{2+} current present in L II SC.

To achieve that, I applied a voltage-dependent activation protocol consisting of 1 s pre-pulse (-100 mV) and ten 1 s pulses at 5 mV intervals (-90 mV to – 45 mV) and steady-state inactivation protocol (starting with 1 s pulses (-100 mV to -55 mV) ending with 1 s post-pulse (-50 mV)) to wild type dorsal (Figure 5.1 A and C) and ventral (Figure 5.2 A and C) L II SC neurons. All of the recordings were then leak-subtracted which allowed me to directly measure the T-type Ca^{2+} currents.

It was apparent that wild type dorsal cells had little T-type Ca^{2+} current present when measured with activation and inactivation protols ('subtracted' traces in Figure 5.1 A and C, respectively). In contrary, the current from wild type ventral neurons was much larger ('subtracted' traces in Figure 5.2 A and C, respectively).

A. $Ca_v3.2$ wild type dorsal activation protocol

B. Eaxmple fit of decay time constant
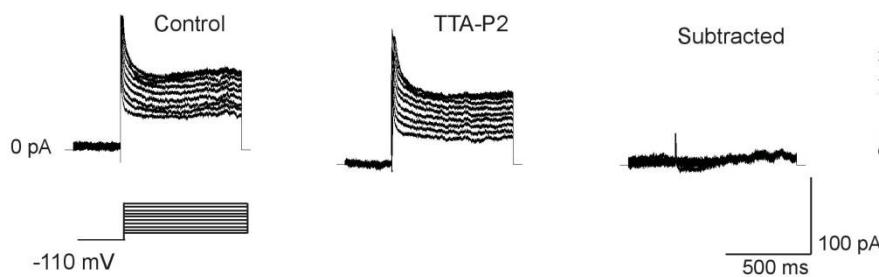
C. $Ca_v3.2$ wild type dorsal inactivation protocol
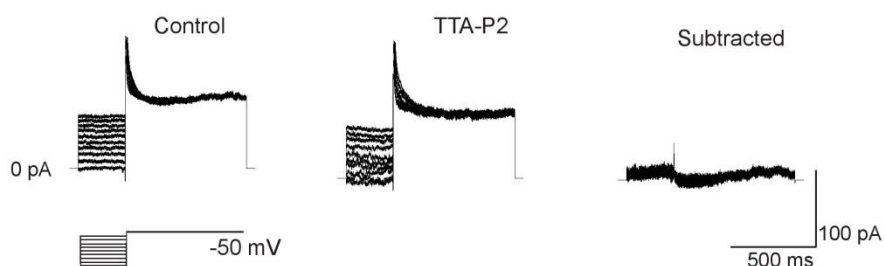
Figure 5.1 Voltage-clamp recordings of isolated T-type Ca²⁺ current obtained from wild type dorsal neurons. A) and C) Example traces of the recordings obtained in before (control) and after (TTA-P2) the application of drug during activation and inactivation protocol, respectively. Subtracted figure show the control minus TTA-P2 condition and reveals the isolated T-type Ca²⁺ current. All of the traces were leak-subtracted. B) An example of the exponential decay fit applied onto the maximal T-type Ca²⁺ current (recorded during the activation protocol at – 45 mV) in order to obtain the inactivation time constant values.
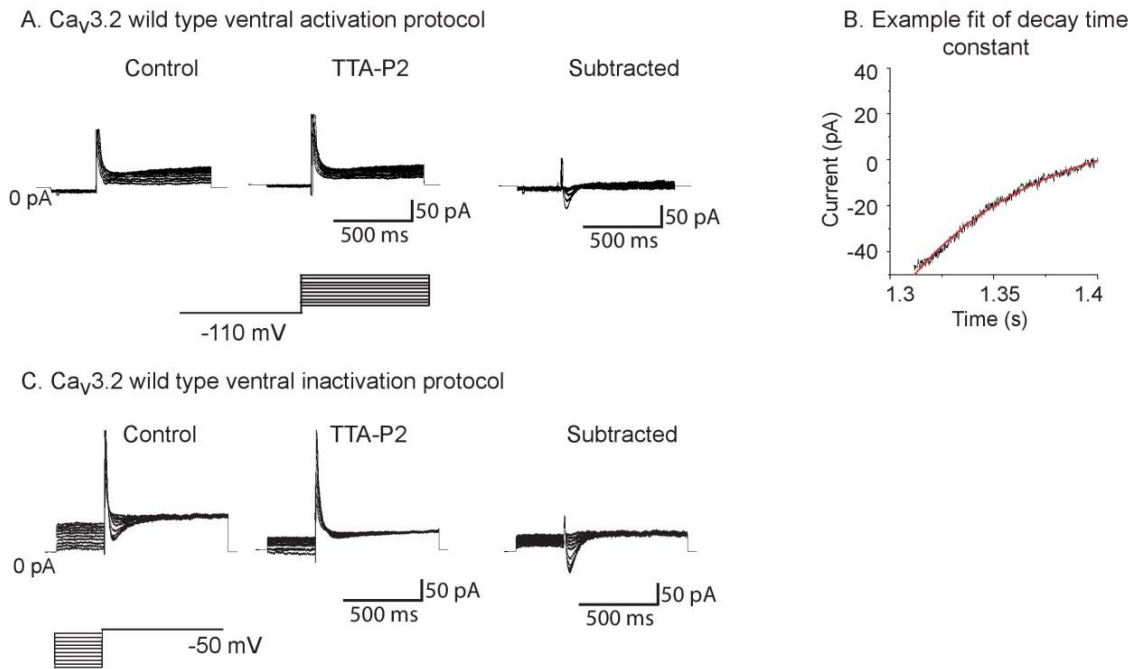
Figure 5.2 Wild type ventral example traces. A) and C) show recordings before and after application of TTA-P2 as well as the subtracted figure (control minus drug) for activation and inactivation protocol, respectively. The traces were leak-subtracted. B) An example of exponentially-fitted inactivation curve obtained from the activation protocol at – 45 mV.

Indeed, when the maximal T-type $Ca_v3.2$ Ca²⁺ current obtained from the actvation protocol was quantified, its maximal amplitude was significantly larger in ventral (74.6±12.3 pA, n=5) compared to dorsal L II SC neurons (33.4±11.3 pA, n=5, p=0.039, 2-tailed t-test, Figure 5.3 A). Furthermore, when current amplitudes were compared across all voltage steps, T-type Ca_v3 channels in the ventral neurons were observed to be activated at more hyperpolarised potentials (approximately -80 mV) than dorsal cells

(approximately -55 mV; Figure 5.5 B). This in turn could differentialy influence the

shape and size of the window current generated by the dorsal and ventral MEC L II SC.
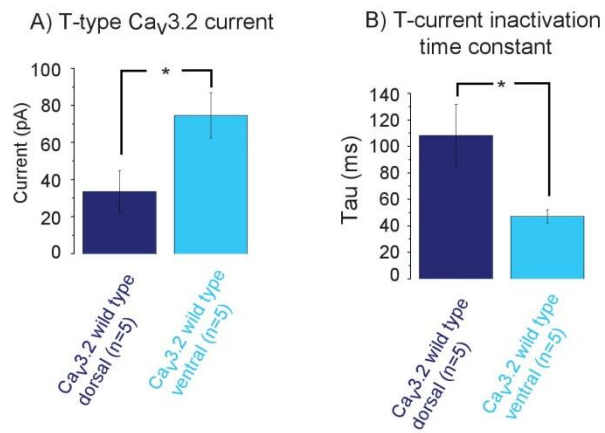
Figure 5.3 Comparison of wild type dorsal (dark blue) and ventral (light blue) T-type Ca$_v$3.2 Ca^{2+} current properties. A) The maximal T-type Ca^{2+} current amplitude measured at – 45 mV B) The inactivation time constant measured at the maximal amplitude current step (-45 mV). Single (*) and two (**) denote significance at $p<0.05$ and $p<0.01$ respectively.

5.3 Wild type dorsal cells displayed slower inactivation kinetics in comparision to L II ventral SC

Having observed the larger T-type Ca^{2+} current amplitudes in ventral L II SC, compared with the dorsal neurons, I was interested to determine whether the kinetics of the T-type Ca^{2+} current in the two cell groups differ. To do this, I measured the time constant of the inactivation part of the isolated maximal T-type Ca^{2+} current obtained using the activation protocol (at – 45 mV). Interestingly, the data showed a larger inactivation time constant in dorsal neurons (108±23.8 ms, n=5) than ventral neurons (47±5 ms, n=5, p=0.037, Figure 5.3 B). These data may indicate that dorsal and ventral L II MEC SC are characterised by T-type Ca^{2+} currents with different kinetics.

5.4 $Ca_V3.2$ null dorsal and ventral L II SC have a negligible amount of T-type Ca^{2+} current

My current-clamp experiments (Chapters III and IV) strongly suggested that T-type Ca^{2+} currents were absent in $Ca_V3.2$ null dorsal and ventral L II SC. Since the T-type Ca^{2+} current is measured much more accurately under voltage-clamp conditions, I used this method to record the current from $Ca_V3.2$ null dorsal and ventral L II SC, to validate the current-clamp data.

As predicted, a negligible amount of TTA-P2-sensitive current was observed when the recordings were obtained from both $Ca_V3.2$ null dorsal (Figure 5.4 A and B for activation and inactivation protocol, respectively) and ventral (Figure 5.4 C for activation and D for the inactivation protocol) L II SC.

Indeed, when quantified, a striking difference between wild type and null currents were observed when the largest amplitude currents obtained from activation protocols were compared (33.3±11.3 pA (n=5) and 74.6±12.3 pA (n=5) for wild type dorsal and ventral, respectively versus 15.7±4 pA (n=5) and 19.3±6 pA (n=4) for null dorsal and ventral, respectively, Figure 5.5 A). The differences between wild type and null currents were

also observed when the data from inactivation protocols were measured (22.2±4.4 pA (n=5) and 59.3±8.6 pA (n=4) versus 6.8±3.3 pA (n=3) and 6.4±3.7 pA (n=3) for wild type dorsal and ventral and null dorsal and ventral, respectively; Figure 5.5 A). This was also confirmed when the data from all volage steps were compared for both activation and inactivation protocols (Figure 5.5 B, Appendix 5). Together, these data confirm that there is very little TTA-P2 sensitive current present in the $Ca_v3.2$ null animals.

A. Ca$_V$3.2 null dorsal activation

B. Ca$_V$3.2 null dorsal inactivation

C. Ca$_V$3.2 null ventral activation

D. Ca$_V$3.2 null ventral inactivation
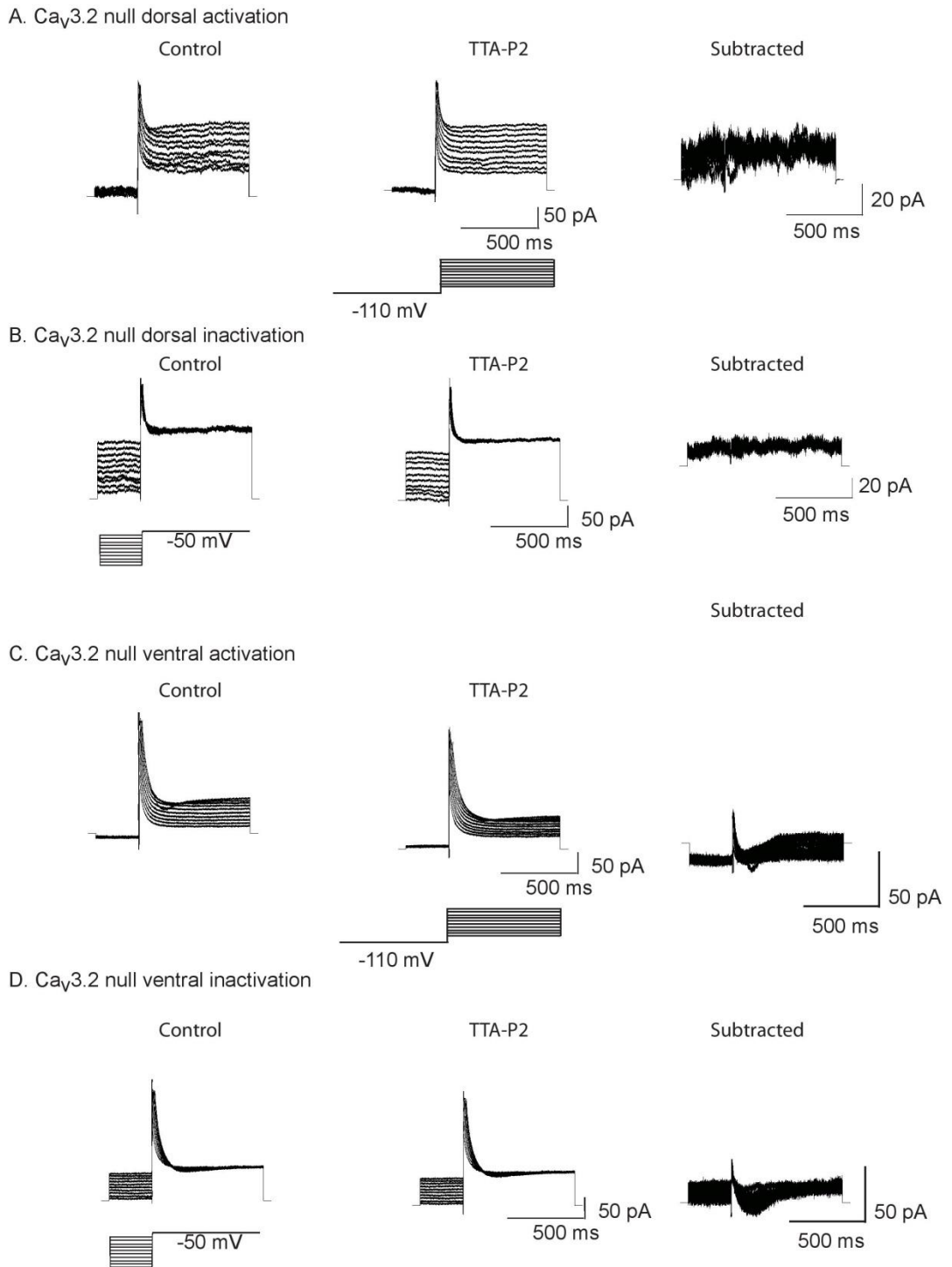
Figure 5.4 Example traces obtained from Ca$_v$3.2 null neurons. The activation (A and C) and inactivation (B and D) protocols were applied onto dorsal (A and B) and ventral (C and D) neurons. The traces represent the currents recorded under control condition and in the drug (TTA-P2) as well as the isolated T-type Ca^{2+} current (subtracted=control-TTAP2). All of the traces were leak-subtracted.
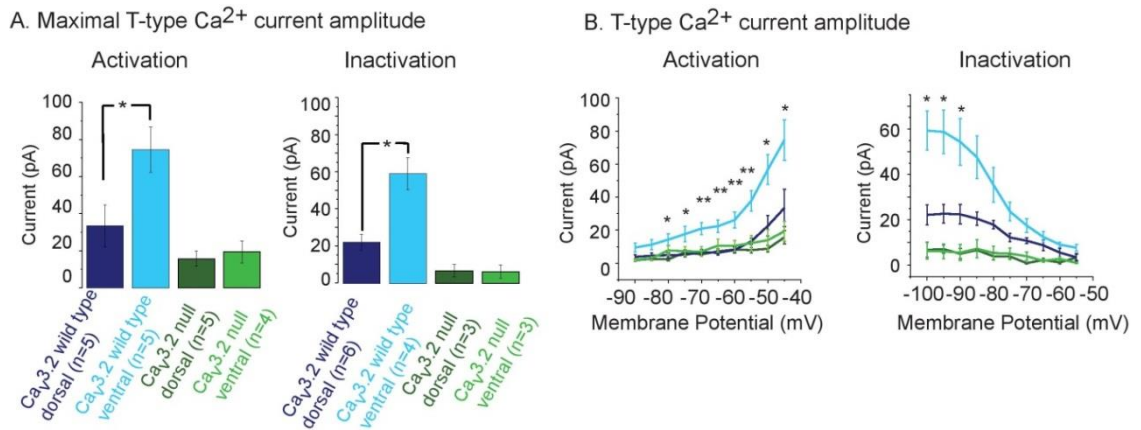
Figure 5.5 Comparison of T-type Ca^{2+} current recorded from Ca$_v$3.2 wild type dorsal (dark blue) and ventral (light blue) with null dorsal (dark green) and ventral (light green) L II SC. A) Bar graph illustrating the difference in the amount of maximal T-type Ca^{2+} current recorded from all four cell groups during the activation and inactivation protocol. B) A comparison between the T-type Ca^{2+} current recorded at various voltage steps during activation (n=5 for Ca$_v$3.2 wild type dorsal and ventral and null dorsal, n=4 for null ventral) and inactivation (n=6 and n=4 Ca$_v$3.2 wild type dorsal and ventral respectively, n=3 for null dorsal and ventral) protocols from wild type and null neurons L II SC (see Appendix 5 for the quantitative data). The stars indicate the difference between the T-type Ca^{2+} current recorded from wild type dorsal and ventral neurons only. Single (*) and two (**) denote significance at $p<0.05$ and $p<0.01$ respectively.

5.5 Summary

My data, using current-clamp electrophysiological recordings, have indicated that MEC L II wild type ventral SC have significantly more $NiCl_2$ and TTA-P2 sensitive $Ca_v3.2$ T-type Ca^{2+} current than dorsal neurons. This most likely contributes towards higher input resistance and excitability of the SC in the ventral ends of MEC. Using whole-cell voltage-clamp recordings and variety of pharmacological blockers, it became clear that wild type ventral cells have 2-3 fold larger peak T-type Ca^{2+} current in comparison to dorsal neurons (74.6±12.3 pA and 33.4±11.3 pA, respectively). The overall amplitude values measured at peak are lower than the ones previously reported in the literature for other neuron subtypes in other brain regions (Huguenard and Prince 1992). However, this is most likely due to differences in expression of channels between different neurons. Nonetheless, these results suggest that wild type ventral cells have larger amounts of T-type $Ca_v3.2$ current compared with dorsal neurons.

Interestingly, the T-type Ca^{2+} current recorded from ventral SC was activated at more hyperpolarised potentials than in the dorsal neurons, which could potentially influence the shape of the window current. This however will have to be further investigated.

The difference in the size of the T-type Ca^{2+} currents could be explained in various ways. One possibility could be that T-type Ca^{2+} $Ca_v3.2$ channels are expressed in different amounts in dorsal and ventral L II SC. This will have to be investigated further with immunohistochemistry experiments once a selective $Ca_v3.2$ antibody become available.

Another possibility is that different Ca_v3 subtypes are active in dorsal and ventral neurons. To investigate this, I measured the kinetics of the recorded T-type Ca^{2+} current. Interestingly, the inactivation time constant of the T-type Ca^{2+} current recorded from ventral neurons (47±5 ms measured at -45 mV test potential) was comparable to those of expressed $Ca_V3.2$ currents reported previously in the literature (e.g. 23.4±0.3

ms in Chemin, Monteil, et al. (2002)). In contrast, the inactivation time constant of the T-type Ca^{2+} current recorded from dorsal neurons (108±23.8 ms measured at -45 mV) was significantly longer and could possibly be attributed, at least partially, to $Ca_v3.3$ subunits, which form currents with much slower time constants when expressed in HEK293 cells (e.g. 122±5 ms in Chemin, Monteil, et al. (2002)). This possibility will, however, have to be investigated further in the future.

Lastly, it is important to acknowledge that limitations in the recording procedures might have had an effect on the obtained data. Due to issues such as space clamp, the shape and amplitude of the recorded currents may have been distorted (Spruston and Johnston 2008). This might be the case if T-type Ca^{2+} currents in SC are located in dendrites, as has been reported for other neurons (Chausson et al. 2013; Destexhe et al. 1998; Egger et al. 2003; Hildebrand et al. 2009). This needs to be further investigated.

Nevertheless, the data clearly show a significant difference in the magnitude of the peak T-type Ca^{2+} current between dorsal and ventral cells. This is very likely to differentially affect the input resistance and the excitability of these neurons and therefore indicates that T-type $Ca_v3.2$ Ca^{2+} currents are likely to contribute towards the dorsal-ventral gradient in the intrinsic properties of the MEC L II SC.

6. Discussion

The MEC is a unique structure of the brain that has been shown to be involved in multiple functions, including spatial navigation (Hafting et al. 2005) and memory (Hasselmo 2006) processing. Despite the importance of MEC, numerous questions about its connectivity, molecular and electrophysiological properties and even detailed structural division, remain unanswered. Over the past decade, the L II of MEC has been a focus of multiple studies, mainly due to its involvement in the spatial navigation (Hafting et al. 2005). Particularly, SC, which constitute a majority of excitatory neurons in L II (69% versus 31% of pyramidal cells, (Alonso and Klink 1993)), have received a lot of attention due to the existence of a dorsal-ventral gradient in their intrinsic membrane properties, the expression and function of ion channels (Garden et al. 2008) and their intrinsic subthreshold oscillation frequency (Giocomo et al. 2007). Due to their properties, SC have been suggested to, at least partially, contribute towards the gird-cell activity (Pastoll, Ramsden, et al. 2012). Thorough investigation of the electrophysiological properties of MEC L II SC is therefore crucial to achieve better understanding of the processes such as spatial navigation, memory and multiple MEC--associated pathologies.

In this thesis, I investigated whether T-type $Ca_v3.2$ Ca^{2+} channels also contribute towards the dorsal-ventral gradient of the MEC L II SC. First, using current-clamp, I recorded from SC obtained from $Ca_v3.2$ wild type and null animals, compared their properties and established that indeed $Ca_v3.2$ calcium channels play a role in the dorsal-ventral gradient by enhancing the activity of ventral, and not dorsal, SC. In order to confirm the results, I used pharmacological blockers, TTA-P2 and $NiCl_2$, of $Ca_v3.2$ calcium channels on both wild type and null animals. These experiments showed that $Ca_V3.2$ Ca^{2+} channels reduced ventral, but not dorsal, SC activity, supporting my notion that $Ca_v3.2$ channels influence the SC dorsal-ventral gradient in intrinsic membrane

excitability. Finally, to verify the conclusions from the current-clamp experiments, using voltage-clamp I was able to isolate the T-type Ca^{2+} current. These experiments showed that $Ca_v3.2$ channels have bigger current density and slightly different kinetics in ventral, compared with dorsal, L II SC of the MEC.

Together, these data strongly support the thesis that T-type $Ca_v3.2$ channels are not only present in the MEC L II SC, but also contribute towards the dorsal-ventral gradient. Below, I will discuss the results of these experiments in detail as well as reiterate and elaborate on the summaries found in previous chapters together with pointing out potential problems and suggesting improvements. Later, I will show how the experiments connect together and explain their relevance to the scientific community in different contexts. Finally, I will introduce prospective directions of this research and point out specific experiments that could contribute to better understanding of the topic in the future.

6.1 The intrinsic properties of the L II SC in the MEC follow the dorsal-ventral gradient

It was previously shown that L II SC intrinsic membrane properties are progressively changing along the dorsal-ventral axes of the MEC (Dodson et al. 2011; Garden et al. 2008; Giocomo et al. 2007; Pastoll, Ramsden, et al. 2012). As neuronal activity can be affected by multiple parameters, including structural differences in the soma size and dendritic processes, in an attempt to explain the dorsal-ventral gradient of SC, their morphology was first assessed. All neurobiotin-filled cells were confirmed to fulfil the criteria of a typical SC morphology (Alonso and Klink 1993; Garden et al. 2008). Additionally, as previously described, dorsal $Ca_v3.2$ wild type neurons had larger cell bodies than ventral neurons (Garden et al. 2008). No difference in dendritic complexity was observed. These findings verified the identity of the patched neurons. I was not

able to see the clear axonal projections of the neurobiotin-filled cells. This is not uncommon and may have been due to difficulties in diffusion of neurobiotin into axons.

Electrophysiological parameters of the patched neurons were also used to confirm their identity (please see the section 2.3.1.3 for more details). In contrast to previous findings (Pastoll, Ramsden, et al. 2012; Boehlen et al. 2010), I observed that ventral SC were significantly more hyperpolarised than dorsal neurons at rest. These results may indicate the variability of the kinetics or density of ion channels present in dorsal and ventral cells. It has been previously shown that I_h contributes to approximately 50 % of the SC membrane conductance at rest (Nolan et al. 2007). Additionally, I_h depolarizes the RMP and has been shown to be more profound in dorsal SC (Garden et al. 2008; Giocomo and Hasselmo 2008). This could explain the slightly more depolarised RMP of SC dorsal neurons. Furthermore, other channels contributing to the RMP should be taken into consideration. For example, Ba^{2+} and quinidine sensitive potassium channels have been shown to follow dorsal-ventral gradient, with more current been present in the dorsal than ventral SC (Garden et al. 2008). It has been previously shown that activation of two pore domain K^+ channels (via serotonin), could induce SC hyperpolarisation (Deng et al. 2007). Although the activity of K^+ channels themselves will not lead to ventral cells being more hyperpolarised, it cannot be excluded that higher activity of these channels in dorsal location induces other depolarising channels (such as HCN) to become more active and consequently depolarising the membrane potential of dorsal SC. The role of other depolarising ion channels active at the RMP, such as Na_p, should also be investigated (French et al. 1990). Finally, the contribution of the $Ca_v3.2$ channels in setting the RMP cannot be excluded and will be discussed further below. It is important to note however, that the observed RMP difference between the dorsal and ventral neurons, although statistically significant, was relatively small (approximately 2 mV). More tests are therefore needed to validate this interpretation of the results as it has been previously shown that such

small fluctuations in the intrinsic properties could depend on the recording method, temperature and the animal's age (Pastoll, Ramsden, et al. 2012). If confirmed, however, these results might shed light on the mechanisms controlling RMP of SC.

Next, we decided to investigate whether any other intrinsic membrane properties also follow the dorsal-ventral gradient in MEC. The values of input resistance observed in our experiments were slightly higher than the previously reported ones, most likely due to the fact that different solutions were used or simply because they were measured at different current injection steps (Boehlen et al. 2010). Nevertheless, a steep dorsal-ventral gradient has been observed in the input resistance measured at both -100 and +100 pA current injection steps. Interestingly, the difference in the latter measurement has been shown to be more prominent than the − 100 pA. Since the +100 pA input resistance has been measured at potentials when $Ca_v3.2$ channels are open, it may suggest the contribution of these channels towards setting this dorsal-ventral gradient.

The phenomenon of dorsal SC having significantly lower input resistance than ventral neurons has already been investigated by multiple groups in the last decade (Garden et al. 2008; Boehlen et al. 2010; Pastoll, Ramsden, et al. 2012). To-date, two ion channels have been pointed out to be major contributors towards the dorsal-ventral gradient in the SC input resistance, I_h and K_{leak}. Voltage-clamp experiments have previously shown larger amplitudes of K_{leak} and I_h currents in dorsal neurons (Garden et al. 2008). In contrast, another study has reported similar I_h amplitudes across MEC SC, but smaller I_h time constants in ventral than dorsal neurons (Giocomo and Hasselmo 2008). Our results were in agreement with this and did not show any difference in the amplitude of I_h sag across the dorsal-ventral MEC axes. Nevertheless, the data from Allen Brain Atlas showed greater mRNA expression levels of HCN1 and HCN2 in dorsal than in ventral neurons supporting the hypothesis that I_h contributes towards the SC gradient in intrinsic properties. As ion channels play the role of resistors in electrical circuits of the cell, the greater activity or expression of I_h and K_{leak} channels could

indeed result in lower input resistance in dorsal ends of L II MEC SC. Interestingly, the contribution of $Ca_v3.2$ ion channels towards the dorsal-ventral gradient is not well defined yet and has been investigated further in this report.

Given the differences in RMP and the input resistance across the dorsal-ventral axis of the MEC, it was expected that the number of action potentials evoked by depolarisation would vary between the dorsal and ventral L II SC. My results were in agreement with this and have shown that $Ca_v3.2$ ventral neurons are significantly more excitable than the dorsal cells.

Following this finding, I investigated whether any properties of an action potential *per se* differ in dorsal and ventral L II SC. Previous reports indeed have shown a decrease in the current threshold of ventral L II SC (Garden et al. 2008), which suggests that the firing of these neurons will also be greater. In contrast, our results did not show any significant differences in action potential threshold, half-with or amplitude. The discrepancies in these results could be partially explained by differences in the protocols used as the action potential waveform will differ when evoked with long continuous current injections and with brief current stimulation.

Ultimately, my data suggest that the difference in the number of action potentials can be purely explained by the increased input resistance in the ventral SC. Alternatively, some other mechanisms that may contribute towards SC excitability and that are active at potentials close to RMP, such as Na_p, should be considered in the future (Alonso and Llinas 1989). Finally, the role of T-type $Ca_v3.2$ channels should also be considered and will be further investigated and explained in the next section of the discussion.

Action potentials in L II SC have been reported to be evoked within a short period of time upon depolarisation (42 ms on average, (Alonso and Klink 1993)). Fuchs et al. distinguished two types of SC in MEC L II: normal and intermediate SC in which action potentials occur with a latency of approximately 24 ms and 350 ms, respectively,

following a given depolarisation (Fuchs et al. 2016). My results have shown that action potentials within MEC L II SC occur within 100 ms and 200 m with depolarization. Most importantly, there was no difference in the latency for a spike to occur with depolarization between dorsal and ventral neurons.

Some studies have reported that L II SC show characteristic clustering firing patterns (Alonso and Klink 1993) which may follow a dorsal-ventral gradient (Pastoll, Ramsden, et al. 2012). A fraction of cells that I recorded from also exhibited this pattern at some membrane potentials. Some studies have suggested that HCN channels can have a significant influence on firing patterns through their effect on AHP (Dudman and Nolan 2009; Nolan et al. 2007). Additionally, the gradient in clustering patterns was shown to be dependent on the method used, with perforated patch, but not whole-cell patch-clamp, showing a gradient in spike frequency within cluster. Instead, a gradient in a probability of a spike occurring as a part of a cluster was observed with whole-cell patch clamp conditions (Pastoll, Ramsden, et al. 2012). The discrepancies were suggested to be explained by washout during whole-cell conditions that could potentially affect HCN channels and result in a voltage dependence shift in their activation curve (Pastoll, Ramsden, et al. 2012). This would affect the AHP which in turn would affect the firing patterns of L II SC (Pastoll, Ramsden, et al. 2012). Since the clustering pattern is relatively sensitive to washout, it is not surprising I did not observe it in all of my recorded cells. Nevertheless, as it is an important feature of SC, it would be important to better understand the mechanisms underlying action potential clustering in the future.

6.2 T-type $Ca_v3.2$ Ca^{2+} channels contribute towards the dorsal-ventral gradient in the MEC L II SC

Having established the basic intrinsic properties of the L II SC, I investigated whether T-type Ca^{2+} channels might contribute to these using global $Ca_v3.2$ knock out mice. My

results have shown that the RMP of $Ca_v3.2$ wild type dorsal cells is more depolarised than in dorsal neurons. Interestingly, no difference between $Ca_v3.2$ null dorsal and ventral neurons was observed. Together these results suggest that $Ca_v3.2$ could potentially contribute towards setting up the RMP of L II SC. Interestingly, the voltage clamp experiments showed that the dorsal cells have less T-type Ca^{2+} current than ventral neurons. This in turn could potentially suggest that ventral L II SC have a larger window current than dorsal neurons. Since a bigger window current would result in a more depolarised RMP, the more hyperpolarised membrane potential of ventral neurons is counterintuitive and has to be further investigated. The possibility, that the activity of other ion channels contributing towards the RMP, such as HCN, surpass the influence of $Ca_v3.2$ (discussed at the beginning of chapter 6.1) cannot be excluded.

Interestingly, my results also showed that the prominent gradient in the input resistance and excitability between the dorsal and ventral SC was significantly decreased in $Ca_V3.2$ null animals. The findings were particularly interesting as the reduction in the dorsal-ventral gradient in input resistance and excitability was due to selective changes in the $Ca_v3.2$ null ventral SC. One possible explanation for this phenomenon could be the interaction of T-type Ca^{2+} and other ion channels. In fact, it has been shown that in the EC layer III, $Ca_v3.2$ and HCN1 are co-localised in pre-synaptic terminals (Huang et al. 2011). Additionally, in the hippocampal CA1 brain region, dendritic HCN1 channels were also shown to decrease the activity of synaptically induced calcium spikes generated by T- and N- type Ca^{2+} channels (Tsay et al. 2007). Recently, Fan et al. (2017) using green fluorescence protein-tagging also showed that HCN1 and $Ca_v3.2$ are associated with each other via N-terminus of both proteins. Furthermore, the group also discovered the downregulating effects of HCN1 channels on the activity of $Ca_v3.2$. This finding is particularly intriguing when considering the $Ca_v3.2$ contribution towards the dorsal-ventral gradient of SC. The larger expression and activity of HCN1 channels in dorsal ends of the L II MEC (Garden et al. 2008), together with the downregulation of

Ca$_V$3.2 via HCN1 channels (Fan et al. 2017), could explain the increase in excitability in Ca$_V$3.2 wild type ventral neurons compared with dorsal cells.

However, multiple issues have to be taken into consideration when using global knockout mice. This includes changes in developmental mechanisms arising due to a lack of a specific gene expression during maturation, or compensatory changes occurring to sustain homeostasis in the organism (Gingrich and Hen 2000). To verify my findings that Ca$_V$3 channels contribute to the intrinsic membrane excitability gradient, I therefore applied two pharmacological antagonists of T-type Ca^{2+} channels, TTA-P2 and NiCl$_2$ onto Ca$_V$3.2 null and wild type L II SC. These compounds caused significant reduction in input resistance and action potential firing in wild type ventral cells and had no effect on the null neurons. Additionally, the extent of the decrease in input resistance in ventral neurons, 20-30 MΩ, was similar when using either TTA-P2 and NiCl$_2$. As TTA-P2 is a selective Ca$_V$3 channel inhibitor at the concentration used, these findings strongly suggest that 50 µM NiCl$_2$ selectively blocked T-type Ca^{2+} channels. Importantly, also the difference in input resistance between ventral wild type and null neurons at +100 pA (when measured at – 70 mv) was similar to the reduction in input resistance at +100 pA caused by the blockers when applied onto wild type ventral L II SC. Together, the pharmacological and knock out data mutually corroborate each other and more importantly confirm that Ca$_V$3.2 T-type Ca^{2+} channels contribute towards the dorsal-ventral gradient in intrinsic membrane properties and excitability in SC. Furthermore, they do so via selectively modulating the activity of ventral MEC L II SC. This findings are in contrast with other ion channels that, to-date, were discovered to be responsible for the dorsal-ventral gradient. When HCN1 channels were blocked with ZD7288, there was a change in input resistance across the dorsal-ventral gradient but this was observed to be smaller in more ventral L II SC (Garden et al. 2008). Similarly, blocking potassium channels with barium (Ba^{2+}) resulted in a change in the input resistance mainly in dorsal MEC L II SC. The potassium channel contributing

towards the gradient was later shown to be quinidine sensitive, which points towards the two-pore-domain ion channels as contributors of the dorsal-ventral intrinsic excitability gradient. Nevertheless, the selective contribution of T-type Ca^{2+} channels in ventral L II SC is therefore unique and has to be investigated further in the future.

6.3 T-type Ca_v3.2 Ca^{2+} channels and integration properties

Due to their properties and activity at subthreshold membrane potentials, T-type Ca^{2+} channels are excellent candidates for contributing towards the synaptic integrative properties of L II SC. In the past, EPSPs were evoked in SC by stimulation of MEC layer I (Garden et al. 2008; Alonso et al. 1990) and parasubiculum (Jones 1994). I, in contrast, decided to use artificially evoked αEPSP and test whether, in addition to input resistance and excitability, T-type Ca_v3.2 integrative properties also follow the dorsal-ventral gradient. Although I did not observe the previously reported gradient in the EPSP half-width, my preliminary results showed that wild type ventral cells have a higher summation ratio for αEPSPs elicited at 50 Hz than wild type dorsal neurons. Importantly, no significant differences between Ca_v3.2 null dorsal and ventral stellate neurons were observed. Therefore, Ca_v3.2 channels in addition to HCN and K_{leak} (Garden et al. 2008) should be considered important contributors in shaping synaptic integration in MEC L II SC. This is particularly important as this gradient can dictate how SC sum gamma frequency inputs and can also influence the size of the window for coincident input detection (Garden et al. 2008).

Similarly to the gradient in synaptic integration, also the dorsal-ventral differences in peri-threshold theta-frequency activity were mainly attributed to the activity of K_{leak} and HCN1 channels. Moreover, they were also shown to be sufficient to explain the existing gradient (Dodson et al. 2011). Although the possibility of other ion channels contributing towards the sMPOs activity of SC cannot be excluded, my data clearly show that T-type Ca^{2+} channels do not influence the membrane oscillations.

6.4 The T-type $Ca_v3.2$ current amplitude is larger in ventral L II SC

During current-clamp experiments, I observed a significant increase in input resistance and excitability in ventral MEC L II SC compared with dorsal MEC L II SC. I therefore decided to directly measure T-type Ca^{2+} currents in dorsal and ventral neurons using voltage-clamp. This was the best method for determining differences in $Ca_v3.2$ channels between dorsal and ventral neurons, as, unfortunately, the available $Ca_v3.2$ antibody (Neuromab) is not suitable for quantification of channels, because of lack of specificity under light microscopy.

To isolate the T-type Ca^{2+} current, a variety of pharmacological agents were applied which blocked all other Ca^{2+} currents, K^+ currents, Na^+ currents and I_h. I observed, that wild type ventral SC had significantly larger T-type Ca^{2+} current amplitudes than dorsal neurons. Since these channels will contribute to the cell depolarisation, larger amplitudes in ventral neurons would explain the higher excitability observed during current-clamp experiments. Furthermore, considering the role of $Ca_v3.2$ channels in the context of the Ohm's Law (see Equation 2.2), larger activity of calcium channels in ventral SC will lead to bigger change (Δ) in voltage (V) and, therefore, a higher input resistance (R) compared with dorsal neurons (where ΔV will be smaller) when measurements are made under current-clamp. Finally, also the recently discovered HCN1-$Ca_v3.2$ complex, where the first channel limits the activity of the latter one, could explain the smaller $Ca_v3.2$ amplitudes in dorsal neurons where, as previously mentioned, I_h is more active (in comparison to ventral neurons (Fan et al. 2017; Garden et al. 2008)). Therefore, the voltage-clamp experiments provided both confirmation and an explanation of the current-clamp data.

Additionally, the T-type Ca^{2+} current inactivation time constant was significantly longer in dorsal than ventral SC. It is intriguing, that the dorsal SC inactivation time constant resembles that of $Ca_v3.3$ rather than $Ca_v3.2$ channels when these are expressed in heterologous systems. In the past, no $Ca_v3.1$ was observed to be present in the MEC

(Huang et al. 2011). However, the possibility that $Ca_v3.3$ contributes towards the observed currents has to be considered. It is, though, unlikely, as there was no effect of TTA-P2 or $NiCl_2$ in $Ca_v3.2$ null neurons during current-clamp recordings. The voltage-clamp data also revealed very small TTA-P2 sensitive currents in null neurones. This leads to the conclusion that, even if present, the $Ca_v3.3$ current is rather small compared with $Ca_v3.2$ currents in these neurons. This possibility could be, though, investigated in the future using a $Ca_v3.3$ global knock out (Astori et al. 2011) or subunit specific antibodies, if available. Additionally, a recent study by Fan et al. (2017) showed that the inactivation time constant of expressed $Ca_v3.2$ channels was significantly longer than when co-expressed with HCN1 subunits than in the absence of these (27.8 ms vs 17.7 ms, respectively). Since I_h was shown to be more active in dorsal, than ventral, L II SC (Garden et al. 2008), it is possible that it affected the inactivation time constant of T-type $Ca_v3.2$ currents in these cells more than in ventral SC, resulting in a slower inactivation time constant.

Altogether, MEC L II ventral SC had a larger T-type $Ca_v3.2$ current amplitudes. This in turn leads to greater input resistance and excitability of ventral neurons compared with dorsal SC, thereby contributing towards the dorsal-ventral gradient.

6.5 Physiological relevance

The dorsal-ventral gradient of the L II SC intrinsic properties has been the attention of multiple research groups, primarily due to the potential role of SC in the generation of grid cells. These are activated when the animal explores the environment and the firing fields they generate form a characteristic hexagonal pattern in the MEC L II; hence, their name 'grid cells' (Fyhn et al. 2004). Interestingly, the size of these fields was smaller in the dorsal ends of the MEC and was enhanced in more ventral locations (Hafting et al. 2005; Fyhn et al. 2008; Sargolini et al. 2006). Since L II SC neuron excitability also exhibits this dorsal-ventral gradient, it is believed that these neurons can be particularly important for the formation of grid cells. This in turn makes it

important for us to understand the cellular mechanisms underlying this dorsal-ventral gradient in SC excitability.

The contribution of T-type $Ca_v3.2$ channels towards shaping the synaptic integration gradient can also have important physiological consequences. Having diverse intrinsic mechanisms shaping dorsal and ventral L II SC integrative properties could allow MEC networks to organise their inputs accordingly and hence increase the efficiency of neural computation and decrease information redundancy (Stemmler and Koch 1999). Interestingly, this could also allow dorsal and ventral L II SC to differentially compute the information they receive, even if the inputs are similar or even identical (Pastoll, Ramsden, et al. 2012). This could be achieved, for example, via dissimilarity in the synaptic integration time window at dorsal and ventral ends of the MEC, where SC could differentially adjust their response to external gamma and theta rhythms (Buzsaki 2002). Moreover, potential differences in synaptic plasticity that depends on spike timing (Dan and Poo 2004) between dorsal and ventral cells could influence how they manage information storing. Furthermore, the difference in the window for detection of coincidence inputs could potentially lead to both dorsal and ventral neurons having different functions in terms of the inputs they respond to. For example, dorsal SC can be potentially responsible for the coincidence input detection, whereas ventral neurons, due to the large windows, could manage the input summation if received multiple times at gamma frequencies (Pastoll, Ramsden, et al. 2012). This dorsal-ventral diversity could have significant physiological consequences and regulate how L II responds to gamma oscillations that were previously observed in superficial layers of EC (Chrobak and Buzsaki 1998). These gamma oriented discharges were also coupled with theta rhythms in behaving animals, and together they are believed to control how spatially dispersed cells create temporally integrated neuronal networks (Chrobak and Buzsaki 1998). A thorough understanding of dorsal-ventral gradient and its intrinsic

mechanisms is therefore crucial for deciphering the role of SC within the MEC as well as within all neural networks, e.g. perforant pathway.

Finally, the MEC as a structure is responsible for multiple crucial neuronal processes such as spatial encoding, learning (Hasselmo 2006; Elvander et al. 2004; Blokland et al. 1992), storage of episodic memories (Lipton and Eichenbaum 2008) and recollection-associated processes (Eichenbaum et al. 2007). Additionally, its malfunction has been associated with numerous diseases including Mild Cognitive Impairment (deToledo-Morrell et al. 2004), or neuropschychological diseases, such as schizophrenia (Arnold et al. 1991). EC is also the first brain region affected in AD (Braak and Braak 1985), a disease which is characterised by i.e. the deficits in spatial recognition.

Since the dorsal-ventral gradient is believed to, at least partially, contribute towards spatial exploration processes, and the T-type Ca^{2+} channels help to establish the gradient in intrinsic properties between dorsal and ventral SC, any malfunctions or mutations of T-type Ca^{2+} channels in these neurons, could therefore potentially contribute towards the development of spatial deficits. A thorough investigation of cellular basis of the MEC L II SC gradient could therefore improve our understanding of AD and other disorders.

6.6 Future research

My experiments have shown that T-type Ca^{2+} channels contribute towards the intrinsic membrane properties dorsal-ventral gradient of the MEC L II SC. The electrophysiology experiments clearly showed that it is the higher activity of $Ca_v3.2$ currents in ventral, rather than dorsal, SC that enhances the input resistance and excitability in these neurons. There is no doubt however that this information raises a lot of questions for future research.

First, more experiments exploring the role of $Ca_v3.2$ towards the dorsal-ventral gradient in synaptic integration should be performed. In order to do that, the αEPSPs should be recorded from $Ca_v3.2$ wild type and null animals in the presence of TTA-P2. This pharmacological approach would allow to confirm the data I obtained so far using the current-clamp recordings.

Additionally, immunohistochemistry experiments with a selective T-type $Ca_v3.2$ Ca^{2+} channel antibody and the use of silver-intensified immunogold reaction with electron microscopy should be designed. This would allow to answer the question, whether larger amplitudes of T-type Ca^{2+} currents present in ventral neurons result from higher $Ca_v3.2$ subunit expression in these parts of the MEC L II.

Another possibility is to confirm the dorsal-ventral gradient of $Ca_v3.2$ channels in the MEC L II using molecular biology methods, such as single cell qPCR. This would allow us to measure the levels of $Ca_v3.2$ mRNA in dorsal and ventral SC. Although it would be technically extremely challenging (Bustin 2002), it would allow a direct quantifiable comparison of $Ca_v3.2$ gene expression between dorsal and ventral SC. Furthermore, generation of genetically modified animals, where $Ca_v3.2$ would be knocked out selectively in the MEC L II SC, would without a doubt be a great advantage for the future research of this topic.

The discovery of $Ca_v3.2$ channels in MEC L II SC also raises multiple questions regarding their location and function on the cellular level. T-type Ca^{2+} channels were shown to be wide spread along different cellular locations in the past (see 1.3.5), which in turn brings into question about their location within SC. My recordings have been performed purely from the somata. It is possible, though, that $Ca_v3.2$ channels are present in dendrites and axons and may contribute to synaptic integration and regulating neuronal excitability.

First, the dendritic patch-clamp could be used to test the presence and activity of T-type Ca^{2+} channels. This method, although successful in cells with large dendritic branches such as pyramidal and Purkinje neurons, is likely to be challenging in SC whose dendrites are much smaller (Davie et al. 2006). That is why alternative methods including immunohistochemistry and electron microscopy should be considered. Also, two-photon imaging of dendritic Ca^{2+} in combination with somatic patch-clamp recordings (Schmidt-Hieber et al. 2017) could be used to investigate the role of $Ca_v3.2$ channels in synaptic integration of SC.

In addition to dendrites, the presence and role of T-type Ca^{2+} channels in axons should also be considered. In order to do that, the appropriate electrophysiological protocols could be used in a way to observe and investigate the back propagation of action potentials (Staley 2004). Additionally, two-photon imaging experiments have shown that T-type Ca^{2+} channels are present in the axon initial segment (AIS) of Purkinje cells, L V cortical pyramidal cells and in some interneurons (Bender and Trussell 2009) where they contribute towards action potential threshold and burst firing as well as influence the EPSPs. It is however important to note, that I did not observe any difference in the action potential threshold between $Ca_v3.2$ null and wild type littermates. Additionally, some studies on dorsal cochlear nucleus cells suggest that T-type Ca^{2+} channels found in AIS constitute for only small part of all of the overall neuronal T-type Ca^{2+} current (Bender et al. 2010). Nevertheless, in order to fully

understand the importance and function of these channels in L II SC, their precise subcellular location should be established in the future.

Also *in vivo* experiments in which grid cell properties are compared between $Ca_v3.2$ wild type and null animals could provide us with some additional information. It has been shown that grid cells produce spatially coherent firing patterns when performing behavioural tasks (Fyhn et al. 2007). It would be therefore interesting to examine how the $Ca_v3.2$ null animals would perform during behavioural tests. Furthermore, it was previously observed that mice lacking HCN1 subunits exhibit significantly larger grid fields sizes which are spaced apart compared with their wild type littermates (Giocomo et al. 2011). This rises the questions whether the grid scale and firing pattern may also change in $Ca_v3.2$ null animals compared with wild types.

Although further work is clearly needed to answer these multiple pressing questions described above, my research clearly showed, that the T-type Ca^{2+} channels helps to set up the dorsal-ventral gradient in intrinsic properties of the MEC L II SC.

7. References

Aggleton, J. P., M. J. Burton, and R. E. Passingham. 1980. 'Cortical and subcortical afferents to the amygdala of the rhesus monkey (Macaca mulatta)', *Brain Res*, 190: 347-68.

Aggleton, J. P., R. Desimone, and M. Mishkin. 1986. 'The origin, course, and termination of the hippocampothalamic projections in the macaque', *J Comp Neurol*, 243: 409-21.

Alonso, A., M. de Curtis, and R. Llinas. 1990. 'Postsynaptic Hebbian and non-Hebbian long-term potentiation of synaptic efficacy in the entorhinal cortex in slices and in the isolated adult guinea pig brain', *Proc Natl Acad Sci U S A*, 87: 9280-4.

Alonso, A., and C. Kohler. 1984. 'A study of the reciprocal connections between the septum and the entorhinal area using anterograde and retrograde axonal transport methods in the rat brain', *J Comp Neurol*, 225: 327-43.

Alonso, A., and R. Klink. 1993. 'Differential electroresponsiveness of stellate and pyramidal-like cells of medial entorhinal cortex layer II', *J Neurophysiol*, 70: 128-43.

Alonso, A., and R. R. Llinas. 1989. 'Subthreshold Na+-dependent theta-like rhythmicity in stellate cells of entorhinal cortex layer II', *Nature*, 342: 175-7.

Amaral, D. G. 1993. 'Emerging principles of intrinsic hippocampal organization', *Curr Opin Neurobiol*, 3: 225-9.

Amaral, D. G., and M. P. Witter. 1995. The Rat Nervous System. *Academic Press*, 443-493.

Amaral, D. G., and R. Insausti. 1992. 'Retrograde transport of D-[3H]-aspartate injected into the monkey amygdaloid complex', *Exp Brain Res*, 88: 375-88.

Amaral, D. G., R. Insausti, and W. M. Cowan. 1984. 'The commissural connections of the monkey hippocampal formation', *J Comp Neurol*, 224: 307-36.

Arnold, S. E., B. T. Hyman, G. W. Van Hoesen, and A. R. Damasio. 1991. 'Some cytoarchitectural abnormalities of the entorhinal cortex in schizophrenia', *Arch Gen Psychiatry*, 48: 625-32.

Arnoult, C., J. R. Lemos, and H. M. Florman. 1997. 'Voltage-dependent modulation of T-type calcium channels by protein tyrosine phosphorylation', *EMBO J*, 16: 1593-9.

Astori, S., R. D. Wimmer, H. M. Prosser, C. Corti, M. Corsi, N. Liaudet, A. Volterra, P. Franken, J. P. Adelman, and A. Luthi. 2011. 'The Ca(V)3.3 calcium channel is the major sleep spindle pacemaker in thalamus', *Proc Natl Acad Sci U S A*, 108: 13823-8.

Autret, L., I. Mechaly, F. Scamps, J. Valmier, P. Lory, and G. Desmadryl. 2005. 'The involvement of Cav3.2/alpha1H T-type calcium channels in excitability of mouse embryonic primary vestibular neurones', *J Physiol*, 567: 67-78.

Barrett, P. Q., H. K. Lu, R. Colbran, A. Czernik, and J. J. Pancrazio. 2000. 'Stimulation of unitary T-type Ca(2+) channel currents by calmodulin-dependent protein kinase II', *Am J Physiol Cell Physiol*, 279: C1694-703.

Beauvais, K., F. Cave-Riant, C. De Barace, M. Tardieu, E. Tournier-Lasserve, and A. Furby. 2004. 'New CACNA1A gene mutation in a case of familial hemiplegic migraine with status epilepticus', *Eur Neurol*, 52: 58-61.

Beckstead, Robert M. 1978. 'Afferent connections of the entorhinal area in the rat as demonstrated b

Beckstead, R. M. 1979. 'An autoradiographic examination of corticocortical and subcortical projections of the mediodorsal-projection (prefrontal) cortex in the rat', *J Comp Neurol*, 184: 43-62.y retrograde cell-labeling with horseradish peroxidase', *Brain research*, 152: 249-64.

Beed, P., M. H. Bendels, H. F. Wiegand, C. Leibold, F. W. Johenning, and D. Schmitz. 2010. 'Analysis of excitatory microcircuitry in the medial entorhinal cortex reveals cell-type-specific differences', *Neuron*, 68: 1059-66.

Beed, P., A. Gundlfinger, S. Schneiderbauer, J. Song, C. Bohm, A. Burgalossi, M. Brecht, I. Vida, and D. Schmitz. 2013. 'Inhibitory gradient along the dorsoventral axis in the medial entorhinal cortex', *Neuron*, 79: 1197-207.

Belardetti, F., and G. W. Zamponi. 2008. 'Linking calcium-channel isoforms to potential therapies', *Curr Opin Investig Drugs*, 9: 707-15.

Bellgowan, P. S., E. A. Buffalo, J. Bodurka, and A. Martin. 2009. 'Lateralized spatial and object memory encoding in entorhinal and perirhinal cortices', *Learn Mem*, 16: 433-8.

Bender, K. J., C. P. Ford, and L. O. Trussell. 2010. 'Dopaminergic modulation of axon initial segment calcium channels regulates action potential initiation', *Neuron*, 68: 500-11.

Bender, K. J., and L. O. Trussell. 2009. 'Axon initial segment Ca2+ channels influence action potential generation and timing', *Neuron*, 61: 259-71.

Bernal Sierra, Y. A., J. Haseleu, A. Kozlenkov, V. Begay, and G. R. Lewin. 2017. 'Genetic Tracing of Cav3.2 T-Type Calcium Channel Expression in the Peripheral Nervous System', *Front Mol Neurosci*, 10: 70.

Biel, M., C. Wahl-Schott, S. Michalakis, and X. Zong. 2009. 'Hyperpolarization-activated cation channels: from genes to function', *Physiol Rev*, 89: 847-85.

Blair, H. T., A. C. Welday, and K. Zhang. 2007. 'Scale-invariant memory representations emerge from moire interference between grid fields that produce theta oscillations: a computational model', *J Neurosci*, 27: 3211-29.

Blethyn, K. L., S. W. Hughes, T. I. Toth, D. W. Cope, and V. Crunelli. 2006. 'Neuronal basis of the slow (<1 Hz) oscillation in neurons of the nucleus reticularis thalami in vitro', *J Neurosci*, 26: 2474-86.

Blokland, A., W. Honig, and W. G. Raaijmakers. 1992. 'Effects of intra-hippocampal scopolamine injections in a repeated spatial acquisition task in the rat', *Psychopharmacology (Berl)*, 109: 373-6.

Boehlen, A., U. Heinemann, and I. Erchova. 2010. 'The range of intrinsic frequencies represented by medial entorhinal cortex stellate cells extends with age', *J Neurosci*, 30: 4585-9.

Bossu, J. L., and A. Feltz. 1986. 'Inactivation of the low-threshold transient calcium current in rat sensory neurones: evidence for a dual process', *J Physiol*, 376: 341-57.

Bourinet, E., A. Alloui, A. Monteil, C. Barrere, B. Couette, O. Poirot, A. Pages, J. McRory, T. P. Snutch, A. Eschalier, and J. Nargeot. 2005. 'Silencing of the Cav3.2 T-type calcium channel gene in sensory neurons demonstrates its major role in nociception', *EMBO J*, 24: 315-24.

Braak, H., and E. Braak. 1985. 'On areas of transition between entorhinal allocortex and temporal isocortex in the human brain. Normal morphology and lamina-specific pathology in Alzheimer's disease', *Acta Neuropathol*, 68: 325-32.

Brodmann, Korbinian. 1909. *Vergleichende Lokalisationslehre der Grosshirnrinde in ihren Prinzipien dargestellt auf Grund des Zellenbaues* (Barth).

Broicher, T., T. Kanyshkova, P. Meuth, H. C. Pape, and T. Budde. 2008. 'Correlation of T-channel coding gene expression, IT, and the low threshold Ca2+ spike in the thalamus of a rat model of absence epilepsy', *Mol Cell Neurosci*, 39: 384-99.

Bruehl, C., and W. J. Wadman. 1999. 'Calcium currents in acutely isolated stellate and pyramidal neurons of rat entorhinal cortex', *Brain Res*, 816: 554-62.

Burwell, R. D., and D. G. Amaral. 1998. 'Perirhinal and postrhinal cortices of the rat: interconnectivity and connections with the entorhinal cortex', *J Comp Neurol*, 391: 293-321.

Bustin, S. A. 2002. 'Quantification of mRNA using real-time reverse transcription PCR (RT-PCR): trends and problems', *J Mol Endocrinol*, 29: 23-39.

Buzsaki, G. 2002. 'Theta oscillations in the hippocampus', *Neuron*, 33: 325-40.

Caballero-Bleda, M., and M. P. Witter. 1993. 'Regional and laminar organization of projections from the presubiculum and parasubiculum to the entorhinal cortex: an anterograde tracing study in the rat', *J Comp Neurol*, 328: 115-29.

Cain, S. M., and T. P. Snutch. 2010. 'Contributions of T-type calcium channel isoforms to neuronal firing', *Channels (Austin)*, 4: 475-82.

Canteras, N. S., R. B. Simerly, and L. W. Swanson. 1994. 'Organization of projections from the ventromedial nucleus of the hypothalamus: a Phaseolus vulgaris-leucoagglutinin study in the rat', *J Comp Neurol*, 348: 41-79.

Canto, C. B., F. G. Wouterlood, and M. P. Witter. 2008. 'What does the anatomical organization of the entorhinal cortex tell us?', *Neural Plast*, 2008: 381243.

Canto, CB, P Ganter, EI Moser, MB Moser, and MP Witter. 2006. 'Neuron diversity in the medial entorhinal cortex of the rat', *Soc Neurosci Abst*, 32.

Carbone, E., and H. D. Lux. 1984. 'A low voltage-activated, fully inactivating Ca channel in vertebrate sensory neurones', *Nature*, 310: 501-2.

Carmichael, S. T., and J. L. Price. 1995. 'Limbic connections of the orbital and medial prefrontal cortex in macaque monkeys', *J Comp Neurol*, 363: 615-41.

Carter, A. G., and B. L. Sabatini. 2004. 'State-dependent calcium signaling in dendritic spines of striatal medium spiny neurons', *Neuron*, 44: 483-93.

Castelli, L., and J. Magistretti. 2006. 'High-voltage-activated Ca2+ currents show similar patterns of expression in stellate and pyramidal cells from rat entorhinal cortex layer II', *Brain Res*, 1090: 76-88.

Chapuis, J., Y. Cohen, X. He, Z. Zhang, S. Jin, F. Xu, and D. A. Wilson. 2013. 'Lateral entorhinal modulation of piriform cortical activity and fine odor discrimination', *J Neurosci*, 33: 13449-59.

Chausson, P., N. Leresche, and R. C. Lambert. 2013. 'Dynamics of intrinsic dendritic calcium signaling during tonic firing of thalamic reticular neurons', *PLoS One*, 8: e72275.

Chemin, J., A. Mezghrani, I. Bidaud, S. Dupasquier, F. Marger, C. Barrere, J. Nargeot, and P. Lory. 2007. 'Temperature-dependent modulation of CaV3 T-type calcium channels by protein kinases C and A in mammalian cells', *J Biol Chem*, 282: 32710-8.

Chemin, J., A. Monteil, E. Perez-Reyes, E. Bourinet, J. Nargeot, and P. Lory. 2002. 'Specific contribution of human T-type calcium channel isotypes (alpha(1G), alpha(1H) and alpha(1I)) to neuronal excitability', *J Physiol*, 540: 3-14.

Chemin, J., J. Nargeot, and P. Lory. 2002. 'Neuronal T-type alpha 1H calcium channels induce neuritogenesis and expression of high-voltage-activated calcium channels in the NG108-15 cell line', *J Neurosci*, 22: 6856-62.

Chen, C. C., K. G. Lamping, D. W. Nuno, R. Barresi, S. J. Prouty, J. L. Lavoie, L. L. Cribbs, S. K. England, C. D. Sigmund, R. M. Weiss, R. A. Williamson, J. A. Hill, and K. P. Campbell. 2003. 'Abnormal coronary function in mice deficient in alpha1H T-type Ca2+ channels', *Science*, 302: 1416-8.

Choe, W., R. B. Messinger, E. Leach, V. S. Eckle, A. Obradovic, R. Salajegheh, V. Jevtovic-Todorovic, and S. M. Todorovic. 2011. 'TTA-P2 is a potent and selective blocker of T-type calcium channels in rat sensory neurons and a novel antinociceptive agent', *Mol Pharmacol*, 80: 900-10.

Choi, S., H. S. Na, J. Kim, J. Lee, S. Lee, D. Kim, J. Park, C. C. Chen, K. P. Campbell, and H. S. Shin. 2007. 'Attenuated pain responses in mice lacking Ca(V)3.2 T-type channels', *Genes Brain Behav*, 6: 425-31.

Chrobak, J. J., and G. Buzsaki. 1998. 'Gamma oscillations in the entorhinal cortex of the freely behaving rat', *J Neurosci*, 18: 388-98.

Connelly, W. M., V. Crunelli, and A. C. Errington. 2017. 'Variable Action Potential Backpropagation during Tonic Firing and Low-Threshold Spike Bursts in

Thalamocortical But Not Thalamic Reticular Nucleus Neurons', *J Neurosci*, 37: 5319-33.

Couey, J. J., A. Witoelar, S. J. Zhang, K. Zheng, J. Ye, B. Dunn, R. Czajkowski, M. B. Moser, E. I. Moser, Y. Roudi, and M. P. Witter. 2013. 'Recurrent inhibitory circuitry as a mechanism for grid formation', *Nat Neurosci*, 16: 318-24.

Crandall, S. R., G. Govindaiah, and C. L. Cox. 2010. 'Low-threshold Ca2+ current amplifies distal dendritic signaling in thalamic reticular neurons', *J Neurosci*, 30: 15419-29.

Cribbs, L. 2010. 'T-type calcium channel expression and function in the diseased heart', *Channels (Austin)*, 4: 447-52.

Cribbs, L. L., J. H. Lee, J. Yang, J. Satin, Y. Zhang, A. Daud, J. Barclay, M. P. Williamson, M. Fox, M. Rees, and E. Perez-Reyes. 1998. 'Cloning and characterization of alpha1H from human heart, a member of the T-type Ca2+ channel gene family', *Circ Res*, 83: 103-9.

Crunelli, V., S. Lightowler, and C. E. Pollard. 1989. 'A T-type Ca2+ current underlies low-threshold Ca2+ potentials in cells of the cat and rat lateral geniculate nucleus', *J Physiol*, 413: 543-61.

Crunelli, V., T. I. Toth, D. W. Cope, K. Blethyn, and S. W. Hughes. 2005. 'The 'window' T-type calcium current in brain dynamics of different behavioural states', *J Physiol*, 562: 121-9.

Dan, Y., and M. M. Poo. 2004. 'Spike timing-dependent plasticity of neural circuits', *Neuron*, 44: 23-30.

Davie, J. T., M. H. Kole, J. J. Letzkus, E. A. Rancz, N. Spruston, G. J. Stuart, and M. Hausser. 2006. 'Dendritic patch-clamp recording', *Nat Protoc*, 1: 1235-47.

Dawodu, S., and M. Thom. 2005. 'Quantitative neuropathology of the entorhinal cortex region in patients with hippocampal sclerosis and temporal lobe epilepsy', *Epilepsia*, 46: 23-30.

Day, M., D. B. Carr, S. Ulrich, E. Ilijic, T. Tkatch, and D. J. Surmeier. 2005. 'Dendritic excitability of mouse frontal cortex pyramidal neurons is shaped by the interaction among HCN, Kir2, and Kleak channels', *J Neurosci*, 25: 8776-87.

Deng, P. Y., S. K. Poudel, L. Rojanathammanee, J. E. Porter, and S. Lei. 2007. 'Serotonin inhibits neuronal excitability by activating two-pore domain k+ channels in the entorhinal cortex', *Mol Pharmacol*, 72: 208-18.

Deng, P. Y., Z. Xiao, C. Yang, L. Rojanathammanee, L. Grisanti, J. Watt, J. D. Geiger, R. Liu, J. E. Porter, and S. Lei. 2009. 'GABA(B) receptor activation inhibits neuronal excitability and spatial learning in the entorhinal cortex by activating TREK-2 K+ channels', *Neuron*, 63: 230-43.

Deschenes, M., M. Paradis, J. P. Roy, and M. Steriade. 1984. 'Electrophysiology of neurons of lateral thalamic nuclei in cat: resting properties and burst discharges', *J Neurophysiol*, 51: 1196-219.

Deshmukh, S. S., and J. J. Knierim. 2011. 'Representation of non-spatial and spatial information in the lateral entorhinal cortex', *Front Behav Neurosci*, 5: 69.

Destexhe, A., M. Neubig, D. Ulrich, and J. Huguenard. 1998. 'Dendritic low-threshold calcium currents in thalamic relay cells', *J Neurosci*, 18: 3574-88.

deToledo-Morrell, L., T. R. Stoub, M. Bulgakova, R. S. Wilson, D. A. Bennett, S. Leurgans, J. Wuu, and D. A. Turner. 2004. 'MRI-derived entorhinal volume is a good predictor of conversion from MCI to AD', *Neurobiol Aging*, 25: 1197-203.

Dhillon, A., and R. S. Jones. 2000. 'Laminar differences in recurrent excitatory transmission in the rat entorhinal cortex in vitro', *Neuroscience*, 99: 413-22.

Diana, M. A., Y. Otsu, G. Maton, T. Collin, M. Chat, and S. Dieudonne. 2007. 'T-type and L-type Ca2+ conductances define and encode the bimodal firing pattern of vestibulocerebellar unipolar brush cells', *J Neurosci*, 27: 3823-38.

Dickson, C. T., J. Magistretti, M. H. Shalinsky, E. Fransen, M. E. Hasselmo, and A. Alonso. 2000. 'Properties and role of I(h) in the pacing of subthreshold oscillations in entorhinal cortex layer II neurons', *J Neurophysiol*, 83: 2562-79.

Dodson, P. D., H. Pastoll, and M. F. Nolan. 2011. 'Dorsal-ventral organization of theta-like activity intrinsic to entorhinal stellate neurons is mediated by differences in stochastic current fluctuations', *J Physiol*, 589: 2993-3008.

Doeller, C. F., C. Barry, and N. Burgess. 2010. 'Evidence for grid cells in a human memory network', *Nature*, 463: 657-61.

Domich, L., G. Oakson, and M. Steriade. 1986. 'Thalamic burst patterns in the naturally sleeping cat: a comparison between cortically projecting and reticularis neurones', *J Physiol*, 379: 429-49.

Dorval, A. D., Jr., and J. A. White. 2005. 'Channel noise is essential for perithreshold oscillations in entorhinal stellate neurons', *J Neurosci*, 25: 10025-8.

Dreyfus, F. M., A. Tscherter, A. C. Errington, J. J. Renger, H. S. Shin, V. N. Uebele, V. Crunelli, R. C. Lambert, and N. Leresche. 2010. 'Selective T-type calcium channel block in thalamic neurons reveals channel redundancy and physiological impact of I(T)window', *J Neurosci*, 30: 99-109.

Du, F., T. Eid, E. W. Lothman, C. Kohler, and R. Schwarcz. 1995. 'Preferential neuronal loss in layer III of the medial entorhinal cortex in rat models of temporal lobe epilepsy', *J Neurosci*, 15: 6301-13.

Du, F., W. O. Whetsell, Jr., B. Abou-Khalil, B. Blumenkopf, E. W. Lothman, and R. Schwarcz. 1993. 'Preferential neuronal loss in layer III of the entorhinal cortex in patients with temporal lobe epilepsy', *Epilepsy Res*, 16: 223-33.

Dubreuil, A. S., H. Boukhaddaoui, G. Desmadryl, C. Martinez-Salgado, R. Moshourab, G. R. Lewin, P. Carroll, J. Valmier, and F. Scamps. 2004. 'Role of T-type calcium current in identified D-hair mechanoreceptor neurons studied in vitro', *J Neurosci*, 24: 8480-4.

Dudman, J. T., and M. F. Nolan. 2009. 'Stochastically gating ion channels enable patterned spike firing through activity-dependent modulation of spike probability', *PLoS Comput Biol*, 5: e1000290.

Dziegielewska, B., L. S. Gray, and J. Dziegielewski. 2014. 'T-type calcium channels blockers as new tools in cancer therapies', *Pflugers Arch*, 466: 801-10.

Eder, C., E. Ficker, J. Gundel, and U. Heinemann. 1991. 'Outward Currents in Rat Entorhinal Cortex Stellate Cells Studied with Conventional and Perforated Patch Recordings', *Eur J Neurosci*, 3: 1271-80.

Egger, V., K. Svoboda, and Z. F. Mainen. 2003. 'Mechanisms of lateral inhibition in the olfactory bulb: efficiency and modulation of spike-evoked calcium influx into granule cells', *J Neurosci*, 23: 7551-8.

Eichenbaum, H., A. P. Yonelinas, and C. Ranganath. 2007. 'The medial temporal lobe and recognition memory', *Annu Rev Neurosci*, 30: 123-52.

Ellinor, P. T., J. Yang, W. A. Sather, J. F. Zhang, and R. W. Tsien. 1995. 'Ca2+ channel selectivity at a single locus for high-affinity Ca2+ interactions', *Neuron*, 15: 1121-32.

Elvander, E., P. A. Schott, J. Sandin, B. Bjelke, J. Kehr, T. Yoshitake, and S. O. Ogren. 2004. 'Intraseptal muscarinic ligands and galanin: influence on hippocampal acetylcholine and cognition', *Neuroscience*, 126: 541-57.

Erchova, I., G. Kreck, U. Heinemann, and A. V. Herz. 2004. 'Dynamics of rat entorhinal cortex layer II and III cells: characteristics of membrane potential resonance at rest predict oscillation properties near threshold', *J Physiol*, 560: 89-110.

Fan, J., M. A. Gandini, F. X. Zhang, L. Chen, I. A. Souza, and G. W. Zamponi. 2017. 'Down-regulation of T-type Cav3.2 channels by hyperpolarization-activated cyclic nucleotide-gated channel 1 (HCN1): Evidence of a signaling complex', *Channels (Austin)*: 1-10.

Fernandez, F. R., and J. A. White. 2008. 'Artificial synaptic conductances reduce subthreshold oscillations and periodic firing in stellate cells of the entorhinal cortex', *J Neurosci*, 28: 3790-803.

Ferron, L., V. Capuano, E. Deroubaix, A. Coulombe, and J. F. Renaud. 2002. 'Functional and molecular characterization of a T-type Ca(2+) channel during fetal and postnatal rat heart development', *J Mol Cell Cardiol*, 34: 533-46.

Finch, D. M., A. M. Tan, and M. Isokawa-Akesson. 1988. 'Feedforward inhibition of the rat entorhinal cortex and subicular complex', *J Neurosci*, 8: 2213-26.

Francois, A., N. Schuetter, S. Laffray, J. Sanguesa, A. Pizzoccaro, S. Dubel, A. Mantilleri, J. Nargeot, J. Noel, J. N. Wood, A. Moqrich, O. Pongs, and E. Bourinet. 2015. 'The Low-Threshold Calcium Channel Cav3.2 Determines Low-Threshold Mechanoreceptor Function', *Cell Rep*.

Fransen, E., A. A. Alonso, C. T. Dickson, J. Magistretti, and M. E. Hasselmo. 2004. 'Ionic mechanisms in the generation of subthreshold oscillations and action potential clustering in entorhinal layer II stellate neurons', *Hippocampus*, 14: 368-84.

Frazier, C. J., J. R. Serrano, E. G. George, X. Yu, A. Viswanathan, E. Perez-Reyes, and S. W. Jones. 2001. 'Gating kinetics of the alpha1I T-type calcium channel', *J Gen Physiol*, 118: 457-70.

French, C. R., P. Sah, K. J. Buckett, and P. W. Gage. 1990. 'A voltage-dependent persistent sodium current in mammalian hippocampal neurons', *J Gen Physiol*, 95: 1139-57.

Fuchs, E. C., A. Neitz, R. Pinna, S. Melzer, A. Caputi, and H. Monyer. 2016. 'Local and Distant Input Controlling Excitation in Layer II of the Medial Entorhinal Cortex', *Neuron*, 89: 194-208.

Fuhs, M. C., and D. S. Touretzky. 2006. 'A spin glass model of path integration in rat medial entorhinal cortex', *J Neurosci*, 26: 4266-76.

Fyhn, M., T. Hafting, A. Treves, M. B. Moser, and E. I. Moser. 2007. 'Hippocampal remapping and grid realignment in entorhinal cortex', *Nature*, 446: 190-4.

Fyhn, M., T. Hafting, M. P. Witter, E. I. Moser, and M. B. Moser. 2008. 'Grid cells in mice', *Hippocampus*, 18: 1230-8.

Fyhn, M., S. Molden, M. P. Witter, E. I. Moser, and M. B. Moser. 2004. 'Spatial representation in the entorhinal cortex', *Science*, 305: 1258-64.

Garden, D. L., P. D. Dodson, C. O'Donnell, M. D. White, and M. F. Nolan. 2008. 'Tuning of synaptic integration in the medial entorhinal cortex to the organization of grid cell firing fields', *Neuron*, 60: 875-89.

Germroth, P., W. K. Schwerdtfeger, and E. H. Buhl. 1989. 'Morphology of identified entorhinal neurons projecting to the hippocampus. A light microscopical study combining retrograde tracing and intracellular injection', *Neuroscience*, 30: 683-91.

Gingrich, J. A., and R. Hen. 2000. 'The broken mouse: the role of development, plasticity and environment in the interpretation of phenotypic changes in knockout mice', *Curr Opin Neurobiol*, 10: 146-52.

Giocomo, L. M., and M. E. Hasselmo. 2008. 'Time constants of h current in layer ii stellate cells differ along the dorsal to ventral axis of medial entorhinal cortex', *J Neurosci*, 28: 9414-25.

Giocomo, L. M., S. A. Hussaini, F. Zheng, E. R. Kandel, M. B. Moser, and E. I. Moser. 2011. 'Grid cells use HCN1 channels for spatial scaling', *Cell*, 147: 1159-70.

Giocomo, L. M., T. Stensola, T. Bonnevie, T. Van Cauter, M. B. Moser, and E. I. Moser. 2014. 'Topography of head direction cells in medial entorhinal cortex', *Curr Biol*, 24: 252-62.

Giocomo, L. M., E. A. Zilli, E. Fransen, and M. E. Hasselmo. 2007. 'Temporal frequency of subthreshold oscillations scales with entorhinal grid cell field spacing', *Science*, 315: 1719-22.

Gloveli, T., T. Dugladze, D. Schmitz, and U. Heinemann. 2001. 'Properties of entorhinal cortex deep layer neurons projecting to the rat dentate gyrus', *Eur J Neurosci*, 13: 413-20.

Gloveli, T., D. Schmitz, R. M. Empson, T. Dugladze, and U. Heinemann. 1997. 'Morphological and electrophysiological characterization of layer III cells of the medial entorhinal cortex of the rat', *Neuroscience*, 77: 629-48.

Goto, M., O. Abe, T. Miyati, T. Yoshikawa, N. Hayashi, H. Takao, S. Inano, H. Kabasawa, H. Mori, A. Kunimatsu, S. Aoki, K. Ino, K. Iida, K. Yano, and K. Ohtomo. 2011. 'Entorhinal cortex volume measured with 3T MRI is positively correlated with the Wechsler Memory Scale-Revised logical/verbal memory score for healthy subjects', *Neuroradiology*, 53: 617-22.

Grubb, M. S., and J. Burrone. 2010. 'Activity-dependent relocation of the axon initial segment fine-tunes neuronal excitability', *Nature*, 465: 1070-4.

Guo, W., K. Kamiya, I. Kodama, and J. Toyama. 1998. 'Cell cycle-related changes in the voltage-gated Ca2+ currents in cultured newborn rat ventricular myocytes', *J Mol Cell Cardiol*, 30: 1095-103.

Haas, J. S., and J. A. White. 2002. 'Frequency selectivity of layer II stellate cells in the medial entorhinal cortex', *J Neurophysiol*, 88: 2422-9.

Hafting, T., M. Fyhn, S. Molden, M. B. Moser, and E. I. Moser. 2005. 'Microstructure of a spatial map in the entorhinal cortex', *Nature*, 436: 801-6.

Hamam, B. N., D. G. Amaral, and A. A. Alonso. 2002. 'Morphological and electrophysiological characteristics of layer V neurons of the rat lateral entorhinal cortex', *J Comp Neurol*, 451: 45-61.

Hamam, B. N., T. E. Kennedy, A. Alonso, and D. G. Amaral. 2000. 'Morphological and electrophysiological characteristics of layer V neurons of the rat medial entorhinal cortex', *J Comp Neurol*, 418: 457-72.

Handforth, A., G. E. Homanics, D. F. Covey, K. Krishnan, J. Y. Lee, K. Sakimura, F. C. Martin, and A. Quesada. 2010. 'T-type calcium channel antagonists suppress tremor in two mouse models of essential tremor', *Neuropharmacology*, 59: 380-7.

Hargreaves, E. L., G. Rao, I. Lee, and J. J. Knierim. 2005. 'Major dissociation between medial and lateral entorhinal input to dorsal hippocampus', *Science*, 308: 1792-4.

Hasselmo, M. E. 2006. 'The role of acetylcholine in learning and memory', *Curr Opin Neurobiol*, 16: 710-5.

Hasselmo, M. E., L. M. Giocomo, and E. A. Zilli. 2007. 'Grid cell firing may arise from interference of theta frequency membrane potential oscillations in single neurons', *Hippocampus*, 17: 1252-71.

Heron, S. E., H. A. Phillips, J. C. Mulley, A. Mazarib, M. Y. Neufeld, S. F. Berkovic, and I. E. Scheffer. 2004. 'Genetic variation of CACNA1H in idiopathic generalized epilepsy', *Ann Neurol*, 55: 595-6.

Heys, J. G., L. M. Giocomo, and M. E. Hasselmo. 2010. 'Cholinergic modulation of the resonance properties of stellate cells in layer II of medial entorhinal cortex', *J Neurophysiol*, 104: 258-70.

Hildebrand, M. E., P. Isope, T. Miyazaki, T. Nakaya, E. Garcia, A. Feltz, T. Schneider, J. Hescheler, M. Kano, K. Sakimura, M. Watanabe, S. Dieudonne, and T. P. Snutch. 2009. 'Functional coupling between mGluR1 and Cav3.1 T-type calcium channels contributes to parallel fiber-induced fast calcium signaling within Purkinje cell dendritic spines', *J Neurosci*, 29: 9668-82.

Honigsperger, C., M. J. Nigro, and J. F. Storm. 2017. 'Physiological roles of Kv2 channels in entorhinal cortex layer II stellate cells revealed by Guangxitoxin-1E', *J Physiol*, 595: 739-57.

Horibe, S., E. Tarusawa, Y. Komatsu, and Y. Yoshimura. 2014. 'Ni(2+)-sensitive T-type Ca(2+) channel currents are regulated in parallel with synaptic and visual response plasticity in visual cortex', *Neurosci Res*, 87: 33-9.

Hu, H., K. Vervaeke, and J. F. Storm. 2007. 'M-channels (Kv7/KCNQ channels) that regulate synaptic integration, excitability, and spike pattern of CA1 pyramidal cells are located in the perisomatic region', *J Neurosci*, 27: 1853-67.

Huang, Z., R. Lujan, I. Kadurin, V. N. Uebele, J. J. Renger, A. C. Dolphin, and M. M. Shah. 2011. 'Presynaptic HCN1 channels regulate Cav3.2 activity and neurotransmission at select cortical synapses', *Nat Neurosci*, 14: 478-86.

Huguenard, J. R., and D. A. Prince. 1992. 'A novel T-type current underlies prolonged Ca(2+)-dependent burst firing in GABAergic neurons of rat thalamic reticular nucleus', *J Neurosci*, 12: 3804-17.

Hutcheon, B., and Y. Yarom. 2000. 'Resonance, oscillation and the intrinsic frequency preferences of neurons', *Trends Neurosci*, 23: 216-22.

Iftinca, M. C. 2011. 'Neuronal T-type calcium channels: what's new? Iftinca: T-type channel regulation', *J Med Life*, 4: 126-38.

Insausti, R., D. G. Amaral, and W. M. Cowan. 1987a. 'The entorhinal cortex of the monkey: II. Cortical afferents', *J Comp Neurol*, 264: 356-95.

———. 1987b. 'The entorhinal cortex of the monkey: III. Subcortical afferents', *J Comp Neurol*, 264: 396-408.

Jahnsen, H., and R. Llinas. 1984. 'Electrophysiological properties of guinea-pig thalamic neurones: an in vitro study', *J Physiol*, 349: 205-26.

Jones, R. S. 1994. 'Synaptic and intrinsic properties of neurons of origin of the perforant path in layer II of the rat entorhinal cortex in vitro', *Hippocampus*, 4: 335-53.

Kaneda, M., and N. Akaike. 1989. 'The low-threshold Ca current in isolated amygdaloid neurons in the rat', *Brain Res*, 497: 187-90.

Kaneda, M., M. Wakamori, C. Ito, and N. Akaike. 1990. 'Low-threshold calcium current in isolated Purkinje cell bodies of rat cerebellum', *J Neurophysiol*, 63: 1046-51.

Kang, H. W., J. Y. Park, S. W. Jeong, J. A. Kim, H. J. Moon, E. Perez-Reyes, and J. H. Lee. 2006. 'A molecular determinant of nickel inhibition in Cav3.2 T-type calcium channels', *J Biol Chem*, 281: 4823-30.

Keene, C. S., J. Bladon, S. McKenzie, C. D. Liu, J. O'Keefe, and H. Eichenbaum. 2016. 'Complementary Functional Organization of Neuronal Activity Patterns in the Perirhinal, Lateral Entorhinal, and Medial Entorhinal Cortices', *J Neurosci*, 36: 3660-75.

Kerr, K. M., K. L. Agster, S. C. Furtak, and R. D. Burwell. 2007. 'Functional neuroanatomy of the parahippocampal region: the lateral and medial entorhinal areas', *Hippocampus*, 17: 697-708.

Khawaja, F. A., A. A. Alonso, and C. W. Bourque. 2007. 'Ca(2+)-dependent K(+) currents and spike-frequency adaptation in medial entorhinal cortex layer II stellate cells', *Hippocampus*, 17: 1143-8.

Khosravani, H., and G. W. Zamponi. 2006. 'Voltage-gated calcium channels and idiopathic generalized epilepsies', *Physiol Rev*, 86: 941-66.

Killian, N. J., M. J. Jutras, and E. A. Buffalo. 2012. 'A map of visual space in the primate entorhinal cortex', *Nature*, 491: 761-4.

Kim, D., I. Song, S. Keum, T. Lee, M. J. Jeong, S. S. Kim, M. W. McEnery, and H. S. Shin. 2001. 'Lack of the burst firing of thalamocortical relay neurons and resistance to absence seizures in mice lacking alpha(1G) T-type Ca(2+) channels', *Neuron*, 31: 35-45.

Kirwan, C. B., and C. E. Stark. 2004. 'Medial temporal lobe activation during encoding and retrieval of novel face-name pairs', *Hippocampus*, 14: 919-30.

Klink, R., and A. Alonso. 1997a. 'Morphological characteristics of layer II projection neurons in the rat medial entorhinal cortex', *Hippocampus*, 7: 571-83.

———. 1997b. 'Muscarinic modulation of the oscillatory and repetitive firing properties of entorhinal cortex layer II neurons', *J Neurophysiol*, 77: 1813-28.

Kloosterman, F., M. P. Witter, and T. Van Haeften. 2003. 'Topographical and laminar organization of subicular projections to the parahippocampal region of the rat', *J Comp Neurol*, 455: 156-71.

Kohler, C. 1985. 'Intrinsic projections of the retrohippocampal region in the rat brain. I. The subicular complex', *J Comp Neurol*, 236: 504-22.

Kohler, C., and V. Chan-Palay. 1983. 'Somatostatin and vasoactive intestinal polypeptide-like immunoreactive cells and terminals in the retrohippocampal region of the rat brain', *Anat Embryol (Berl)*, 167: 151-72.

Kohler, C., L. Eriksson, S. Davies, and V. Chan-Palay. 1986. 'Neuropeptide Y innervation of the hippocampal region in the rat and monkey brain', *J Comp Neurol*, 244: 384-400.

Komatsu, Y., and M. Iwakiri. 1992. 'Low-threshold Ca2+ channels mediate induction of long-term potentiation in kitten visual cortex', *J Neurophysiol*, 67: 401-10.

Krayniak, P. F., R. C. Meibach, and A. Siegel. 1981. 'A projection from the entorhinal cortex to the nucleus accumbens in the rat', *Brain Res*, 209: 427-31.

Krettek, J. E., and J. L. Price. 1974. 'Projections from the amygdala to the perirhinal and entorhinal cortices and the subiculum', *Brain Res*, 71: 150-4. bbbbbbbbbv

Kumar, S. S., and P. S. Buckmaster. 2006. 'Hyperexcitability, interneurons, and loss of GABAergic synapses in entorhinal cortex in a model of temporal lobe epilepsy', *J Neurosci*, 26: 4613-23.

Kumar, S. S., X. Jin, P. S. Buckmaster, and J. R. Huguenard. 2007. 'Recurrent circuits in layer II of medial entorhinal cortex in a model of temporal lobe epilepsy', *J Neurosci*, 27: 1239-46.

Lee, J. H., A. N. Daud, L. L. Cribbs, A. E. Lacerda, A. Pereverzev, U. Klockner, T. Schneider, and E. Perez-Reyes. 1999. 'Cloning and expression of a novel member of the low voltage-activated T-type calcium channel family', *J Neurosci*, 19: 1912-21.

Lee, J. H., J. C. Gomora, L. L. Cribbs, and E. Perez-Reyes. 1999. 'Nickel block of three cloned T-type calcium channels: low concentrations selectively block alpha1H', *Biophys J*, 77: 3034-42.

Lein, E. S., M. J. Hawrylycz, N. Ao, M. Ayres, A. Bensinger, A. Bernard, A. F. Boe, M. S. Boguski, K. S. Brockway, E. J. Byrnes, L. Chen, L. Chen, T. M. Chen, M. C. Chin, J. Chong, B. E. Crook, A. Czaplinska, C. N. Dang, S. Datta, N. R. Dee, A. L. Desaki, T. Desta, E. Diep, T. A. Dolbeare, M. J. Donelan, H. W. Dong, J. G. Dougherty, B. J. Duncan, A. J. Ebbert, G. Eichele, L. K. Estin, C. Faber, B. A. Facer, R. Fields, S. R. Fischer, T. P. Fliss, C. Frensley, S. N. Gates, K. J. Glattfelder, K. R. Halverson, M. R. Hart, J. G. Hohmann, M. P. Howell, D. P. Jeung, R. A. Johnson, P. T. Karr, R. Kawal, J. M. Kidney, R. H. Knapik, C. L. Kuan, J. H. Lake, A. R. Laramee, K. D. Larsen, C. Lau, T. A. Lemon, A. J. Liang, Y. Liu, L. T. Luong, J. Michaels, J. J. Morgan, R. J. Morgan, M. T. Mortrud, N. F. Mosqueda, L. L. Ng, R. Ng, G. J. Orta, C. C. Overly, T. H. Pak, S. E. Parry, S. D. Pathak, O. C. Pearson, R. B. Puchalski, Z. L. Riley, H. R. Rockett, S. A. Rowland, J. J. Royall, M. J. Ruiz, N. R. Sarno, K. Schaffnit, N. V. Shapovalova, T. Sivisay, C. R. Slaughterbeck, S. C. Smith, K. A. Smith, B. I. Smith, A. J. Sodt, N. N. Stewart, K. R. Stumpf, S. M. Sunkin, M. Sutram, A. Tam, C. D. Teemer, C. Thaller, C. L. Thompson, L. R. Varnam, A. Visel, R. M. Whitlock, P. E. Wohnoutka, C. K. Wolkey, V. Y. Wong, M. Wood, M. B. Yaylaoglu, R. C. Young, B. L. Youngstrom, X. F. Yuan, B. Zhang, T. A. Zwingman, and A. R. Jones. 2007. 'Genome-wide atlas of gene expression in the adult mouse brain', *Nature*, 445: 168-76.

Leitner, F. C., S. Melzer, H. Lutcke, R. Pinna, P. H. Seeburg, F. Helmchen, and H. Monyer. 2016. 'Spatially segregated feedforward and feedback neurons support differential odor processing in the lateral entorhinal cortex', *Nat Neurosci*, 19: 935-44.

Leresche, N., H. R. Parri, G. Erdemli, A. Guyon, J. P. Turner, S. R. Williams, E. Asprodini, and V. Crunelli. 1998. 'On the action of the anti-absence drug ethosuximide in the rat and cat thalamus', *J Neurosci*, 18: 4842-53.

Leuranguer, V., A. Monteil, E. Bourinet, G. Dayanithi, and J. Nargeot. 2000. 'T-type calcium currents in rat cardiomyocytes during postnatal development:

contribution to hormone secretion', *Am J Physiol Heart Circ Physiol*, 279: H2540-8.

Levisohn, L. F., and O. Isacson. 1991. 'Excitotoxic lesions of the rat entorhinal cortex. Effects of selective neuronal damage on acquisition and retention of a non-spatial reference memory task', *Brain Res*, 564: 230-44.

Levitsky, K. L., and J. Lopez-Barneo. 2009. 'Developmental change of T-type Ca2+ channel expression and its role in rat chromaffin cell responsiveness to acute hypoxia', *J Physiol*, 587: 1917-29.

Li, Y., J. Xu, Y. Liu, J. Zhu, N. Liu, W. Zeng, N. Huang, M. J. Rasch, H. Jiang, X. Gu, X. Li, M. Luo, C. Li, J. Teng, J. Chen, S. Zeng, L. Lin, and X. Zhang. 2017. 'A distinct entorhinal cortex to hippocampal CA1 direct circuit for olfactory associative learning', *Nat Neurosci*, 20: 559-70.

Lingenhohl, K., and D. M. Finch. 1991. 'Morphological characterization of rat entorhinal neurons in vivo: soma-dendritic structure and axonal domains', *Exp Brain Res*, 84: 57-74.

Lipton, P. A., and H. Eichenbaum. 2008. 'Complementary roles of hippocampus and medial entorhinal cortex in episodic memory', *Neural Plast*, 2008: 258467.

Llinas, R., and H. Jahnsen. 1982. 'Electrophysiology of mammalian thalamic neurones in vitro', *Nature*, 297: 406-8.

Llinas, R., and Y. Yarom. 1981. 'Electrophysiology of mammalian inferior olivary neurones in vitro. Different types of voltage-dependent ionic conductances', *J Physiol*, 315: 549-67.

Lorente de Nó, R. 1933. 'Studies on the struture of the cerebral cortex I: The area entorhinalis', *J. Psychol. Neurol.(Leipzig)*, 45: 381-438.

Louhivuori, L. M., V. Louhivuori, H. K. Wigren, E. Hakala, L. C. Jansson, T. Nordstrom, M. L. Castren, and K. E. Akerman. 2013. 'Role of low voltage activated calcium channels in neuritogenesis and active migration of embryonic neural progenitor cells', *Stem Cells Dev*, 22: 1206-19.

Lu, H. K., R. J. Fern, J. J. Nee, and P. Q. Barrett. 1994. 'Ca(2+)-dependent activation of T-type Ca2+ channels by calmodulin-dependent protein kinase II', *Am J Physiol*, 267: F183-9.

Magistretti, J., and A. Alonso. 1999. 'Biophysical properties and slow voltage-dependent inactivation of a sustained sodium current in entorhinal cortex layer-II principal neurons: a whole-cell and single-channel study', *J Gen Physiol*, 114: 491-509.

Magistretti, J., and A. Alonso. 2006. 'Multiple conductance substates in pharmacologically untreated Na(+) channels generating persistent openings in rat entorhinal cortex neurons', *J Membr Biol*, 214: 165-80.

Magistretti, J., D. S. Ragsdale, and A. Alonso. 2003. 'Kinetic diversity of single-channel burst openings underlying persistent Na(+) current in entorhinal cortex neurons', *Biophys J*, 85: 3019-34.

Marger, F., A. Gelot, A. Alloui, J. Matricon, J. F. Ferrer, C. Barrere, A. Pizzoccaro, E. Muller, J. Nargeot, T. P. Snutch, A. Eschalier, E. Bourinet, and D. Ardid. 2011. 'T-type calcium channels contribute to colonic hypersensitivity in a rat model of irritable bowel syndrome', *Proc Natl Acad Sci U S A*, 108: 11268-73.

Martin, R. L., J. H. Lee, L. L. Cribbs, E. Perez-Reyes, and D. A. Hanck. 2000. 'Mibefradil block of cloned T-type calcium channels', *J Pharmacol Exp Ther*, 295: 302-8.

Martinello, K., Z. Huang, R. Lujan, B. Tran, M. Watanabe, E. C. Cooper, D. A. Brown, and M. M. Shah. 2015. 'Cholinergic afferent stimulation induces axonal function plasticity in adult hippocampal granule cells', *Neuron*, 85: 346-63.

Masurkar, A. V., K. V. Srinivas, D. H. Brann, R. Warren, D. C. Lowes, and S. A. Siegelbaum. 2017. 'Medial and Lateral Entorhinal Cortex Differentially Excite Deep versus Superficial CA1 Pyramidal Neurons', *Cell Rep*, 18: 148-60.

McGivern, J. G. 2006. 'Pharmacology and drug discovery for T-type calcium channels', *CNS Neurol Disord Drug Targets*, 5: 587-603.

McNaughton, B. L., F. P. Battaglia, O. Jensen, E. I. Moser, and M. B. Moser. 2006. 'Path integration and the neural basis of the 'cognitive map'', *Nat Rev Neurosci*, 7: 663-78.

Mesulam, M. M., and E. J. Mufson. 1984. 'Neural inputs into the nucleus basalis of the substantia innominata (Ch4) in the rhesus monkey', *Brain*, 107 (Pt 1): 253-74.

Meunier, M., J. Bachevalier, M. Mishkin, and E. A. Murray. 1993. 'Effects on visual recognition of combined and separate ablations of the entorhinal and perirhinal cortex in rhesus monkeys', *J Neurosci*, 13: 5418-32.

Miwa, H., J. Koh, Y. Kajimoto, and T. Kondo. 2011. 'Effects of T-type calcium channel blockers on a parkinsonian tremor model in rats', *Pharmacol Biochem Behav*, 97: 656-9.

Mizuseki, K., A. Sirota, E. Pastalkova, and G. Buzsaki. 2009. 'Theta oscillations provide temporal windows for local circuit computation in the entorhinal-hippocampal loop', *Neuron*, 64: 267-80.

Molineux, M. L., J. E. McRory, B. E. McKay, J. Hamid, W. H. Mehaffey, R. Rehak, T. P. Snutch, G. W. Zamponi, and R. W. Turner. 2006. 'Specific T-type calcium channel isoforms are associated with distinct burst phenotypes in deep cerebellar nuclear neurons', *Proc Natl Acad Sci U S A*, 103: 5555-60.

Morikawa, H., K. Fukuda, H. Mima, T. Shoda, S. Kato, and K. Mori. 1998. 'Tyrosine kinase inhibitors suppress N-type and T-type Ca2+ channel currents in NG108-15 cells', *Pflugers Arch*, 436: 127-32.

Morris, R., M. Petrides, and D. N. Pandya. 1999. 'Architecture and connections of retrosplenial area 30 in the rhesus monkey (Macaca mulatta)', *Eur J Neurosci*, 11: 2506-18.

Nagahara, A. H., T. Otto, and M. Gallagher. 1995. 'Entorhinal-perirhinal lesions impair performance of rats on two versions of place learning in the Morris water maze', *Behav Neurosci*, 109: 3-9.

Nelson, M. T., P. M. Joksovic, P. Su, H. W. Kang, A. Van Deusen, J. P. Baumgart, L. S. David, T. P. Snutch, P. Q. Barrett, J. H. Lee, C. F. Zorumski, E. Perez-Reyes, and S. M. Todorovic. 2007. 'Molecular mechanisms of subtype-specific inhibition of neuronal T-type calcium channels by ascorbate', *J Neurosci*, 27: 12577-83.

Newmark, R. E., K. Schon, R. S. Ross, and C. E. Stern. 2013. 'Contributions of the hippocampal subfields and entorhinal cortex to disambiguation during working memory', *Hippocampus*, 23: 467-75.

Nigro, M. J., P. Mateos-Aparicio, and J. F. Storm. 2014. 'Expression and functional roles of Kv7/KCNQ/M-channels in rat medial entorhinal cortex layer II stellate cells', *J Neurosci*, 34: 6807-12.

Nolan, M. F., J. T. Dudman, P. D. Dodson, and B. Santoro. 2007. 'HCN1 channels control resting and active integrative properties of stellate cells from layer II of the entorhinal cortex', *J Neurosci*, 27: 12440-51.

Nolan, M. F., G. Malleret, J. T. Dudman, D. L. Buhl, B. Santoro, E. Gibbs, S. Vronskaya, G. Buzsaki, S. A. Siegelbaum, E. R. Kandel, and A. Morozov. 2004. 'A behavioral role for dendritic integration: HCN1 channels constrain spatial memory and plasticity at inputs to distal dendrites of CA1 pyramidal neurons', *Cell*, 119: 719-32.

Nowycky, M. C., A. P. Fox, and R. W. Tsien. 1985. 'Three types of neuronal calcium channel with different calcium agonist sensitivity', *Nature*, 316: 440-3.

O'Donnell, C., and M. F. Nolan. 2011. 'Tuning of synaptic responses: an organizing principle for optimization of neural circuits', *Trends Neurosci*, 34: 51-60.

Ohkuma, M., F. Kawai, and E. Miyachi. 2013. 'Acetylcholine enhances excitability by lowering the threshold of spike generation in olfactory receptor cells', *J Neurophysiol*, 110: 2082-9.

Ono, K., and T. Iijima. 2010. 'Cardiac T-type Ca(2+) channels in the heart', *J Mol Cell Cardiol*, 48: 65-70.

Oswald, C. J., and M. Good. 2000. 'The effects of combined lesions of the subicular complex and the entorhinal cortex on two forms of spatial navigation in the water maze', *Behav Neurosci*, 114: 211-7.

Otto, T., and H. Eichenbaum. 1992. 'Neuronal activity in the hippocampus during delayed non-match to sample performance in rats: evidence for hippocampal processing in recognition memory', *Hippocampus*, 2: 323-34.

Pastoll, H., H. L. Ramsden, and M. F. Nolan. 2012. 'Intrinsic electrophysiological properties of entorhinal cortex stellate cells and their contribution to grid cell firing fields', *Front Neural Circuits*, 6: 17.

Pastoll, H., M. White, and M. Nolan. 2012. 'Preparation of parasagittal slices for the investigation of dorsal-ventral organization of the rodent medial entorhinal cortex', *J Vis Exp*.

Perez-Reyes, E. 2003. 'Molecular physiology of low-voltage-activated t-type calcium channels', *Physiol Rev*, 83: 117-61.

Perez-Reyes, E., L. L. Cribbs, A. Daud, A. E. Lacerda, J. Barclay, M. P. Williamson, M. Fox, M. Rees, and J. H. Lee. 1998. 'Molecular characterization of a neuronal low-voltage-activated T-type calcium channel', *Nature*, 391: 896-900.

Quilichini, P., A. Sirota, and G. Buzsaki. 2010. 'Intrinsic circuit organization and theta-gamma oscillation dynamics in the entorhinal cortex of the rat', *J Neurosci*, 30: 11128-42.

Ramirez, J. J., and D. G. Stein. 1984. 'Sparing and recovery of spatial alternation performance after entorhinal cortex lesions in rats', *Behav Brain Res*, 13: 53-61.

Reid, C. A., S. Xu, and D. A. Williams. 2008. 'Spontaneous release from mossy fiber terminals inhibits Ni2+-sensitive T-type Ca2+ channels of CA3 pyramidal neurons in the rat organotypic hippocampal slice', *Hippocampus*, 18: 623-30.

Robinson, R. B., and S. A. Siegelbaum. 2003. 'Hyperpolarization-activated cation currents: from molecules to physiological function', *Annu Rev Physiol*, 65: 453-80.

Rodo, C., F. Sargolini, and E. Save. 2017. 'Processing of spatial and non-spatial information in rats with lesions of the medial and lateral entorhinal cortex: Environmental complexity matters', *Behav Brain Res*, 320: 200-09.

Saleem, K. S., and K. Tanaka. 1996. 'Divergent projections from the anterior inferotemporal area TE to the perirhinal and entorhinal cortices in the macaque monkey', *J Neurosci*, 16: 4757-75.

Sargolini, F., M. Fyhn, T. Hafting, B. L. McNaughton, M. P. Witter, M. B. Moser, and E. I. Moser. 2006. 'Conjunctive representation of position, direction, and velocity in entorhinal cortex', *Science*, 312: 758-62.

Schenk, F., and R. G. Morris. 1985. 'Dissociation between components of spatial memory in rats after recovery from the effects of retrohippocampal lesions', *Exp Brain Res*, 58: 11-28.

Schmidt-Hieber, C., G. Toleikyte, L. Aitchison, A. Roth, B. A. Clark, T. Branco, and M. Hausser. 2017. 'Active dendritic integration as a mechanism for robust and precise grid cell firing', *Nat Neurosci*.

Schwerdtfeger, W. K., E. H. Buhl, and P. Germroth. 1990. 'Disynaptic olfactory input to the hippocampus mediated by stellate cells in the entorhinal cortex', *J Comp Neurol*, 292: 163-77.

Senatore, A., W. Guan, and J. D. Spafford. 2014. 'Cav3 T-type channels: regulators for gating, membrane expression, and cation selectivity', *Pflugers Arch*, 466: 645-60.

Serrano, J. R., E. Perez-Reyes, and S. W. Jones. 1999. 'State-dependent inactivation of the alpha1G T-type calcium channel', *J Gen Physiol*, 114: 185-201.

Shipe, W. D., J. C. Barrow, Z. Q. Yang, C. W. Lindsley, F. V. Yang, K. A. Schlegel, Y. Shu, K. E. Rittle, M. G. Bock, G. D. Hartman, C. Tang, J. E. Ballard, Y. Kuo, E.

D. Adarayan, T. Prueksaritanont, M. M. Zrada, V. N. Uebele, C. E. Nuss, T. M. Connolly, S. M. Doran, S. V. Fox, R. L. Kraus, M. J. Marino, V. K. Graufelds, H. M. Vargas, P. B. Bunting, M. Hasbun-Manning, R. M. Evans, K. S. Koblan, and J. J. Renger. 2008. 'Design, synthesis, and evaluation of a novel 4-aminomethyl-4-fluoropiperidine as a T-type Ca2+ channel antagonist', *J Med Chem*, 51: 3692-5.

Silver, R. A., and S. R. Bolsover. 1991. 'Expression of T-type calcium current precedes neurite extension in neuroblastoma cells', *J Physiol (Paris)*, 85: 79-83.

Simms, B. A., and G. W. Zamponi. 2014. 'Neuronal voltage-gated calcium channels: structure, function, and dysfunction', *Neuron*, 82: 24-45.

Spitzer, N. C. 1994. 'Spontaneous Ca2+ spikes and waves in embryonic neurons: signaling systems for differentiation', *Trends Neurosci*, 17: 115-8.

Splawski, I., D. S. Yoo, S. C. Stotz, A. Cherry, D. E. Clapham, and M. T. Keating. 2006. 'CACNA1H mutations in autism spectrum disorders', *J Biol Chem*, 281: 22085-91.

Spruston, N., and D. Johnston. 2008. 'Out of control in the dendrites', *Nat Neurosci*, 11: 733-4.

Squire, L. R., and P. Alvarez. 1995. 'Retrograde amnesia and memory consolidation: a neurobiological perspective', *Curr Opin Neurobiol*, 5: 169-77.

Staley, K. 2004. 'Neuroscience. Epileptic neurons go wireless', *Science*, 305: 482-3.

Stemmler, M., and C. Koch. 1999. 'How voltage-dependent conductances can adapt to maximize the information encoded by neuronal firing rate', *Nat Neurosci*, 2: 521-7.

Stern, C. E., S. J. Sherman, B. A. Kirchhoff, and M. E. Hasselmo. 2001. 'Medial temporal and prefrontal contributions to working memory tasks with novel and familiar stimuli', *Hippocampus*, 11: 337-46.

Steward, O. 1976. 'Topographic organization of the projections from the entorhinal area to the hippocampal formation of the rat', *J Comp Neurol*, 167: 285-314.

Steward, O., and S. A. Scoville. 1976. 'Cells of origin of entorhinal cortical afferents to the hippocampus and fascia dentata of the rat', *J Comp Neurol*, 169: 347-70.

Stewart, M., G. J. Quirk, M. Barry, and S. E. Fox. 1992. 'Firing relations of medial entorhinal neurons to the hippocampal theta rhythm in urethane anesthetized and walking rats', *Exp Brain Res*, 90: 21-8.

Surmeli, G., D. C. Marcu, C. McClure, D. L. F. Garden, H. Pastoll, and M. F. Nolan. 2015. 'Molecularly Defined Circuitry Reveals Input-Output Segregation in Deep Layers of the Medial Entorhinal Cortex', *Neuron*, 88: 1040-53.

Suthana, N., Z. Haneef, J. Stern, R. Mukamel, E. Behnke, B. Knowlton, and I. Fried. 2012. 'Memory enhancement and deep-brain stimulation of the entorhinal area', *N Engl J Med*, 366: 502-10.

Suzuki, W. A., and D. G. Amaral. 1994. 'Topographic organization of the reciprocal connections between the monkey entorhinal cortex and the perirhinal and parahippocampal cortices', *J Neurosci*, 14: 1856-77.

Tahvildari, B., and A. Alonso. 2005. 'Morphological and electrophysiological properties of lateral entorhinal cortex layers II and III principal neurons', *J Comp Neurol*, 491: 123-40.

Talley, E. M., L. L. Cribbs, J. H. Lee, A. Daud, E. Perez-Reyes, and D. A. Bayliss. 1999. 'Differential distribution of three members of a gene family encoding low voltage-activated (T-type) calcium channels', *J Neurosci*, 19: 1895-911.

Talley, E. M., G. Solorzano, A. Depaulis, E. Perez-Reyes, and D. A. Bayliss. 2000. 'Low-voltage-activated calcium channel subunit expression in a genetic model of absence epilepsy in the rat', *Brain Res Mol Brain Res*, 75: 159-65.

Tamamaki, N., and Y. Nojyo. 1993. 'Projection of the entorhinal layer II neurons in the rat as revealed by intracellular pressure-injection of neurobiotin', *Hippocampus*, 3: 471-80.

Tang, A. H., M. A. Karson, D. A. Nagode, J. M. McIntosh, V. N. Uebele, J. J. Renger, M. Klugmann, T. A. Milner, and B. E. Alger. 2011. 'Nerve terminal nicotinic acetylcholine receptors initiate quantal GABA release from perisomatic interneurons by activating axonal T-type (Cav3) Ca(2)(+) channels and Ca(2)(+) release from stores', *J Neurosci*, 31: 13546-61.

Tao, J., M. E. Hildebrand, P. Liao, M. C. Liang, G. Tan, S. Li, T. P. Snutch, and T. W. Soong. 2008. 'Activation of corticotropin-releasing factor receptor 1 selectively inhibits CaV3.2 T-type calcium channels', *Mol Pharmacol*, 73: 1596-609.

Tigaret, C. M., V. Olivo, J. H. Sadowski, M. C. Ashby, and J. R. Mellor. 2016. 'Coordinated activation of distinct Ca(2+) sources and metabotropic glutamate receptors encodes Hebbian synaptic plasticity', *Nat Commun*, 7: 10289.

Todorovic, S. M., and V. Jevtovic-Todorovic. 2007. 'Regulation of T-type calcium channels in the peripheral pain pathway', *Channels (Austin)*, 1: 238-45.

Todorovic, S. M., and C. J. Lingle. 1998. 'Pharmacological properties of T-type Ca2+ current in adult rat sensory neurons: effects of anticonvulsant and anesthetic agents', *J Neurophysiol*, 79: 240-52.

Truett, G. E., P. Heeger, R. L. Mynatt, A. A. Truett, J. A. Walker, and M. L. Warman. 2000. 'Preparation of PCR-quality mouse genomic DNA with hot sodium hydroxide and tris (HotSHOT)', *Biotechniques*, 29: 52, 54.

Tsao, A., M. B. Moser, and E. I. Moser. 2013. 'Traces of experience in the lateral entorhinal cortex', *Curr Biol*, 23: 399-405.

Tsay, D., J. T. Dudman, and S. A. Siegelbaum. 2007. 'HCN1 channels constrain synaptically evoked Ca2+ spikes in distal dendrites of CA1 pyramidal neurons', *Neuron*, 56: 1076-89.

Tscherter, A., F. David, T. Ivanova, C. Deleuze, J. J. Renger, V. N. Uebele, H. S. Shin, T. Bal, N. Leresche, and R. C. Lambert. 2011. 'Minimal alterations in T-type calcium channel gating markedly modify physiological firing dynamics', *J Physiol*, 589: 1707-24.

Uebachs, M., C. Schaub, E. Perez-Reyes, and H. Beck. 2006. 'T-type Ca2+ channels encode prior neuronal activity as modulated recovery rates', *J Physiol*, 571: 519-36.

Uebele, V. N., C. E. Nuss, V. P. Santarelli, S. L. Garson, R. L. Kraus, J. C. Barrow, S. R. Stauffer, K. S. Koblan, J. J. Renger, S. Aton, J. Seibt, M. Dumoulin, S. K. Jha, T. Coleman, and M. G. Frank. 2009. 'T-type calcium channels regulate cortical plasticity in-vivo. [corrected]', *Neuroreport*, 20: 257-62.

Uslaner, J. M., S. M. Smith, S. L. Huszar, R. Pachmerhiwala, R. M. Hinchliffe, J. D. Vardigan, S. J. Nguyen, N. O. Surles, L. Yao, J. C. Barrow, V. N. Uebele, J. J. Renger, J. Clark, and P. H. Hutson. 2012. 'T-type calcium channel antagonism produces antipsychotic-like effects and reduces stimulant-induced glutamate release in the nucleus accumbens of rats', *Neuropharmacology*, 62: 1413-21.

van Groen, T. 2001. 'Entorhinal cortex of the mouse: cytoarchitectonical organization', *Hippocampus*, 11: 397-407.

van Groen, T., I. Kadish, and J. M. Wyss. 1999. 'Efferent connections of the anteromedial nucleus of the thalamus of the rat', *Brain Res Brain Res Rev*, 30: 1-26.

van Groen, T., P. Miettinen, and I. Kadish. 2003. 'The entorhinal cortex of the mouse: organization of the projection to the hippocampal formation', *Hippocampus*, 13: 133-49.

Van Hoesen, G., D. N. Pandya, and N. Butters. 1975. 'Some connections of the entorhinal (area 28) and perirhinal (area 35) cortices of the rhesus monkey. II. Frontal lobe afferents', *Brain Res*, 95: 25-38.

Van Hoesen, Gary W, and Deepak N Pandya. 1975. 'Some connections of the entorhinal (area 28) and perirhinal (area 35) cortices of the rhesus monkey. I. Temporal lobe afferents', *Brain research*, 95: 1-24.

Varga, C., S. Y. Lee, and I. Soltesz. 2010. 'Target-selective GABAergic control of entorhinal cortex output', *Nat Neurosci*, 13: 822-4.

Vitko, I., Y. Chen, J. M. Arias, Y. Shen, X. R. Wu, and E. Perez-Reyes. 2005. 'Functional characterization and neuronal modeling of the effects of childhood absence epilepsy variants of CACNA1H, a T-type calcium channel', *J Neurosci*, 25: 4844-55.

Wang, F., Y. Zhang, X. Jiang, Y. Zhang, L. Zhang, S. Gong, C. Liu, L. Zhou, and J. Tao. 2011. 'Neuromedin U inhibits T-type Ca2+ channel currents and decreases membrane excitability in small dorsal root ganglia neurons in mice', *Cell Calcium*, 49: 12-22.

Wang, M., B. P. Ramos, C. D. Paspalas, Y. Shu, A. Simen, A. Duque, S. Vijayraghavan, A. Brennan, A. Dudley, E. Nou, J. A. Mazer, D. A. McCormick, and A. F. Arnsten. 2007. 'Alpha2A-adrenoceptors strengthen working memory networks by inhibiting cAMP-HCN channel signaling in prefrontal cortex', *Cell*, 129: 397-410.

White, J. A., A. Alonso, and A. R. Kay. 1993. 'A heart-like Na+ current in the medial entorhinal cortex', *Neuron*, 11: 1037-47.

Witter, M. P. 1993. 'Organization of the entorhinal-hippocampal system: a review of current anatomical data', *Hippocampus*, 3 Spec No: 33-44.

Witter, M. P. 2007. 'The perforant path: projections from the entorhinal cortex to the dentate gyrus', *Prog Brain Res*, 163: 43-61.

Witter, M. P., and D. G. Amaral. 1991. 'Entorhinal cortex of the monkey: V. Projections to the dentate gyrus, hippocampus, and subicular complex', *J Comp Neurol*, 307: 437-59.

Witter, M. P., G. W. Van Hoesen, and D. G. Amaral. 1989. 'Topographical organization of the entorhinal projection to the dentate gyrus of the monkey', *J Neurosci*, 9: 216-28.

Witter, M. P., P. Room, H. J. Groenewegen, and A. H. Lohman. 1988. 'Reciprocal connections of the insular and piriform claustrum with limbic cortex: an anatomical study in the cat', *Neuroscience*, 24: 519-39.

Wouterlood, F. G., E. Mugnaini, and J. Nederlof. 1985. 'Projection of olfactory bulb efferents to layer I GABAergic neurons in the entorhinal area. Combination of anterograde degeneration and immunoelectron microscopy in rat', *Brain Res*, 343: 283-96.

Wouterlood, F. G., and H. Pothuizen. 2000. 'Sparse colocalization of somatostatin- and GABA-immunoreactivity in the entorhinal cortex of the rat', *Hippocampus*, 10: 77-86.

Wouterlood, F. G., J. C. van Denderen, T. van Haeften, and M. P. Witter. 2000. 'Calretinin in the entorhinal cortex of the rat: distribution, morphology, ultrastructure of neurons, and co-localization with gamma-aminobutyric acid and parvalbumin', *J Comp Neurol*, 425: 177-92.

Wouterlood, FG. 2002. 'Spotlight on the neurones (I): cell types, local connectivity, microcircuits, and distribution of markers', *The Parahippocampal Region*: 61-88.

y Cajal, Santiago Ramón. 1902. *Sobre un ganglio especial de la corteza esfeno occipital*.

Yaari, Y., B. Hamon, and H. D. Lux. 1987. 'Development of two types of calcium channels in cultured mammalian hippocampal neurons', *Science*, 235: 680-2.

Yang, Z. Q., J. C. Barrow, W. D. Shipe, K. A. Schlegel, Y. Shu, F. V. Yang, C. W. Lindsley, K. E. Rittle, M. G. Bock, G. D. Hartman, V. N. Uebele, C. E. Nuss, S. V. Fox, R. L. Kraus, S. M. Doran, T. M. Connolly, C. Tang, J. E. Ballard, Y. Kuo, E. D. Adarayan, T. Prueksaritanont, M. M. Zrada, M. J. Marino, V. K. Graufelds, A. G. DiLella, I. J. Reynolds, H. M. Vargas, P. B. Bunting, R. F. Woltmann, M. M. Magee, K. S. Koblan, and J. J. Renger. 2008. 'Discovery of 1,4-substituted piperidines as potent and selective inhibitors of T-type calcium channels', *J Med Chem*, 51: 6471-7.

Yartsev, M. M., M. P. Witter, and N. Ulanovsky. 2011. 'Grid cells without theta oscillations in the entorhinal cortex of bats', *Nature*, 479: 103-7.

Yoshida, M., L. M. Giocomo, I. Boardman, and M. E. Hasselmo. 2011. 'Frequency of subthreshold oscillations at different membrane potential voltages in neurons at different anatomical positions on the dorsoventral axis in the rat medial entorhinal cortex', *J Neurosci*, 31: 12683-94.

Yoshida, M., M. Teramura, M. Sakai, N. Karasawa, T. Nagatsu, and I. Nagatsu. 1987. 'Immunohistochemical visualization of glutamate- and aspartate-containing nerve terminal pools in the rat limbic structures', *Brain Res*, 410: 169-73.

Yoshimura, Y., M. Inaba, K. Yamada, T. Kurotani, T. Begum, F. Reza, T. Maruyama, and Y. Komatsu. 2008. 'Involvement of T-type Ca2+ channels in the potentiation of synaptic and visual responses during the critical period in rat visual cortex', *Eur J Neurosci*, 28: 730-43.

Young, B. J., T. Otto, G. D. Fox, and H. Eichenbaum. 1997. 'Memory representation within the parahippocampal region', *J Neurosci*, 17: 5183-95.

Zamponi, G. W., E. Bourinet, D. Nelson, J. Nargeot, and T. P. Snutch. 1997. 'Crosstalk between G proteins and protein kinase C mediated by the calcium channel alpha1 subunit', *Nature*, 385: 442-6.

Zhang, S. J., J. Ye, C. Miao, A. Tsao, I. Cerniauskas, D. Ledergerber, M. B. Moser, and E. I. Moser. 2013. 'Optogenetic dissection of entorhinal-hippocampal functional connectivity', *Science*, 340: 1232627.

Zhang, Y., X. Jiang, T. P. Snutch, and J. Tao. 2013. 'Modulation of low-voltage-activated T-type Ca(2)(+) channels', *Biochim Biophys Acta*, 1828: 1550-9.

8. Appendix

			Ca$_v$3.2 wild type			
			Dorsal	*p*-value	**Ventral**	*p*-value
Input Resistance (MΩ) +100 pA		**Control**	48.6±5.6		119±15.1	
		NiCl$_2$	45.9±8.5	0.49	93.5±13.5	*p*<0.002
		Washout	53.6±7.4		110±11.9	
Input Resistance (MΩ) -100 pA		**Control**	35.6±2.8		65.8±10.7	
		NiCl$_2$	32.2±4.1	0.17	66.2±9.4	0.92
		Washout	38.4±4.1		75.2±8.7	
Number of action potentials	**50 pA**	**Control**	0		0	
		NiCl$_2$	0	N/A	0	N/A
		Washout	0		0	
	100 pA	**Control**	0		0	
		NiCl$_2$	0	N/A	0	N/A
		Washout	0		0	
	150 pA	**Control**	0		1.8±1.6	
		NiCl$_2$	0	N/A	0.5±0.5	0.26
		Washout	0		1.1±1.1	
	200 pA	**Control**	1.9±1.9		6.9±2.8	
		NiCl$_2$	1.5±1.5	0.36	2.9±1.6	0.06
		Washout	1.4±1.4		6.6±3	
	250 pA	**Control**	4.9±4.3		11.6±4.3	
		NiCl$_2$	3.3±3.3	0.19	7.7±3.2	0.02
		Washout	4.5±4.5		13.2±5.7	
	300 pA	**Control**	9.4±5.9		15.3±5.6	
		NiCl$_2$	4.8±4.5	0.1	11.7±5.3	0.046
		Washout	7.9±6.6		20.2±7.5	

Appendix 1. Table with the supplementary data for the Figure 4.2. The measurements of the input resistance at +100 pA and 100 pA and action potential number at set membrane potential of -70 mV from Ca$_v$3.2 wild type dorsal and ventral cells. The numbers were recorded before, during and after treatment with 50 μM NiCl$_2$.

			Ca$_v$3.2 wild type			
			Dorsal	*p*-value	**Ventral**	*p*-value
Input Resistance (MΩ) +100 pA		**Control**	62.7±7.6	0.13	96.7±11.3	*p*<0.003
		TTA-P2	58.9±7.4		78.5±8.5	
		Washout	67.8±7.7		88.9±10.1	
Input Resistance (MΩ) -100 pA		**Control**	38.7±4.2	0.67	49.2±5.2	0.98
		TTA-P2	36.7±4.		49.2±6	
		Washout	47.2±6.6		62±7.8	
Number of action potentials	**50 pA**	**Control**	0	N/A	0	N/A
		TTA-P2	0		0	
		Washout	0		0	
	100 pA	**Control**	0	N/A	0	N/A
		TTA-P2	0		0	
		Washout	0		0	
	150 pA	**Control**	0.08±0.08	0.36	1.97±0.9	0.07
		TTA-P2	0		0.3±0.3	
		Washout	0		1.1±1.1	
	200 pA	**Control**	5.17±2.5	0.19	8.5±2.1	0.007
		TTA-P2	3.1±2		3.2±1.6	
		Washout	3±1.9		6.6±3	
	250 pA	**Control**	12.3±5.6	0.2	15.6±3.2	0.013
		TTA-P2	9±3.9		9.2±3.6	
		Washout	8.3±3.7		13.2±5.7	
	300 pA	**Control**	18.3±7.5	0.18	21.4±4.3	0.057
		TTA-P2	14±5.3		15.3±5	
		Washout	14±5.3		20.2±7.5	

Appendix 2. The table showing supplementary information for the Figure 4.4. The data were obtained before during and after treatment with 100 nM TTA-P2 and show changes in the input resistance (+100 pA and – 100 pA) and excitability of Ca$_v$3.2 wild type dorsal and ventral neurons at set membrane potential of – 70 mV.

			Ca$_v$3.2 null			
			Dorsal	*p*-value	**Ventral**	*p*-value
Input Resistance (MΩ) +100 pA		**Control**	71.4±9.3		81.7±18.9	
		NiCl$_2$	76.7±9.8	0.16	79±15.3	0.51
		Washout	73.6±9.3		80.7±15.2	
Input Resistance (MΩ) -100 pA		**Control**	48.5±6.3		46±4.2	
		NiCl$_2$	51.9±7.2	0.19	55.1±6.8	0.17
		Washout	52±4.4		56.4±8	
Number of action potentials	**50 pA**	**Control**	0		0	
		NiCl$_2$	0	N/A	0	N/A
		Washout	0		0	
	100 pA	**Control**	0		0	
		NiCl$_2$	0	N/A	0	N/A
		Washout	0		0	
	150 pA	**Control**	0		2.4±2.4	
		NiCl$_2$	0	N/A	0.5±0.5	0.37
		Washout	0		0.47±0.47	
	200 pA	**Control**	0		4.6±4.6	
		NiCl$_2$	0.2±0.2	0.37	4.1±3.6	0.65
		Washout	0		3.47±0.47	
	250 pA	**Control**	0.53±0.03		8.13±5.6	
		NiCl$_2$	0.4±0.4	0.87	13±5.9	0.31
		Washout	0.2±0.2		10±5.4	
	300 pA	**Control**	2.3±1.3		19.9±5	
		NiCl$_2$	1.7±0.93	0.7	25.3±7.8	0.39
		Washout	1.5±0.74		22.8±6.6	

Appendix 3. Supplementary numerical values for the Figure 4.6. The input resistance (+100 pA and -100 pA) and excitability changes in Ca$_v$3.2 null dorsal and ventral neurons were recorded at – 70 mV. The data were obtained in before, during and after application of 50 µM NiCl$_2$. .

174

			Ca$_v$3.2 null			
			Dorsal	*p*-value	**Ventral**	*p*-value
Input Resistance (MΩ) +100 pA		**Control**	72.5±5		86.9±6.8	
		TTA-P2	71.8±5	0.92	87.8±8.5	0.91
		Washout	75.9±6.2		87.1±6.6	
Input Resistance (MΩ) -100 pA		**Control**	43.7±4.8		38.4±5.4	
		TTA-P2	48.3±4.9	0.34	46.6±6.9	0.28
		Washout	49.2±4.5		53.9±8.8	
Number of action potentials	**50 pA**	**Control**	0		0	
		TTA-P2	0	N/A	0	N/A
		Washout	0		0	
	100 pA	**Control**	0		0	
		TTA-P2	0	N/A	0	N/A
		Washout	0		0	
	150 pA	**Control**	0.33±0.33		1.6±1	
		TTA-P2	0.2±0.2	0.36	0.6±0.3	0.2
		Washout	1±1		0.97±0.88	
	200 pA	**Control**	2.5±1.9		8.5±2.1	
		TTA-P2	2.7±1.9	0.43	5.4±2.1	0.06
		Washout	4.2±3.3		5.4±2.5	
	250 pA	**Control**	8.1±3.1		16.8±2.7	
		TTA-P2	9.1±3.6	0.61	12.3±2.7	0.11
		Washout	9.5±5.2		12.7±3.7	
	300 pA	**Control**	15.8±4.4		23.4±3.6	
		TTA-P2	14.1±5.8	0.56	19.9±3.4	0.12
		Washout	16.9±7.6		19.6±4.6	

Appendix 4. The supplementary table for the Figure 4.8. Data show the effects of TTA-P2 (100 nM) treatment on the input resistance (+100 pA and -100 pA) and excitability of Ca$_v$3.2 null dorsal and ventral L II SC when recorded at set membrane potential of – 70 mV.

	Wild type dorsal (n=5)	Wild type ventral (n=5)	Null dorsal (n=5)	Null ventral (n=4)
-90	3.8±1.3	9.5±2.6	1.8±0.6	2.1±0.7
-85	4.6±1.8	11.3±3.1	2.7±0.9	3±1
-80	4.9±1.5	14.3±3.5	2.4±1	7.8±2.8
-75	5.1±1.3	17.7±4.7	6.5±1.7	7.3±2.8
-70	6.7±1.6	21±3.6	5.4±1.1	7.1±3.1
-65	6.3±1.3	22.4±3.7	7.2±1.4	10.7±3.9
-60	8±1.8	26.2±4.7	8.3±1.5	10.5±3.3
-55	13.3±1.8	37.7±6.2	7.9±1.5	12.2±4.5
-50	22.6±6.2	56.7±9.1	8.8±2	14±6.3
-45	33.4±11.3	74.6±12.3	15.7±4	19.3±6
	Wild type dorsal (n=5)	**Wild type ventral (n=4)**	**Null dorsal (n=3)**	**Null ventral (n=3)**
-100	22.2±4.4	59.3±8.6	6.8±3.3	6.4±3.7
-95	22.7±4	58.7±9.7	7.1±1.8	6.1±3.2
-90	22.4±4.3	54.3±10.2	5.1±2.3	5.6±3.5
-85	20.5±3	47.6±9.4	6.7±0.4	7.3±4.0
-80	17.9±1.8	35.4±7.6	4±1.5	5.4±2.9
-75	12.2±1.8	23.6±4.1	3.9±1	5.2±2.5
-70	10.9±1.2	17.6±3	1±0.3	4±1.9
-65	8.8±2.4	12.5±2.3	2.3±0.7	2±0.6
-60	5.6±1.9	9.1±1.1	1.3±0.6	2.8±0.9
-55	3.5±1.4	7.7±1.4	3.4±1.8	1.1±0.3

Appendix 5. Supplementary data for Figure 5.5 B. Quantitative comparison of T-type Ca^{2+} current recorded from $Ca_v3.2$ wild type dorsal and ventral with null dorsal and ventral neurons. The -90 mV to -45 mV rows (top) represent the activation protocol whereas the -100 mV to -55 mV (bottom) show the numbers recorded during the inactivation protocol.

RMP					
		n	**1-4 Hz**	**4-8 Hz**	**8-12 Hz**
WT Dorsal	**>-55 mV**	23	0,040±0,01	0,01±0,0007	0,001±0,0003
WT Ventral		24	0,023±0,005	0,005±0,001	0,002±0,0008
Null Dorsal		17	0,022±0,004	0,008±0,002	0,003±0,0009
Null Ventral		12	0,024±0,007	0,005±0,001	0,002±0,0007
		n	**1-4 Hz**	**4-8 Hz**	**8-12 Hz**
WT Dorsal	**>-50 mV**	14	0,059±0,01	0,01±0,003	0,04±0,0008
WT Ventral		6	0,03±0,007	0,01±0,002	0,004±0,001
Null Dorsal		14	0,045±0,008	0,02±0,004	0,004±0,0009
Null Ventral		6	0,036±0,03	0,014±0,01	0,003±0,001
		n	**1-4 Hz**	**4-8 Hz**	**8-12 Hz**
WT Dorsal	**>-45 mV**	6	0,049±0,02	0,018±0,004	0,009±0,003
WT Ventral		2	0,055±0,006	0,013±0,0002	0,007±0,0009
Null Dorsal		11	0,028±0,005	0,02±0,005	0,009±0,002
Null Ventral		N/A	N/A	N/A	
-70 mV					
		n	**1-4 Hz**	**4-8 Hz**	**8-12 Hz**
WT Dorsal	**>-55 mV**	21	0,04±0,008	0,006±0,0009	0,002±0,0004
WT Ventral		21	0,03±0005	0,006±0,001	0,002±0,0009
Null Dorsal		17	0,02±0,007	0,008±0,003	0,003±0,0009
Null Ventral		13	0,03±0,009	0,005±0,001	0,002±0,0006
		n	**1-4 Hz**	**4-8 Hz**	**8-12 Hz**
WT Dorsal	**>-50 mV**	15	0,04±0,009	0,01±0,004	0,01±0,002
WT Ventral		14	0,04±0,007	0,01±0,003	0,004±0,001
Null Dorsal		22	0,03±0,005	0,02±0,003	0,006±0,002
Null Ventral		6	0,04±0,03	0,016±0,01	0,003±0,002
		n	**1-4 Hz**	**4-8 Hz**	**8-12 Hz**
WT Dorsal	**>-45 mV**	7	0,03±0,005	0,02±0,004	0,008±0,001
WT Ventral		N/A	N/A	N/A	N/A
Null Dorsal		5	0,03±0,006	0,02±0,004	0,008±0,002
Null Ventral		5	0,05±0,01	0,02±0,008	0,003±0,0004

Appendix 6. The table showing numerical values of the sMPOs power obtained from Cav3.2 wild type (WT) and null cells at different membrane potentials. The data were grouped into three frequencies: 1-4 Hz, 4-8 Hz and 8-12 Hz.